DYNAMIC ACCURACY AND STABILITY OF MACHINE-TOOL HYDRAULIC COPYING SYSTEMS

by

Seshadri Sankar

A THESIS

IN THE

FACULTY OF ENGINEERING

Presented in Partial Fulfilment of the Requirements

for the

Degree of DOCTOR OF ENGINEERING

at

Sir George Williams University

Montreal, Canada

March, 1973

ABSTRACT

The dynamic accuracy and stability of machine-tool hydraulic copying systems are investigated by formulating a mathematical model of a copying unit, which takes into account the following features: a) dynamic cutting force and its interaction with the velocity response of the system, b) dynamic behavior of the copying slide with the dry friction in its mountings, c) dynamic behavior of the control valve and the action of the flow forces, and d) dynamic behavior of the stylus.

The time domain model of the kinematic input due to the template configuration which gives the actual motion of the stylus during copying is used as the input function in the analysis. This procedure makes both analysis and results applicable to all types of machine-tool hydraulic copying systems, including electro-hydraulic and numerically-controlled devices.

The governing equations of the system are non-dimensionalized and simulated on an analog computer to study the effects of various influencing parameters on the dynamic accuracy and stability. For this purpose, a dynamic accuracy criterion which is a function of the manufacturing tolerance of the produced parts is developed. The comparison of theoretical results with experimental data have been achieved by

comparing the theoretical results with actual test data supplied by the manufacturers. Close agreement is observed.

The results indicate that the stability of copying depends to a great extent on the amount of dry friction, inertia, size, and stiffness of the stylus, the supply pressure and the cross-sectional area of the piston. The results also show that the system accuracy is increased by decreasing the inertia and increasing the stiffness of the stylus. Increasing the supply pressure and the cross-sectional area of the piston also improves the dynamic accuracy of the system.

Further results in this investigation are outlined as:

- dry friction in the system increases the stability but decreases the dynamic accuracy.
- dynamic accuracy increases by increasing the kinematic gain K_g but decreases the stability.
- leakage flow increases the stability at the cost of a decrease in the dynamic accuracy.
- increasing the angle γ and decreasing the velocity v of the machine-tool slide increases the dynamic accuracy.
- decrease of the exhaust pressure increases the dynamic accuracy and decreases the stability.
- from the stability point of view, the dry friction in the system should be higher for finishing operation than for roughing operation.

The results also provide some useful informations on:

- control of stability of existing devices.
- optimization of existing copying devices for maximum accuracy under stable operation.

Plots are developed to be used as a guide for the design and operation of hydraulic copying systems.

ACKNOWLEDGEMENTS

The author wishes to express his gratitude and deep appreciation to this thesis supervisor, Dr. M.O.M. Osman, for initiating the project and providing continued guidance throughout the investigation.

The technical information and assistance provided by the manufacturers of hydraulic copying systems, listed in Appendix I of this thesis, are greatly appreciated.

The author gratefully acknowledges the Government of Quebec for offering a Post-Graduate Scholarship which makes this work possible. The financial support of the National Research Council of Canada, Grant No. A5181, and la Formation de Chercheurs et d'Action Concertée, of the Government of Quebec, Grant No. 242-110 is also acknowledged.

TABLE OF CONTENTS

page

ABSTRACT i

ACKNOWLEDGEMENT. iv

LIST OF FIGURES. viii

LIST OF TABLES xi

NOMENCLATURE xii

CHAPTER I

INTRODUCTION 1

1.1 Background. 1
1.2 Review of Previous Work 11
1.3 Scope of the Research Work. 16

CHAPTER II

MATHEMATICAL MODEL OF HYDRAULIC COPYING SYSTEMS. . . 19

2.1 Description and Operating Principle of Hydraulic Copying Systems 19
2.2 A Comparison of Error in Copying Systems. . . . 26
2.3 Formulation of the Governing System Equations 32
2.4 Stylus Motion in Time Domain. 45
2.4.1 Introduction 45
2.4.2 Transformation of Template Profile in Time Domain 46

CHAPTER III

STABILITY OF HYDRAULIC COPYING SYSTEMS 50

3.1 General 50
3.2 Stability Analysis Using Linearization Method. 50
3.3 Stability Analysis Using Matrix Theory. 56
3.4 Stability Analysis Using Simulation Procedures. 63

page

CHAPTER IV

DYNAMIC ACCURACY OF HYDRAULIC COPYING SYSTEMS. . . . 66

4.1 General 66
4.2 Dynamic Accuracy Criterion for Hydraulic Copying Systems 66

CHAPTER V

SIMULATION OF HYDRAULIC COPYING SYSTEM FOR DYNAMIC ACCURACY AND STABILITY 71

5.1 General 71
5.2 Non-Dimensionalization of System Equations. . . 71
5.3 Simulation of Governing Equations 81

CHAPTER VI

SYSTEM PARAMETER ANALYSIS AND CASE STUDIES 85

6.1 General 85
6.2 Effects of System Parameters on the Dynamic Accuracy and Stability. 87
6.2.1 Effect of Dry Friction 87
6.2.2 Effect of Cross-Sectional Area of the Piston 90
6.2.3 Effect of Inertia of the Stylus 91
6.2.4 Effect of Contact Spring in the Stylus System. 94
6.2.5 Effect of Spring Stiffness K_s. 98
6.2.6 Effect of Initial Spring Force λ_k. . . . 98
6.2.7 Effect of Kinematic Gain K_g. 99
6.2.8 Effect of Leakage Coefficient. 102
6.2.9 Effect of Supply and Exhaust Pressures. 104
6.2.10 Influence of Other System Parameters 108
6.3 Effect of Dynamic Cutting Force 110
6.4 Effect of Cutting Force Fluctuation Frequency and the Coefficient ε 110
6.5 Effect of Velocity v and Angle γ. 112
6.6 Effect of Leakage Flow. 118

CHAPTER VII

CONCLUSIONS AND RECOMMENDATIONS FOR FUTURE WORK. . . 122

page

REFERENCES 129

APPENDIX I

MANUFACTURERS OF HYDRAULIC COPYING SYSTEMS 133

APPENDIX II

CALCULATION OF THE CUTTING FORCE F_s. 135

APPENDIX III

AMPLITUDE AND TIME SCALING IN ANALOG COMPUTER. . . . 148

APPENDIX IV

FORTRAN PROGRAM FOR STYLUS MOTION IN TIME DOMAIN 157

APPENDIX V

SYSTEM PARAMETERS. 161

APPENDIX VI

CALCULATION OF HYDRO-MECHANICAL STIFFNESS C_h AND ITS CONDITION ON STABILITY 163

LIST OF FIGURES

FIGURE		PAGE
1	Two-Dimensional Hydraulic Copying System for a Lathe	3
2	Two-Dimensional Hydraulic Copying System in a Milling Machine.	4
3	Two-Dimensional Hydraulic Copying System with Automatic Feed Control	5
4	Three-Dimensional Hydraulic Copying System in a Milling Machine.	7
5	Sectional View of an Electro-Hydraulic Servovalve.	8
6	A Schematic Layout of a Numerically Controlled Copying System	9
7	Two-Dimensional Hydraulic Copying System with its Control Elements.	20
8	Four-Edge Controlled, Symmetrical Cylinder Hydraulic Copying System.	22
9	Two-Edge Controlled, Symmetrical Cylinder Hydraulic Copying System.	24
10	Two-Edge Controlled, Unsymmetrical Cylinder Hydraulic Copying System.	25
11	One-Edge Controlled, Unsymmetrical Cylinder Hydraulic Copying System.	27
12	Block Diagram of Copying Systems.	28
13	Control Error e Against Velocity Response $\dot{z}$ . .	31
14	Effect of Dry Friction on the Control Error . .	33

FIGURE		PAGE
15	Effect of Feed on ω_f and ε for Steel CK60 . .	37
16	An Equivalent Spring, Mass and Damper System for the Copying System	39
17	Schematic Diagram of a Hydraulic Servomotor.	40
18	A Schematic Diagram for the Stylus System . .	42
19	Velocity Diagram for Stylus Motion.	47
20	Flow Chart for Stability Analysis	64
21	Schematic Input and Error Function of the Copying System.	68
22	Analog Circuit Diagram of the Copying System.	82
23	Template Profile and its Configuration in Time Domain.	83
24	Typical Error Function of the Copying System.	86
25	Effect of Dry Friction on the Total Error Zone.	88
26	Stabilizing Effect of Dry Friction.	89
27	Effect of Cross-Sectional Area of Piston A on Δ_e and F_w.	92
28	Error Plots for the Cross-Sectional Area of the Piston A = 9 in^2	93
29	Effect of Mass Moment of Inertia of Stylus I_m on Δ_e and F_w.	95
30	Error Plots for the Contact Spring Stiffness $K_m = 4\times10^4$ lb/in...	96
31	Effect of Spring Stiffness K_m on the Total Error Zone Δ_e	97

FIGURE		PAGE
32	Effect of Kinematic Gain on the Total Error Zone.	103
33	Effect of Leakage Coefficient on the Total Error Zone.	105
34	Effect of Supply and Exhaust Pressures on the Total Error Zone	106
35	Effect of Supply Pressure Pulsation	109
36	Effects of F_1 and F_2 on F_w and Δ_e	111
37	Effect of ω_f on the Error Function.	113
38	Effect of Velocity of Slide on the Stylus Displacement.	115
39	Effect of Angle γ on the Stylus Displacement	116
40	Effect of Velocity of Slide on the Total Error Zone.	117
41	Effect of Laminar Leakage Coefficient on Δ_e and F_w.	120
42	Effect of Turbulent Leakage Coefficient on Δ_e and F_w.	121
A.1	Representation of Cutting Force in Three Mutually Perpendicular Axes.	137
A.2	Cutting Forces in a Hydraulic Copying System.	140
A.3	Flow Chart for Computing F_1 and F_2.	142
A.4	The Coefficients K_q and K_r for Steel 4340 . .	145
A.5	Amplitude and Time Scaled Analog Computer Diagrams.	152

LIST OF TABLES

TABLE		PAGE
1	Effect of Initial Spring Force λ_k on the Steady State Error.	126
2	Effect of Mass of Spool Valve on the Total Error Zone	127
3	Effect of Angle γ on the Total Error Zone of the Workpiece Diamter.	128

NOMENCLATURE

A	effective cross-sectional area of piston; in^2.
a	linear dimension of the stylus; in.
a*, b*	a/u; b/u; dimensionless
B	bulk modulus of elasticity of fluid, lb/in^2.
b	linear dimension of the stylus; in.
b_o	depth of cut; in.
C	viscous damping coefficient between the piston and the cylinder; lb.sec/in.
C_d	coefficient of discharge, dimensionless
C_e	flow gain coefficient; in^2/sec.
C_h	hydro-mechanical stiffness; lb/in.
C_l	laminar leakage coefficient; $in^5/lb.sec$.
C_m	damping coefficient in the stylus; lb.in.sec
C_m^*	$C_m\omega_n^2/P_s\hat{Q}$; non-dimensional friction in the stylus
C_o	hydraulic stiffness; lb/in.
C_p	flow-pressure coefficient; $in^5/lb.sec$.
C_s	viscous damping coefficient in the spool; lb.sec/in.
ds	the elemental displacement of the stylus along the profile; in.
dt	the elemental increment of the independent variable, time; sec.
dx	the elemental displacement of the stylus along the copying axis; in.
e	the error between the input and the output; in.

F	force transmitted to valve from the stylus; lb.
$F_{1,2}$	coefficients as defined in equation (A.13); lb. and lb.sec/in.
F_d	total dynamic cutting force; lb.
F_f	steady state flow force on the valve; lb.
F_k	initial spring force of the spring between the spool and the slide; lb.
F_{km}	initial spring force of the contact spring; lb.
F_s	dynamic cutting force as defined by equation (2.11); lb.
F_w	magnitude of dry friction in the copying slide; lb.
f	feed of machine tool slide; in/rev.
F^*	F/P_sA; dimensionless force
I_m	mass moment of inertia of the stylus; lb.in.sec^2.
I_m^*	$I_m\omega_n^3/P_s\hat{Q}$; non-dimensional mass moment of inertia of stylus
i_o	oblique angle of the cutting tool; deg.
j	$\sqrt{-1}$
K	$(I_m^*\omega^{*2} + \alpha_s\omega^{*2}u^{*2}a^{*2}) / a^*u^*$; a constant
K_m	stiffness of the contact spring; lb/in.
K_o	material constant
$K_{p,q,r}$	coefficients as defined in equation (A.8)
K_s	stiffness of the spring between the control valve and the copying slide; lb/in.
K_1	$C_m^*\omega^* / a^*u^*$; a constant
k	$0.43\ W\ u\ /\ A$; dimensionless
k_g	a/b, kinematic gain; dimensionless

$\hat{L}$	$\hat{Q} / A\omega_n$; reference length; in.
M	mass of the copying slide; lb.sec^2 / in.
m_s	mass of the spool valve; lb.sec^2 / in.
n	workpiece rotational speed; rev/sec.
$P_{1,2}$	pressures in the cylinder chambers; lb/in^2.
$P^*_{1,2}$	$P_{1,2} / P_s$; dimensionless
$P_{e,s}$	constant exhaust and supply pressures; lb/in^2.
P^*_e	P_e/P_s; dimensionless
$Q_{1,2}$	flow through the valve into cylinder chambers; in^3 / sec.
$Q^*_{1,2}$	$Q_{1,2} / \hat{Q}$; dimensionless
r_t	the ratio of the undeformed to the deformed chip thickness; dimensionless
sgn	signum function
S_n	shear stress of material at zero normal stress; lb/in^2.
S_o	feed of the copying slide; in/rev.
S_s	shear stress of material; lb/in^2.
t	time; sec.
u	reference length; in.
u*	u / $\hat{L}$; dimensionless
V	total volume of oil compressed in the servo; in^3.
v	velocity of the machine-tool slide; in/sec.
W	area gradient of the valve; in^2/in.
x	template ordinates along the axis of copying system; in.
x_o	displacement of the stylus as in Figure 18; in.

x^*, x_o^*	x/u; x_o/u; dimensionless
y	absolute displacement of the valve; in.
y^*	y/u; dimensionless
z	output response of the copying system along its axis; in.
z^*	z/u; dimensionless
α	$M\hat{Q}\omega_n / P_s A^2$; non-dimensional inertial parameter of the copying slide
α_o	normal rake angle of cutting tool; deg.
α_s	$m_s\hat{Q}\omega_n / P_s A^2$; non-dimensional inertial parameter of the valve
β	B/P_s; non-dimensional Bulkmodulus parameter
β_o	normal friction angle of cutting tool; deg.
β_t	time scale factor
γ	angle between the power cylinder and the workpiece axis; deg.
Δ_d	total error zone in workpiece diameter; in.
Δ_e	total error zone in copying; in.
ε	nondimensional ratio of the magnitude of the fluctuating cutting force to the mean value
η_o	chip flow angle; deg.
θ	angular displacement of the stylus; radians
λ_k, λ_{km}	$F_k / P_s A$, $F_{km} / P_s A$; non-dimensional initial spring force parameter
μ_{km}	$K_m\hat{Q} / P_s A^2\omega_n$; non-dimensional spring stiffness factor
μ_s	$K_s\hat{Q} / P_s A^2\omega_n$; non-dimensional spring stiffness factor
ν	$C\hat{Q} / P_s A^2$; non-dimensional cylinder friction factor

ν_c	$F_2\hat{Q} / P_sA^2$; non-dimensional cutting force friction factor
ν_s	$C_s\hat{Q} / P_sA^2$; non-dimensional valve friction factor
ρ	mass density of the fluid; $lb.sec^2/in^4$.
σ	F_w / P_sA ; non-dimensional dry friction parameter
σ_c	F_1 / P_sA ; non-dimensional cutting force parameter
ΣP	the total load on the copying slide; lb.
τ	$\hat{\omega}t$; dimensionless time
τ_v	velocity time constant; sec.
ϕ	$C_l P_s / \hat{Q}$; non-dimensional leakage parameter
ϕ_o	normal shear angle of cutting tool; deg.
ψ	side cutting edge angle for cutting tool; deg.
ω_f	frequency of cutting force; radians/sec.
ω_n	$[4BA^2/MV]^{\frac{1}{2}}$; natural frequency of the oil column and mass; radians/sec.
$\hat{\omega}$	reference frequency; radians/sec.
ω^*	$\hat{\omega}/\omega_n$; dimensionless
ω_f^*	$\omega_f/\hat{\omega}$; dimensionless

C H A P T E R I

INTRODUCTION

1.1 Background

Positioning systems such as copying systems have been widely used in machining operations to produce identical parts. It has become an important means of automation of profile-products manufacture as it enables a considerable increase of productivity. Two- and three-dimensional copying systems have found wide application in machine-tool industries. Two-dimensional systems are used in lathes and those of two- and three-dimensional systems on milling or grinding machines. Every operation of copying starts from the source of information which describes the shape of the workpiece to be produced. This source of information may be stored in the form of templates and/or cams, which are essentially two-dimensional storage elements. Punched or magnetic tapes can also be used as data storage elements in discrete forms. Depending on the type of storage elements and on the type of input, copying systems are generally classified as:

1) Hydro-Mechanical or Hydraulic Copying Systems,
2) Electro-Hydraulic Copying Systems,
3) Numerically Controlled Copying Systems.

In all these different types of copying system, the input signal is hydraulically amplified (force amplification) which controls the movement of the cutting tool across the work in the case of a lathe and the movement of the worktable in the case of a milling machine. Figures 1 and 2 show the schematic layouts of two-dimensional hydraulic copying systems used in a lathe and in a milling machine. The input in these types of copy system is stored in the form of a template and a stylus which follows the template actuates the hydraulic power source to control the motion of the cutting tool or the worktable. A detailed description and the operating principle of the different kinds of two-dimensional hydraulic copying systems used in lathes are outlined in Chapter II.

The main criterion in copying systems is that the direction of the speed of advance of the cutting tool has to coincide at every point of the profile with the tangent at that precise moment. Hence, two- and three-dimensional systems may be used to control the motion of the cutting tool in the individual coordinates so that the absolute speed of the cutting tool along the profile will coincide with the value of the tangent at any given moment. Figure 3 shows a schematic layout of a two-dimensional hydraulic copying system in which the longitudinal and the vertical movements are controlled by separate control valve-cylinder units which have a common supply from a single pump. For machining 360° profiles, a three-dimensional copying system

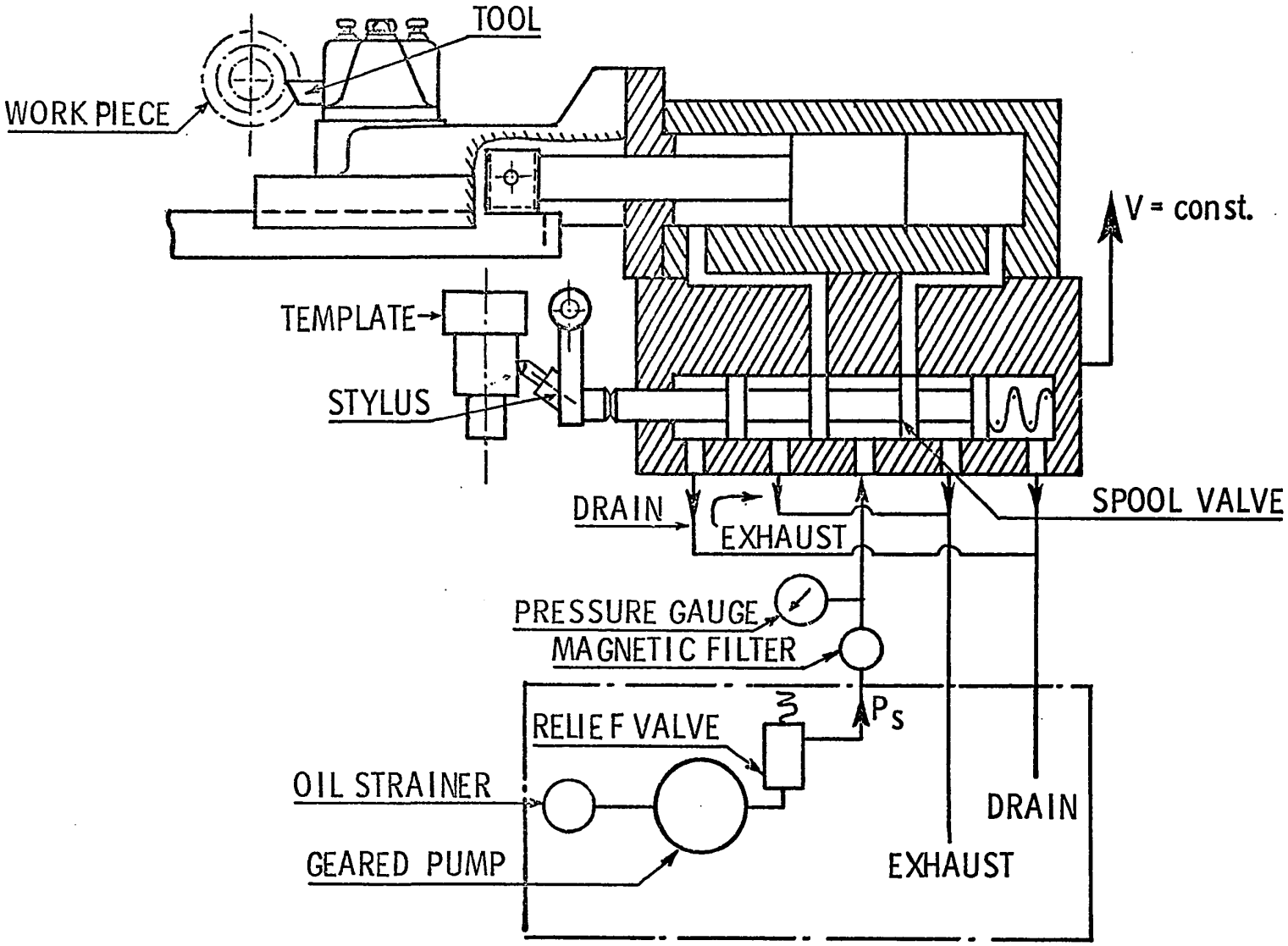

FIGURE 1 TWO-DIMENSIONAL HYDRAULIC COPYING SYSTEM FOR A LATHE

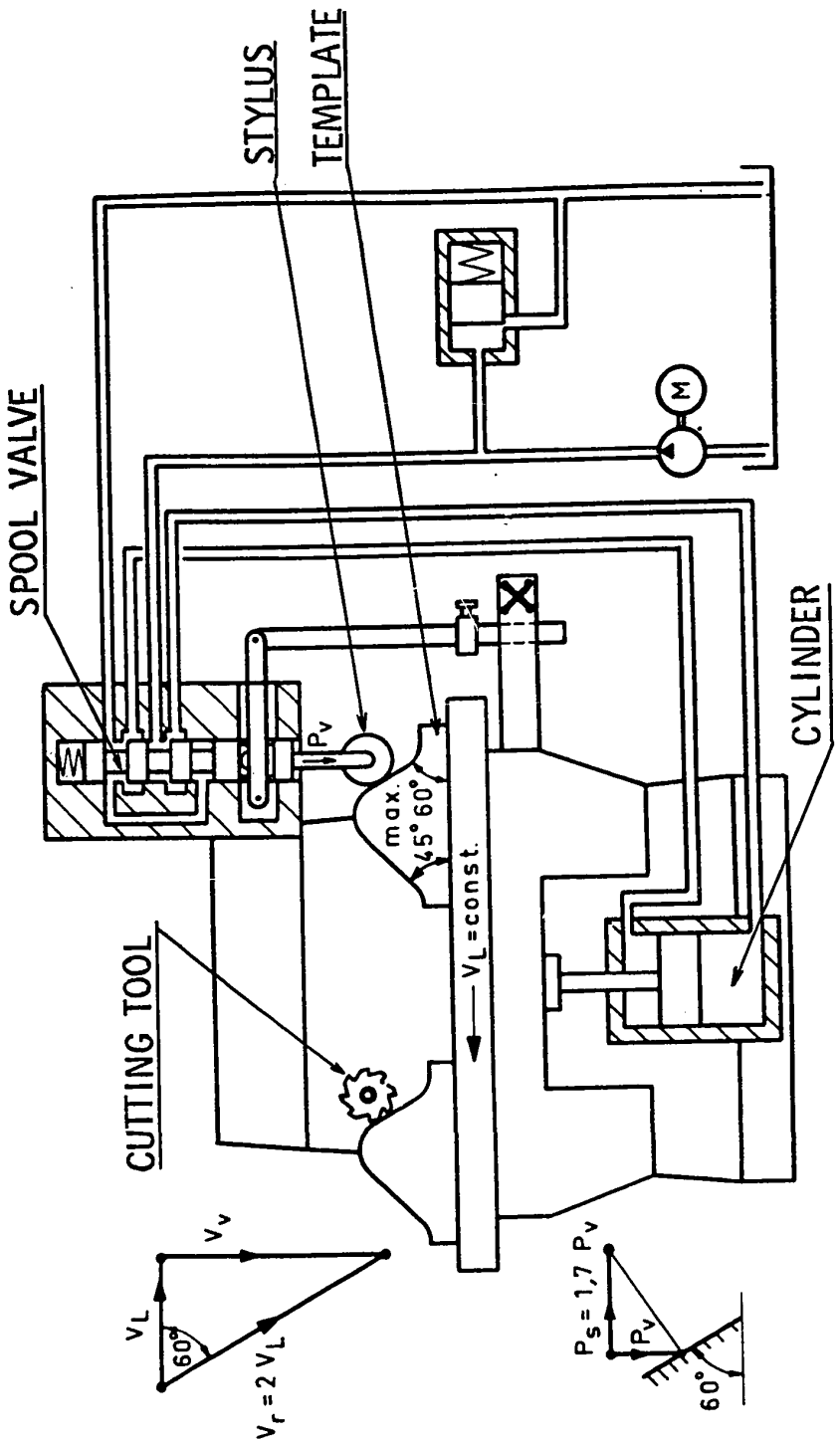

FIGURE 2 TWO-DIMENSIONAL HYDRAULIC COPYING SYSTEM IN A MILLING MACHINE

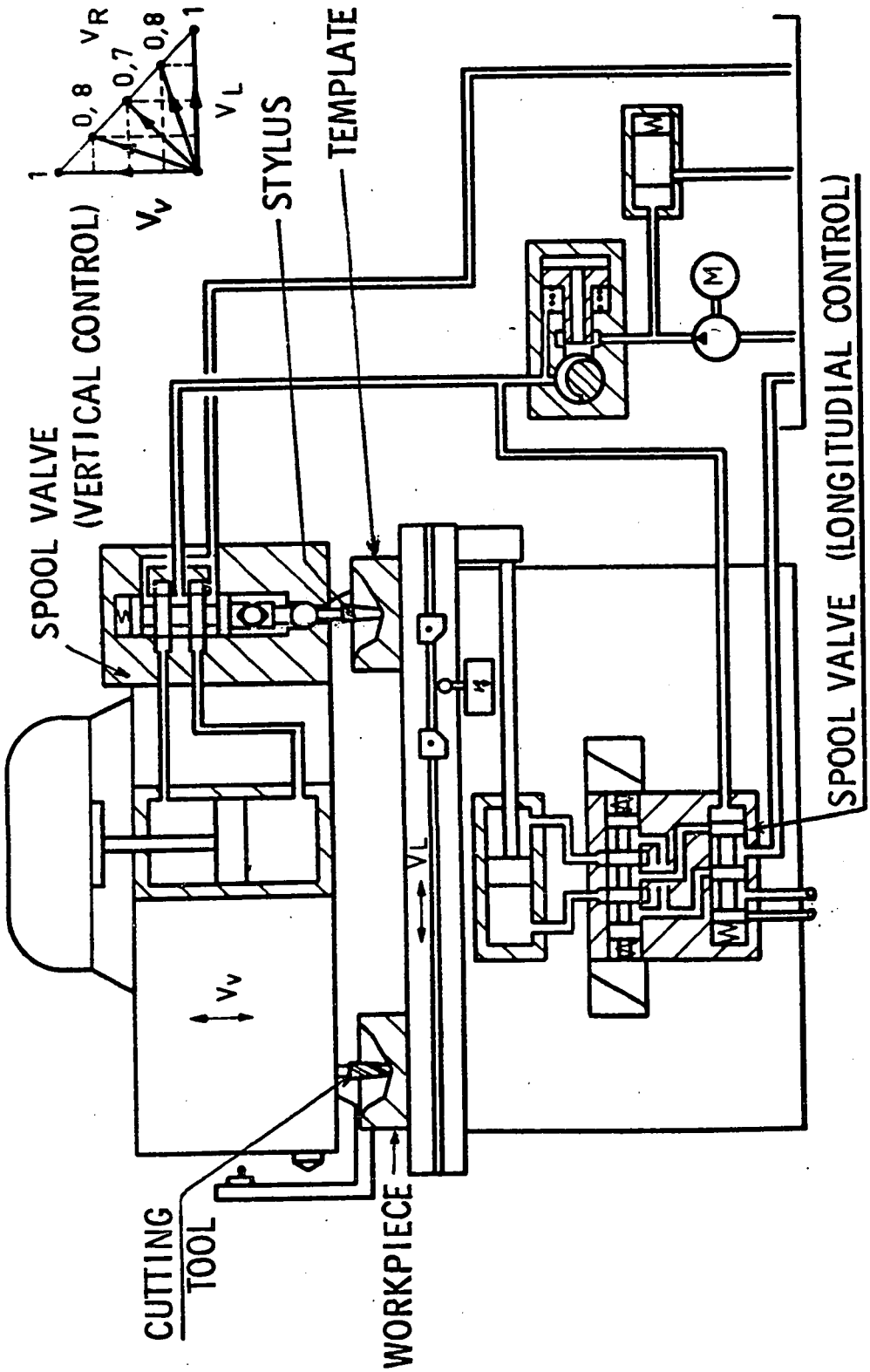

FIGURE 3 TWO-DIMENSIONAL HYDRAULIC COPYING SYSTEM WITH AUTOMATIC FEED CONTROL

may be utilized. A sectional layout of a three-dimensional hydraulic copying system for milling is shown in Figure 4. In this system, three separate control valve-cylinder units are used to control the motion of the cutting tool for milling a 360^{0} profile.

An electro-hydraulic copying system utilizes an electro-hydraulic servovalve which actuates the hydraulic power source to control the motion of the cutting tool. The basic principle of operation of this type of copying system is exactly the same as in a hydro-mechanical copying system except that the displacement of the stylus is being converted to an electric signal in an electronic transducer and further amplified to drive the spool valve through a solenoid. A cross-sectional view of an electro-hydraulic servovalve that is normally used in this type of copying system is shown in Figure 5.

Copying with information derived from punched or magnetic tape is denoted as numerical controls. Every movement along the coordinates is subject to a comparison between nominal and actual values, in which the nominal value of the position is taken from the stored information and the actual value of the position is obtained from the measuring system. Figure 6 shows a schematic diagram of a numerically controlled copying system. Essentially, it consists of a tape reader which reads the punched tape and sends the signal to a computer which produces the command signals. These command pulses are sent to a counter, which

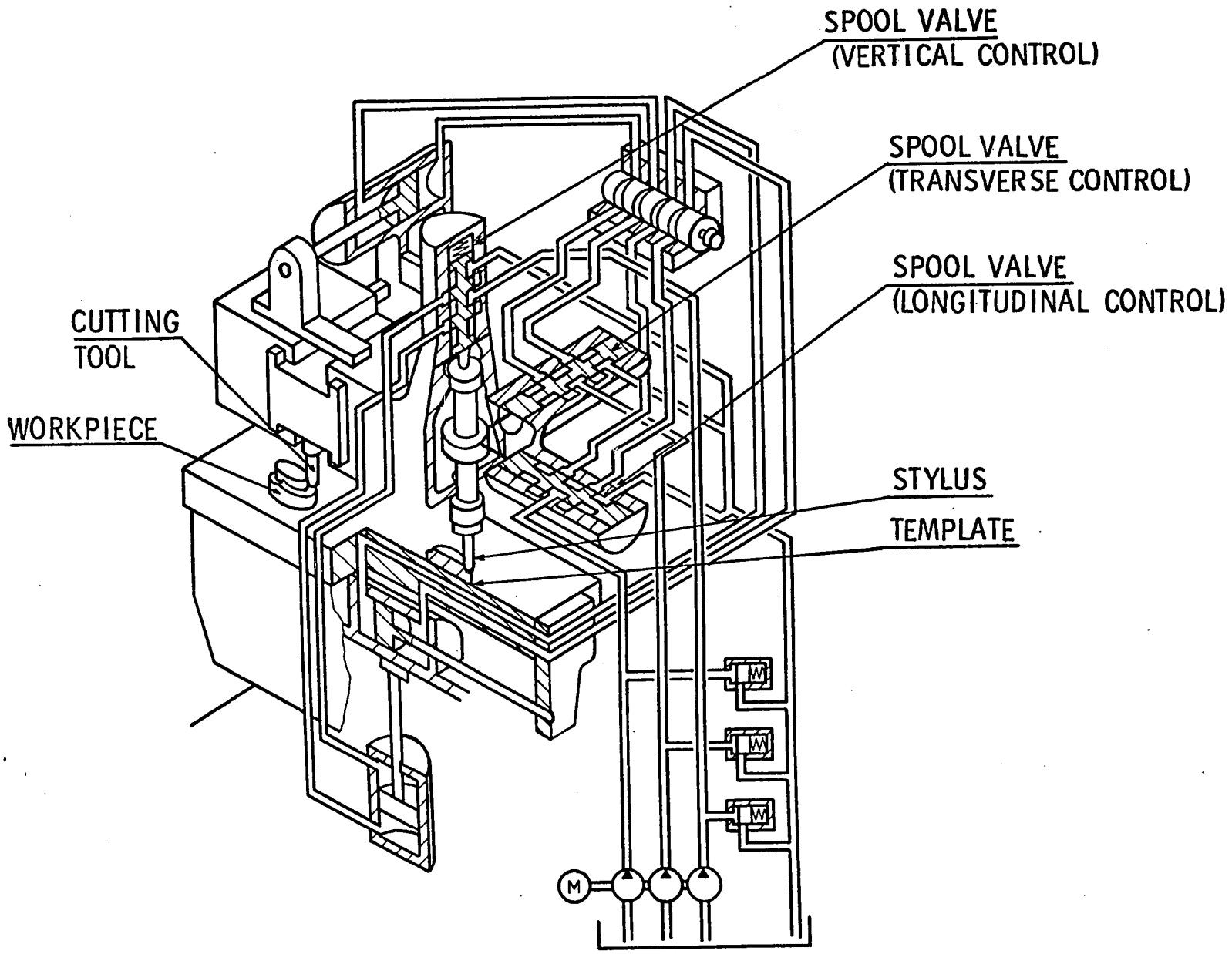

FIGURE 4 THREE-DIMENSIONAL HYDRAULIC COPYING SYSTEM IN A MILLING MACHINE

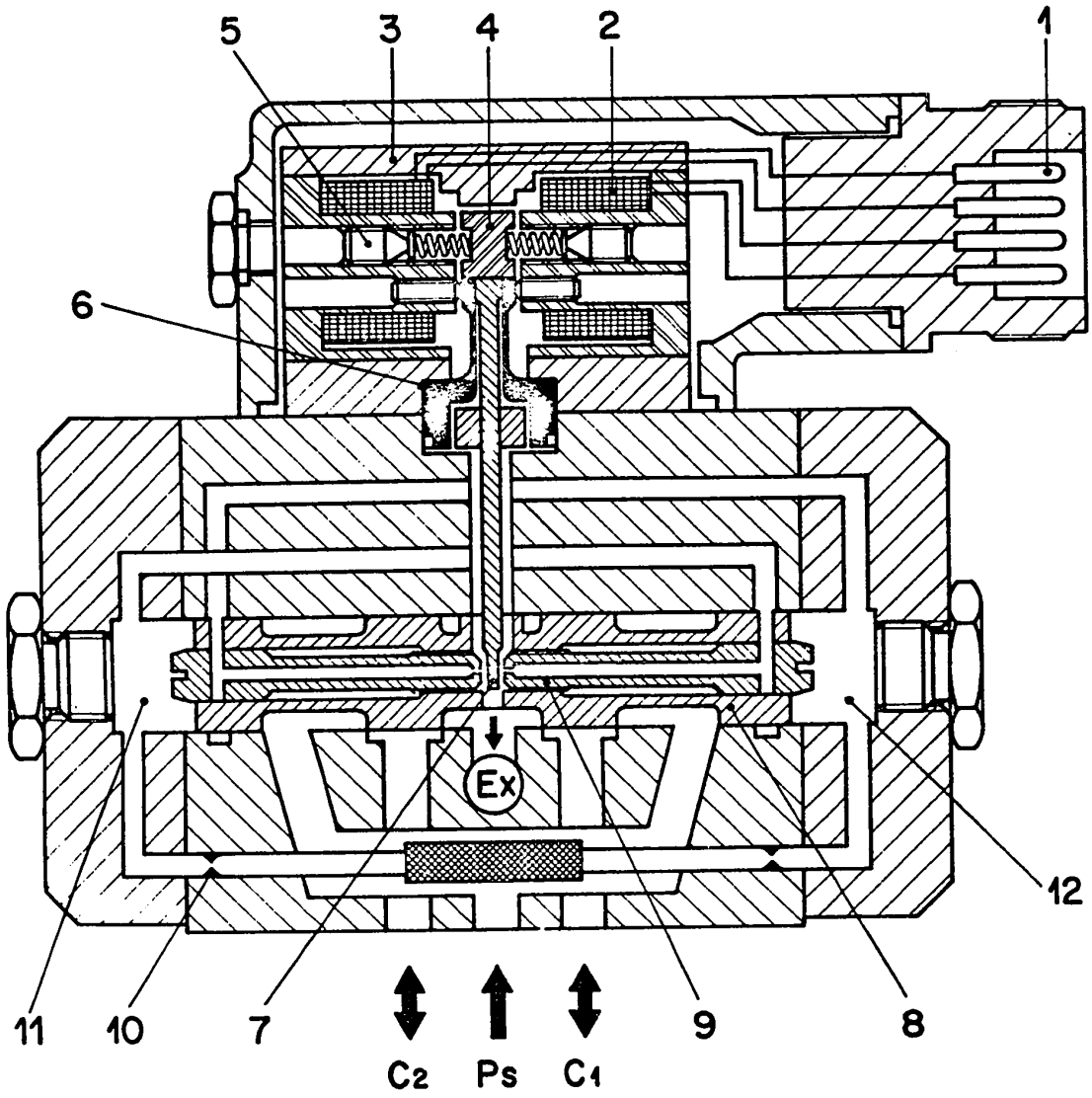

1 ELECTRICAL CONNECTION
2 COILS
3 PERMANENT MAGNET
4 ARMATURE
5 MECHANICAL POSITIONER
6 FLEXIBLE TUBE
7 BAFFLE PLATE
8 CONTROL PISTON
9 NOZZLE
10 THROTTLE
11 AND 12 INTERMEDIATE CHAMBERS

FIGURE 5 SECTIONAL VIEW OF AN ELECTRO-HYDRAULIC SERVOVALVE

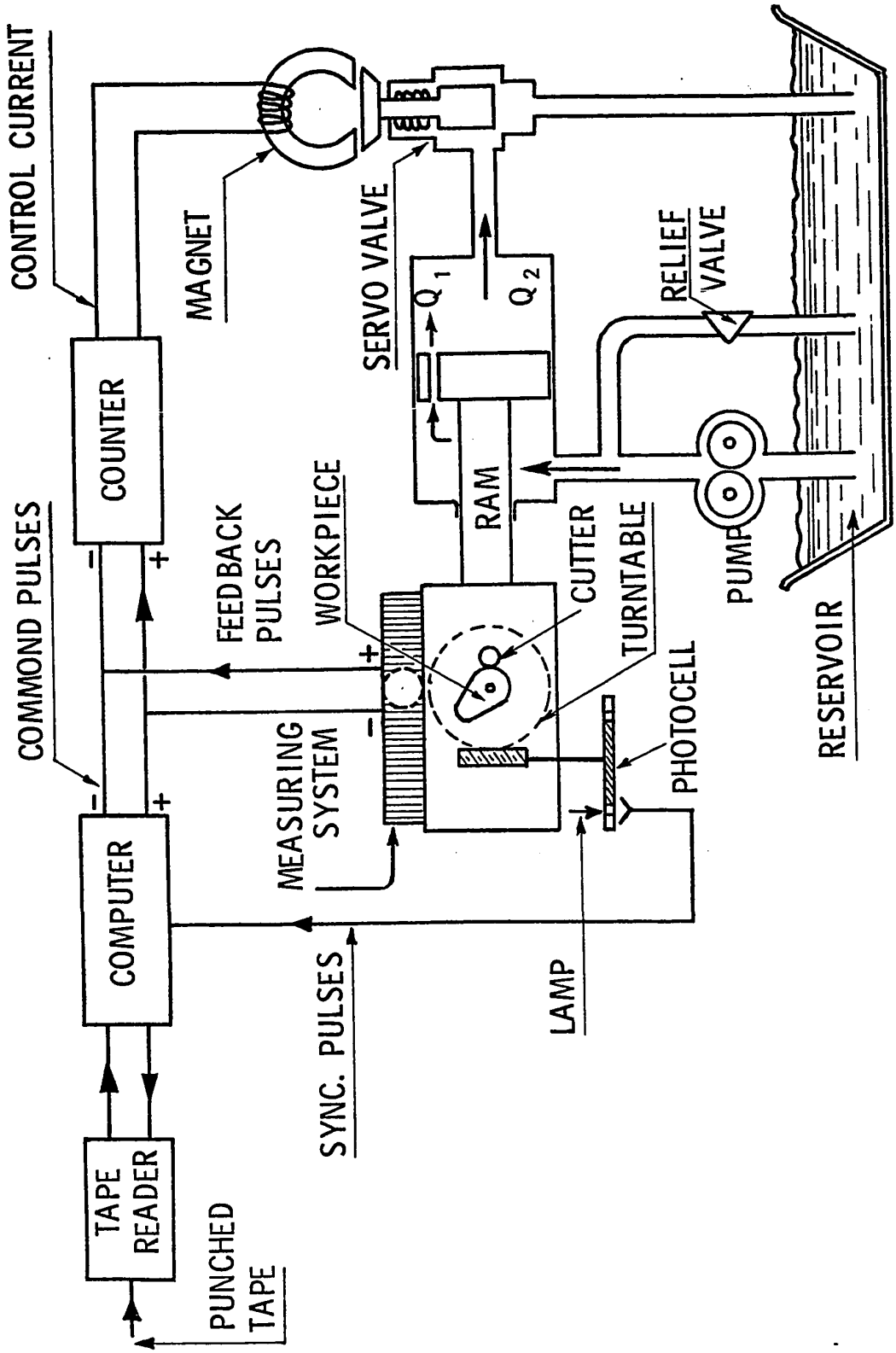

FIGURE 6 A SCHEMATIC LAYOUT OF A NUMERICALLY CONTROLLED COPYING SYSTEM

produces a control current of such magnitude that the hydraulic servomotor will move to either side depending on the polarity of the command pulses and actuates flow into the cylinder to control the movement of the worktable. Feedback pulses which correspond to the actual motion are also fed back to the counter and hence any deviation of the counter from its central position corresponds to the difference between the command and the feedback pulses. Syncronizing pulses are also provided to correct any error in the required velocity of the slide.

To acquire general information about the available commercial copying systems in North America and Europe, a survey was carried out and found that 87% of the manufacturers produce hydro-mechanical copying systems, 31% produce electro-hydraulic copying systems and 16% produce numerically controlled copying systems. The names of the manufacturers and the types of copying system they produce are given in Appendix I.

Dynamic accuracy and stability of commercial copying devices prove to be the major requirements which characterize the quality of the copying process. Any hydraulic copying system, regardless of its type and the number of dimensions, the basic copying unit consists of: a) a source of information, b) control valve, and c) power cylinder. In this

investigation the dynamic accuracy and stability are considered for such a unit. The source of information which constitutes the kinematic input of the system is expressed mathematically as a two-dimensional template function transformed in the time domain. Such a method of analysis generalizes the results of this investigation which are applicable to all types of machine-tool hydraulic positioning systems.

1.2 Review of Previous Work

To gain qualitative and quantitative information regarding the dynamic accuracy of copying systems with the simultaneous preservation of their stability, a systematic study of the principles of hydraulic servomechanisms must be carried out. Hydraulic servomechanisms employing a control valve to control the fluid flow to an actuator positioning a load has been the subject of many authors [1-16] during the last twenty years. Harpur [1] analyzed the basic equations of motion by utilizing the classical small perturbation technique. This method permits a linear approach of describing the dynamic behavior of the hydraulic servo system by considering small excursions about an equilibrium position. He showed, among other things, that the symmetrical underlap increases the stability of the follow-up system but the amount of underlap was such that the

leakage would be excessive. Thomasson [2] used Harpur's method to investigate the effect of other parameters when leakage and valve underlap are unacceptable, showing that the structural damping and jack friction are important stabilizing parameters.

Lambert and Davies [3] verified the analysis of Harpur, who also took some account of Coulomb friction in the jack. The use of analog computer in investigating hydraulic servos has been demonstrated by Glaze [4], who showed that in a real system Coulomb friction could not be ignored, and Parnaby [5], who took account of both static and Coulomb friction in a particular type of servo.

Royle [6] showed that it was necessary to include the inherent non-linear effects of hydraulic servos and used an analog simulation to investigate the performance of the system. His work indicated that within certian limitations, the non-linear and linear theories could be related and that there was some validity to the small perturbation theory.

Analytical design for time optimum transient response of a hydraulic servomechanism under variably loaded condition was carried out by Davies [7]. His work discussed the design feature of a hydraulic control system whose valve is operated in such a way as to provide time optimum system

response to step inputs of various magnitudes for various inertial loads.

Urata [8] discussed the response of a loaded hydraulic servomechanism under ramp input. Exact solutions with closed form were obtained for the cases where the inertial load does not exist. The response characteristics under inertial load were analyzed using phase plane and perturbation methods. The paper also discusses an analytical method such as the power series method near the initial point for an inertial loaded system since the regular numerical technique fails at the origin because of the singularity at the initial point. The analysis was also extended for a hydraulic servo system with non-symmetrical cylinder.

Stability and step response of hydraulic servo systems with special reference to unsymmetrical oil volumes on the two sides of the power cylinder were studied by Martin [9]. Application of small perturbation theory to the closed loop system showed that the loop gain for the marginal stability is least when oil volumes are equal and that when these volumes are unequal, the response of the system is faster and less oscillatory. A study on the instability of a loaded hydraulic servomechanism was carried out by Ito and others [10]. The investigation was carried out mainly on a system with underlapped valve. The effects of compressibility

of oil on the system instability were examined. The results obtained are summarized as follows:

1. The system is completely stable under the assumption of incompressible oil flow, regardless of constant-pressure or constant-flow operation.
2. Compressibility of oil often makes the system unstable, and sustained oscillation can occur.

McCloy and Martin [11] examined an open loop system with inertial loading for harmonic inputs. By means of digital computer they studied the effects of leakage and viscous damping on the boundary. McCloy [12] analyzed the effect of valve lap on the peak pressure excursions that occur when large inertial loads are subjected to harmonic inputs. Asymmetrical lap and other non-linearities in valve-controlled hydraulic actuators were carried out by Montgomery and Lichtarowicz [13]. In their analysis, they included the non-linear port area-valve displacement characteristics and the supply-exhaust valve lap combinations.

The development of the electro-hydraulic servo-system was initiated by Enyon [14]. The electro-hydraulic servovalve provides the interface between the versatility of low power electrical input signals and the high power output of the hydraulic actuators. The use of electrical signals further facilitates the improvement of the system

performance by the use of feedback loops.

Bell and dePennington [15] discussed the use of acceleration and pressure feedbacks to introduce active damping into the cylinder drive of a lightly damped electro-hydraulic servosystem. Their analysis is based on the optimization of a linear model.

An investigation of a harmonic response of an electro-hydraulic servomechanism was carried out by Davies [16] on an inertially loaded system. He found that such an analysis gives rise to the jump phenomenon characteristics for the non-linear system which indicates that there exists one more possible output state which is not observable because it is unstable. The analysis indicates that these jump resonances arise from the basic fact that the flow through an orifice is proportional to the square root of the pressure difference across the orifice. Since the orifice size in a spool type valve changes with respect to the instantaneous position of the spool, the flow through such orifices is a function of two variables: the size of the orifice and the pressure difference across the orifice. Linear equations therefore can be used only when the pressure difference can be considered constant. Deviation from the linear behavior can be expected when large pressure differences appear across the piston.

Chiappulini [17,18] has extended the study of hydraulic servomechanisms to the stability aspect of a hydraulic copying system. In his work, the flow characteristic equations are linearized, the dry friction in the copying slide was assumed to be zero and the cutting forces were assumed to be a constant. The dry friction in the copying slide always has an effect on both the dynamic accuracy and the stability of the system, and must be considered in studying hydraulic copying systems [19].

It has been found by experimental studies [20,21] that the cutting forces in an actual cutting process are always dynamic in nature. Hence a study of hydraulic copying systems should consider the dynamic cutting forces. This thesis investigates the dynamic accuracy and stability of hydraulic copying systems and explores the effects of various influencing parameters on its accuracy and stability.

1.3 Scope of the Research Work

The scope of this thesis is to investigate the dynamic accuracy and stability of hydraulic copying systems by formulating a mathematical model of a two-dimensional hydraulic copying system, utilizing a four-way, critical centered spool valve and a symmetrical volume power cylinder.

The mathematical model of the copying system is

formulated in Chapter II, by taking into account the following features:

a) Dynamic behavior of the copying slide with the dry friction in its mountings.

b) Dynamic behavior of the control valve and the action of the flow forces.

c) Dynamic behavior of the stylus.

d) Dynamic input that accounts for the cutting force fluctuations and its interaction with the velocity response of the system.

A method to evaluate the time domain model of the kinematic input due to the template configuration and the feed rate of the machine tool slide is also outlined in Chapter II.

In Chapter III, a brief investigation on the stability of hydraulic copying systems using different techniques is presented. The dynamic accuracy of the copying system is investigated in Chapter IV by formulating a dynamic accuracy criterion. This dynamic accuracy criterion is chosen to be a function of the specified manufacturing tolerance of the produced workpiece and is directly evaluated from the system analysis.

In Chapter V, a detailed procedure of non-dimensionalizing the system equations and their simulation on an analog computer are presented. The effects of various influ-

encing parameters on the dynamic accuracy and stability of copying systems are studied using the analog simulation and are presented in Chapter VI.

Finally, in Chapter VII, a conclusion on the dynamic accuracy and stability of hydraulic copying systems is drawn from the simulation and the various techniques adopted. Recommendations for future research in the area of hydraulic copying systems are also outlined.

C H A P T E R II

MATHEMATICAL MODEL OF HYDRAULIC COPYING SYSTEMS

2.1 Description and Operating Principle of Hydraulic Copying Systems

The principle of copying systems is to reproduce the shape of a template profile by controlling the cutting tool through the action of the follower which moves over the surface of the template. In copying systems, the follower controls the source of power for the copying slide, thus controlling the movement of the tool across the work. Two-dimensional hydraulic copying systems that are used on lathes can be divided into two major groups:

1) A copying system which produces contours that can be defined in a single plane and traces from a stationary template.
2) A copying system which requires contouring both around its periphery and along its axis of rotation (i.e., tracing from a rotating master).

A pictorial view of a two-dimensional hydraulic copying system with its control elements is shown in Figure 7. These two-dimensional hydraulic copying systems have been normally classified according to the number of control valve metering edges and according to the symmetry of the power cylinder. Based on this, the hydraulic copying systems can

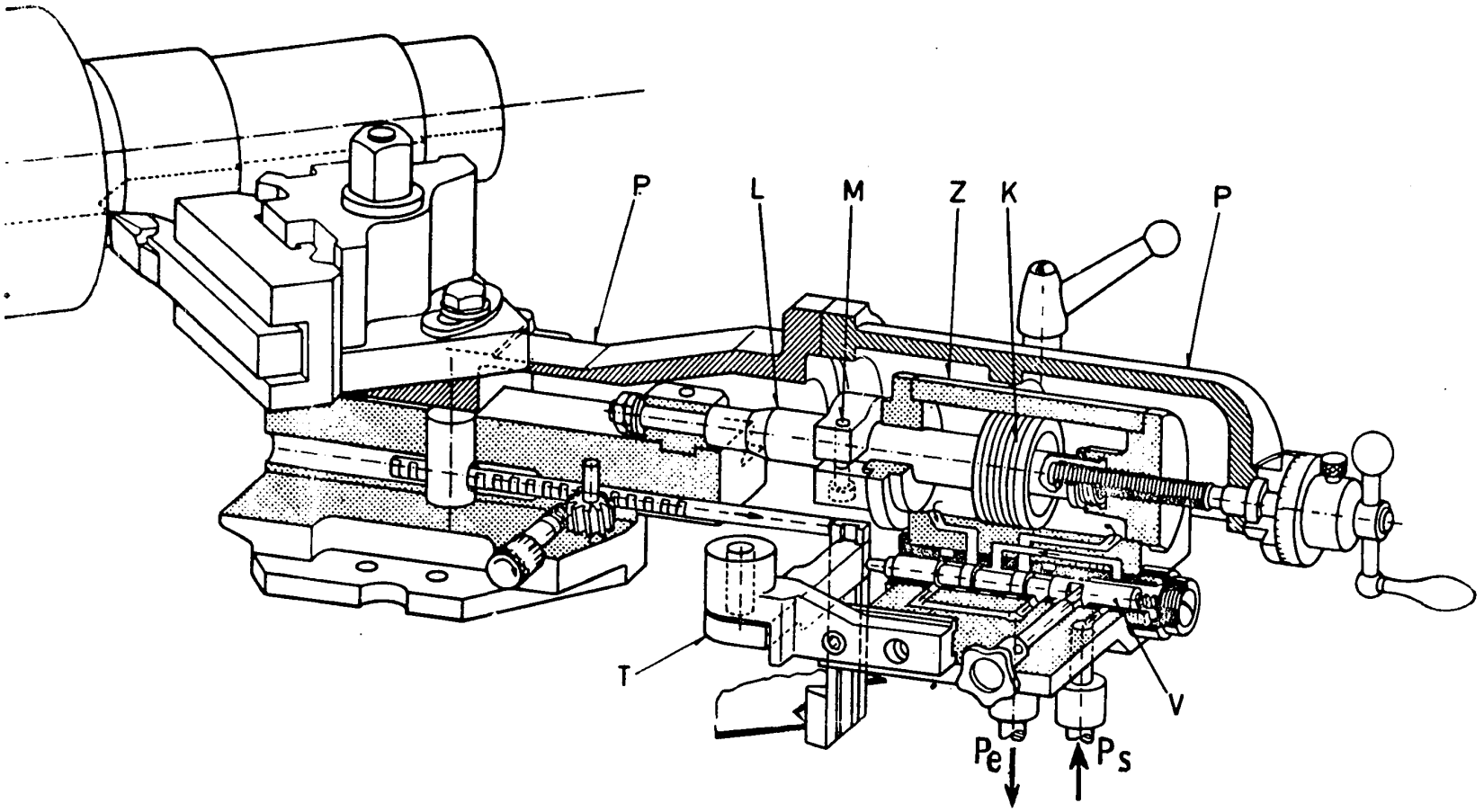

P COPYING SLIDE; L PISTON ROD; M ADJUSTING SCREW; Z CYLINDER;
K PISTON; T TEMPLATE; V SPOOL VALVE.

FIGURE 7 TWO-DIMENSIONAL HYDRAULIC COPYING SYSTEM WITH ITS CONTROL ELEMENTS

be designated as:

(a) Four-edge controlled, symmetrical cylinder copying system.

(b) Two-edge controlled, symmetrical cylinder copying system.

(c) Two-edge controlled, unsymmetrical cylinder copying system.

(d) One-edge controlled, unsymmetrical cylinder copying system.

A schematic diagram of a four-edge controlled, symmetrical cylinder hydraulic copying system is shown in Figure 8. The main component of the hydraulic copying system is a copying slide, consisting of a four-edge controlled, critical-centered spool valve and a symmetrical cylinder with a fixed piston. The copying slide is mounted on an adjustable slide and can move freely on its slideways, due to any pressure difference across the piston. This adjustable slide in turn is mounted on the machine tool slide and moves with a constant feed dictated by the lead screw. A stylus is connected to the spool valve and is mounted as shown in Figure 8. Due to the constant feed of the machine tool slide, the stylus is forced to move and trace the template. The motion of the stylus causes the spool valve to move from its initial position and actuates flow into the cylinder chambers, thus driving the copying slide. Since the cutting tool is rigidly

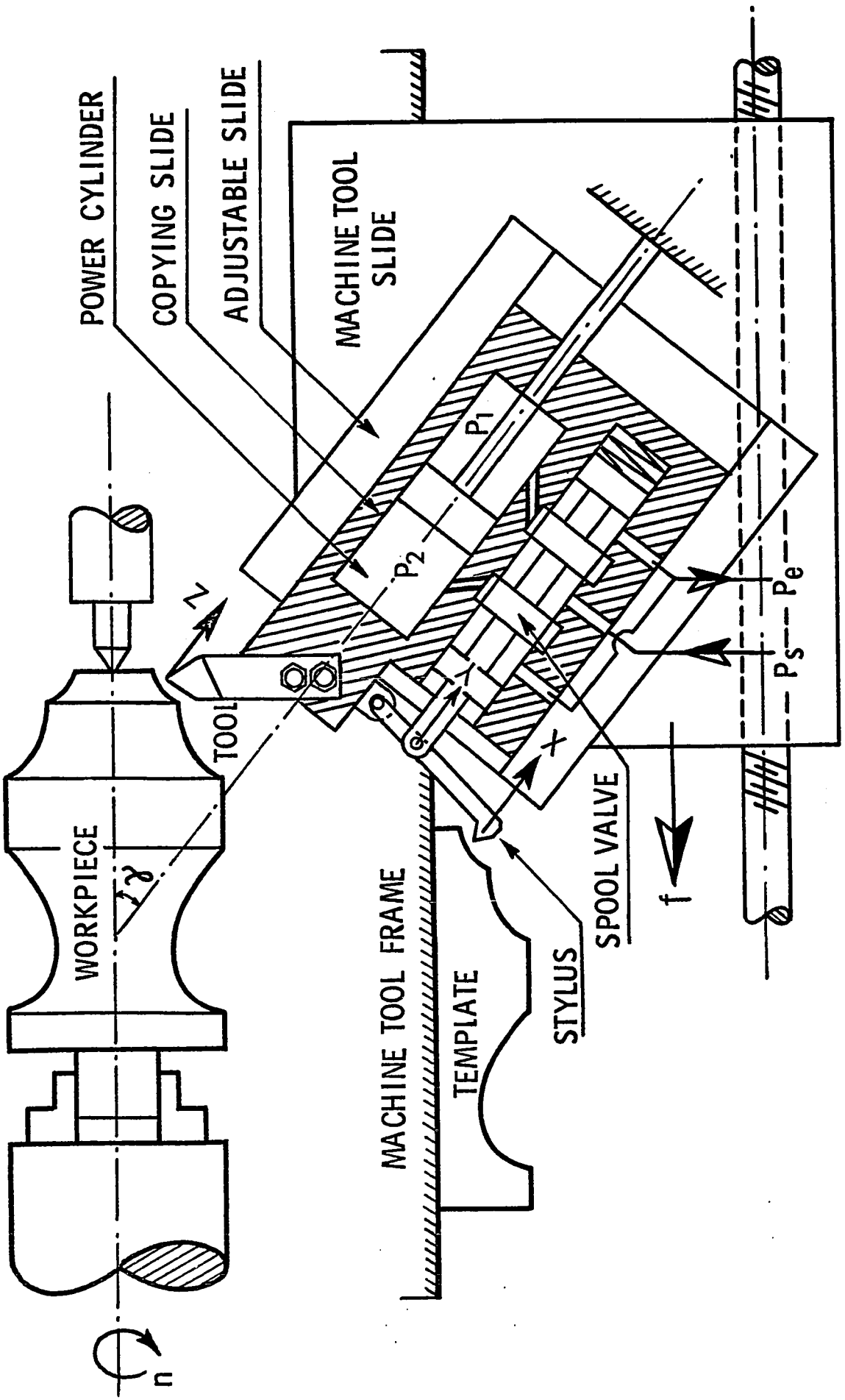

FIGURE 8 FOUR-EDGE CONTROLLED, SYMMETRICAL CYLINDER HYRAULIC COPYING SYSTEM

fixed to the copying slide, it moves along with the copying slide and removes metal from the workpiece according to the template. In practice, the copying slide is always mounted at an angle to the workpiece axis to machine shoulders and other surfaces which lie at right angles to the workpiece axis.

The operating principle of other types of copying systems (types b, c, and d) are exactly the same as in a four-edge controlled system, except for some constructional changes. The hydraulic copying system of type b is shown in Figure 9 and it needs two pumps to supply fluid into the two sides of the symmetrical power cylinder. The two control edges of the spool valve control the pressure in the cylinder chambers by restricting the flow to the exhaust and thus control the movement of the copying slide. Since in this type of copying system two pumps are required, both the initial and operating costs are relatively higher [22].

Figure 10 shows a two-edge controlled, unsymmetrical cylinder copying system of type c. A constant supply pressure P_s is supplied to one of the cylinder chambers and the pressure in the other cylinder chamber is controlled by the control edges. Since an equilibrium of forces has to be maintained when the spool is in the neutral position, the piston rod in this type of system is designed to be thicker, in fact it is designed to be one half of the effective piston

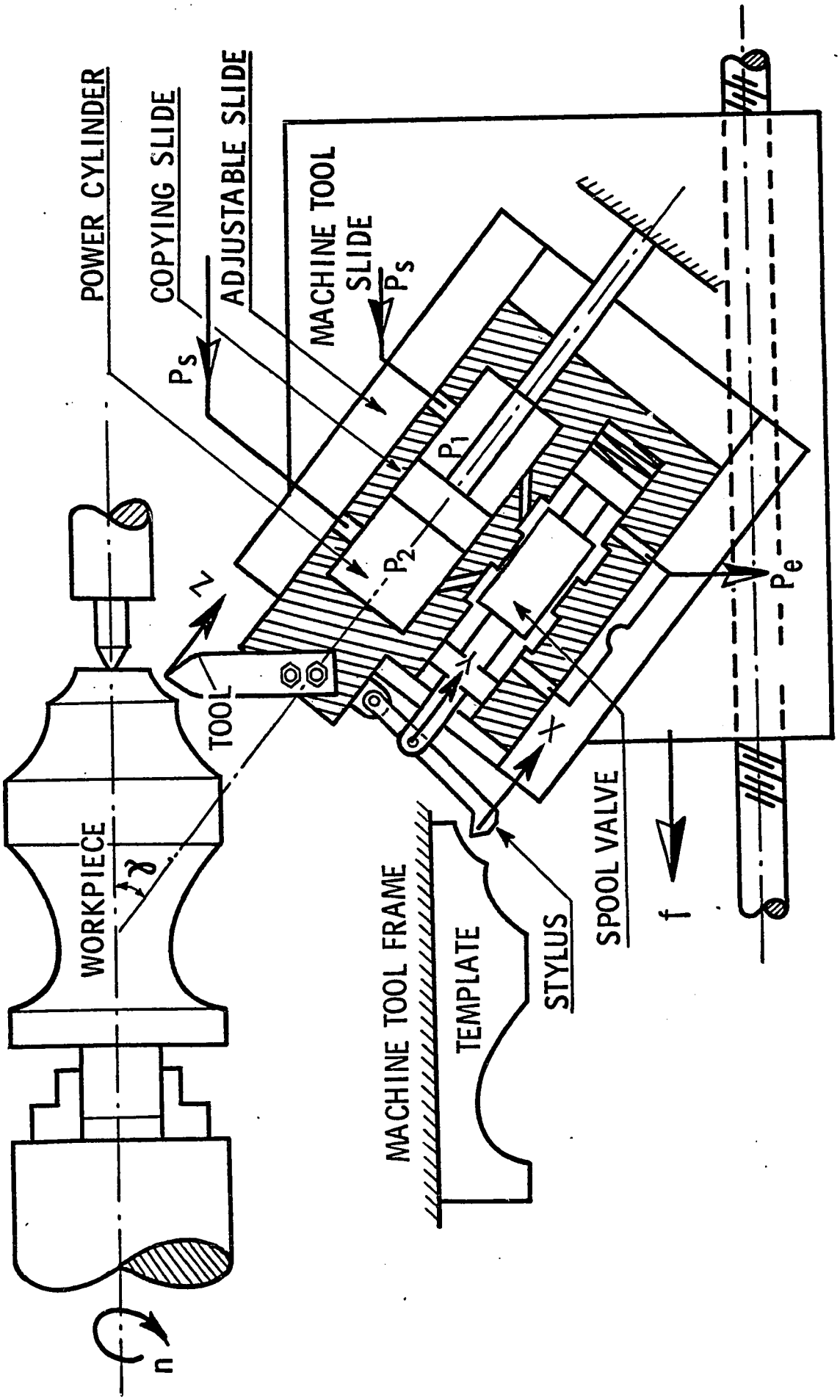

FIGURE 9 TWO-EDGE CONTROLLED, SYMMETRICAL CYLINDER HYDRAULIC COPYING SYSTEM

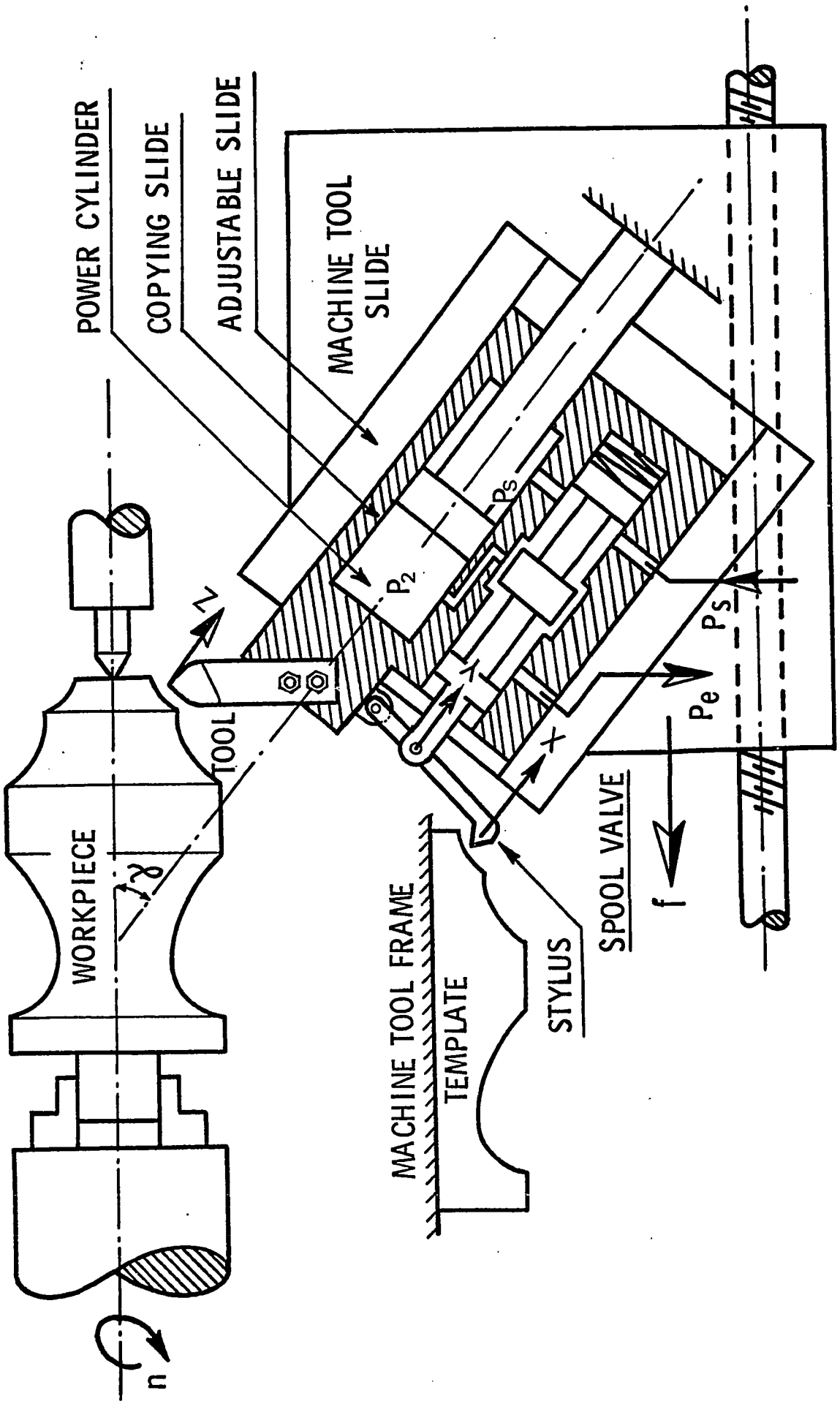

FIGURE 10 TWO-EDGE CONTROLLED, UNSYMMETRICAL CYLINDER HYDRAULIC COPYING SYSTEM

area as shown in Figure 10.

In the case of a one-edge controlled unsymmetrical cylinder copying system (type d), only one of the ports is variable and the other one is fixed. A schematic diagram of this type of system is shown in Figure 11. The piston rod in this system is also designed to be thicker for the same reason as outlined for a two-edge controlled, unsymmetrical cylinder copying system.

2.2 A Comparison of Error in Copying Systems

Hydraulic copying systems are closed loop positional servo systems which receive a positional input x(t) from a template and provides an output position z(t). Such a system can be expressed in the form of a block diagram as shown in Figure 12. The error e, between the intended and the actual displacement of the cutting tool can be considered to be made up of errors due to the velocity and load of the system. Hence, the control error e can be expressed as:

$$e = f(\dot{z}, \Sigma P) \tag{2.1}$$

where $\dot{z}$ is the velocity of the copying slide

ΣP is the total load on the copying slide which is the sum of external, inertial and frictional forces.

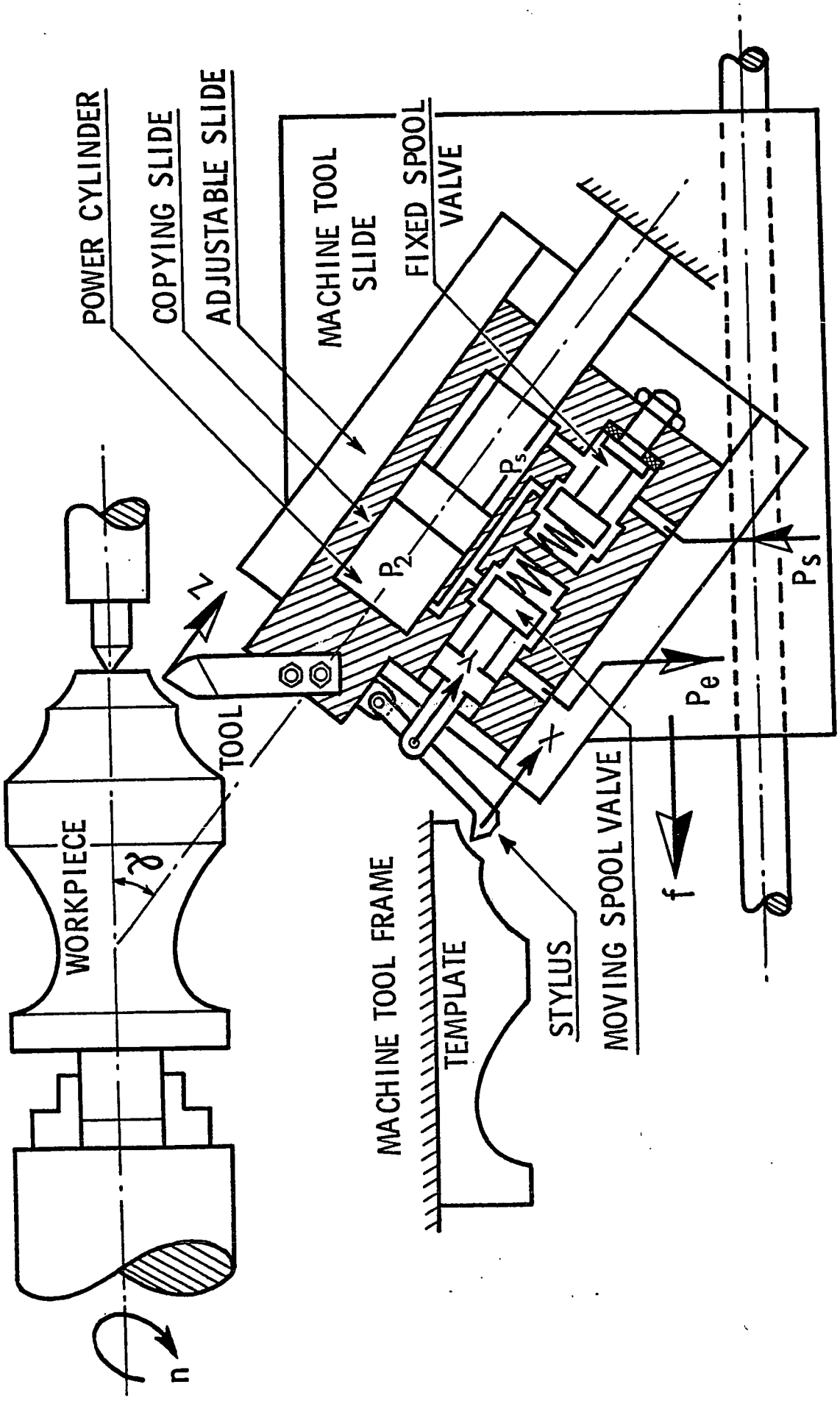

FIGURE 11 ONE-EDGE CONTROLLED, UNSYMMETRICAL CYLINDER HYDRAULIC COPYING SYSTEM

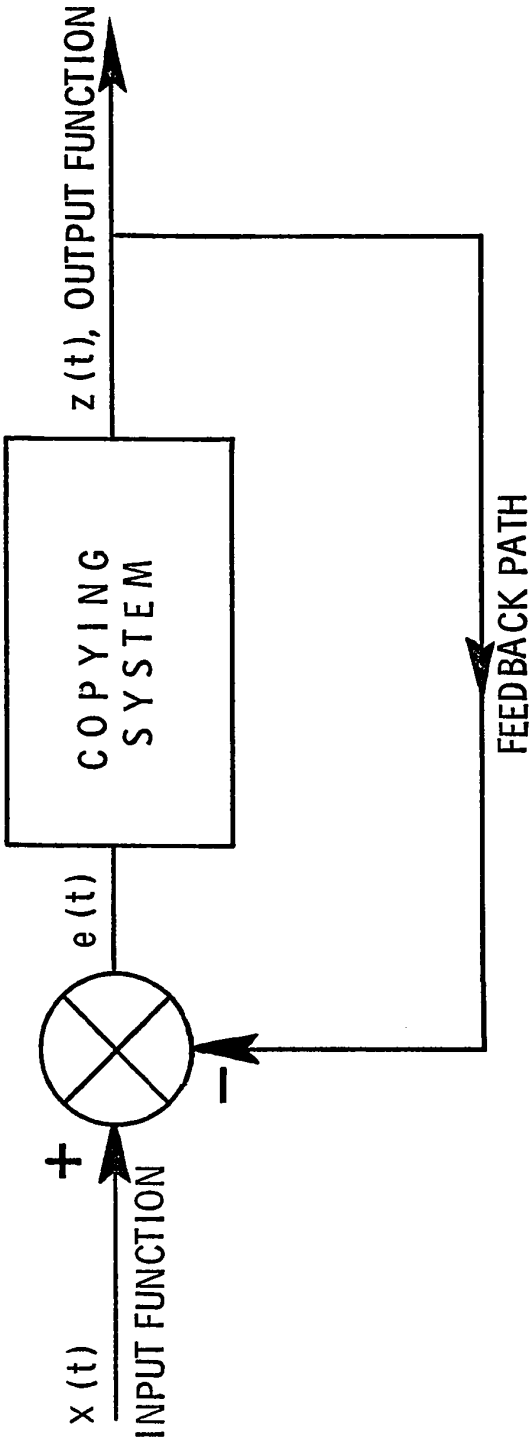

FIGURE 12 BLOCK DIAGRAM OF COPYING SYSTEMS

Considering a small elemental change in the error e, the equation (2.1) becomes:

$$de = \left.\frac{\delta e}{\delta \dot{z}}\right|_{\Sigma P=0} \cdot d\dot{z} + \left.\frac{\delta e}{\delta \Sigma P}\right|_{\dot{z}=0} \cdot d\Sigma P \qquad (2.2)$$

Let τ_v and C_h be the velocity time constant and the hydro-mechanical stiffness of the copying system and are defined as:

$$\tau_v = \left.\frac{\delta e}{\delta \dot{z}}\right|_{\Sigma P=0}$$

$$C_h = \left.\frac{\delta \Sigma P}{\delta z}\right|_{\dot{z}=0}$$

Since $\delta e = -\delta z$

$$C_h = -\left.\frac{\delta \Sigma P}{\delta e}\right|_{\dot{z}=0}$$

Then, rewriting equation (2.2) in terms of τ_v and C_h gives:

$$de = \tau_v \cdot d\dot{z} - \frac{d\Sigma P}{C_h} \qquad (2.3)$$

For a linear system, the equation (2.3) can be written as:

$$e = \tau_v \dot{z} - \frac{\Sigma P}{C_h} \tag{2.4}$$

Thus, the total error expressed by the equation (2.4) may be plotted against the velocity response of the system $\dot{z}$ with the total load ΣP as a parameter and is shown in Figure 13. But since the total load ΣP is the sum of the cutting force, inertial and frictional forces, it is expressed in the absence of viscous friction as:

$$\Sigma P = F_d - F_w \, \mathrm{sgn}(\dot{z}) - M\ddot{z} \tag{2.5}$$

where F_d is the total dynamic cutting force

F_w is the magnitude of dry-friction in the copying slide

If the inertial forces are neglected and the cutting forces are assumed to be constant, then the equations (2.4) and (2.5) are combined to give:

$$e = \tau_v \dot{z} + \frac{F_w}{C_h} \mathrm{sgn}(\dot{z}) - \frac{F_d}{C_h} \tag{2.6}$$

Thus the total control error is made up of three components:

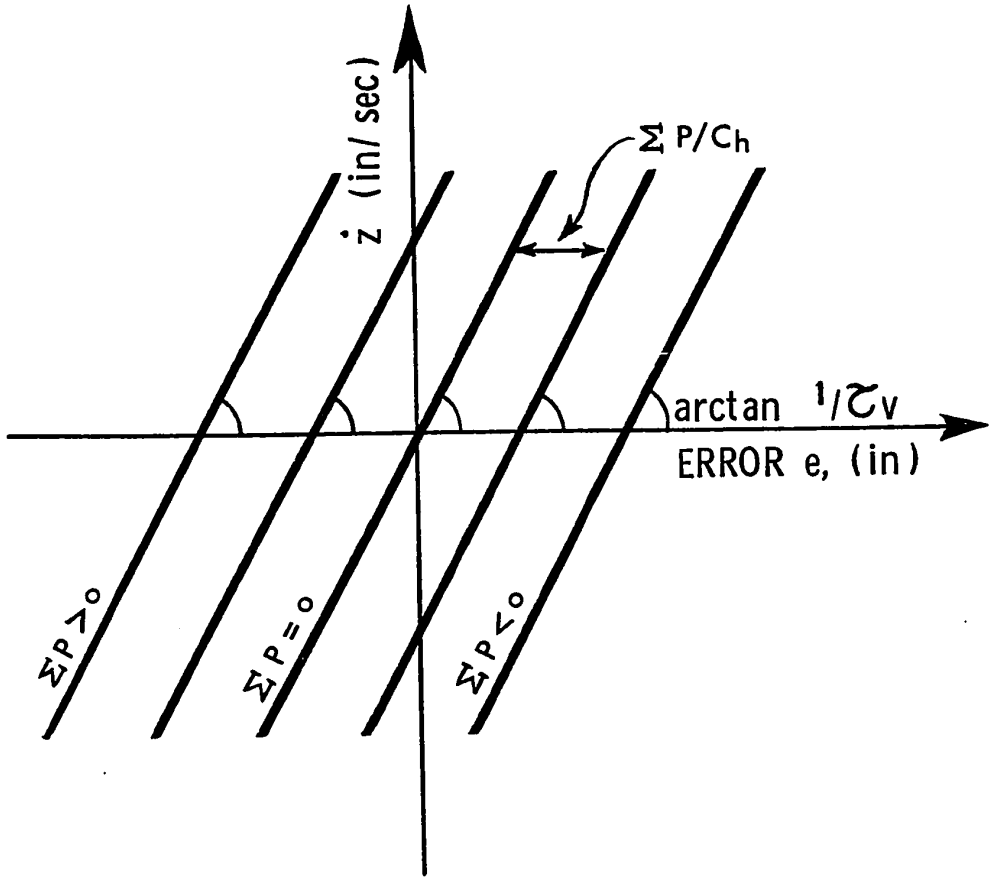

FIGURE 13 CONTROL ERROR e AGAINST VELOCITY RESPONSE ż

$$\text{a) Dry frictional error} = \frac{F_w}{C_h}$$

$$\text{b) Velocity error} = \tau_v \dot{z} \qquad (2.7)$$

$$\text{c) Load error} = \frac{F_d}{C_h}$$

Figure 14 shows the relationship between the total control error e and the velocity response $\dot{z}$ as described by equation (2.6). It can be seen from Figure 14 that for a small value of control error e in copying, the velocity-time constant τ_v should be minimized and the hydro-mechanical stiffness C_h must be maximized. Viersma [23] has shown that under quasi-steady state condition, the hydro-mechanical stiffness C_h for a two-edge controlled servo system is one half of the value for that of a four-edge controlled system and twice that of a single edge controlled servo system. Hence, it can be concluded that a four-edge controlled copying system will have the highest accuracy and rigidity among the different types of hydraulic copying systems. Thus, in order to study the dynamic accuracy and stability of hydraulic copying systems, only a four-edge controlled copying system is considered in this thesis.

2.3 Formulation of the Governing System Equations

The governing equations in hydraulic copying systems are characterized by:

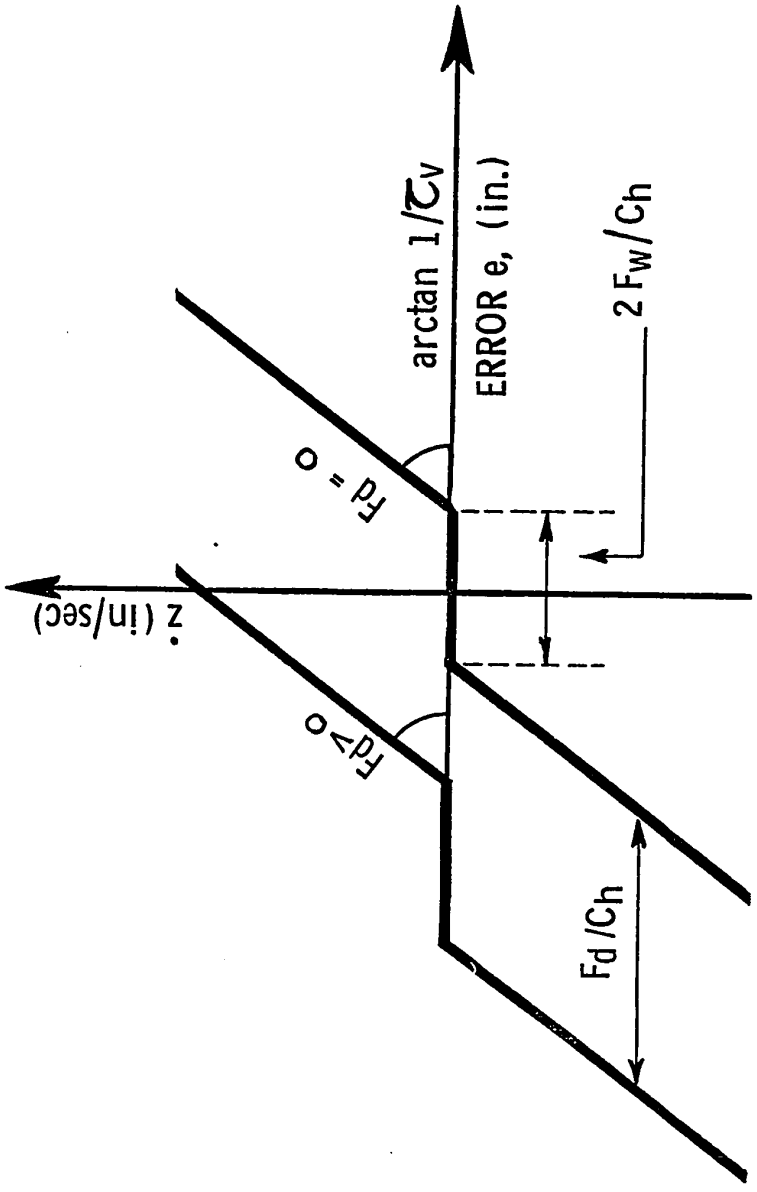

FIGURE 14. EFFECT OF DRY FRICTION ON THE CONTROL ERROR

1) The force balance equations;

2) The flow characteristic equations;

3) The flow continuity equations.

The force balance equations describe the dynamic behavior of the copying slide, the control valve and the stylus. The dependence of the flow rate through a control valve on the position of the valve and the pressure difference across the valve are given by the flow characteristic equations. The flow continuity equations describe the relationship between the quantity of flow into and out of the cylinder chambers.

By considering the dynamic nature of the cutting forces and the presence of dry-friction between the copying slide and its mountings, the dynamic behavior of the copying slide can be characterized by the following equation:

$$M\frac{d^2z}{dt^2} + C\frac{dz}{dt} + K_s(z-y) + F_w\ \mathrm{sgn}\left(\frac{dz}{dt}\right) = A(P_1-P_2) + F_k + F_d \qquad (2.8)$$

where F_w is the dry friction between the copying slide and its mountings

F_d is the dynamic cutting force

In actual cutting process the dynamic cutting forces are random in nature [20] and hence as a first approximation, a sinusoidal signal with frequency ω_f superimposed over a mean value F_s is chosen to represent this dynamic cutting force F_d. Under this assumption the total dynamic cutting force F_d is defined as:

$$F_d = F_s \left[1 + \varepsilon \sin\omega_f t \right] \tag{2.9}$$

where ω_f is the fluctuating frequency of the cutting force

ε is the non-dimensional ratio of the magnitude of the fluctuating force to the mean value

The circular frequency ω_f of the fluctuating force is closely related to the frequency ω_c of the chip formation, which can be calculated using the continuity of volume flow [24] and is given by:

$$\omega_c = 4\pi^2 \, n \, n_c \, r \, r_t \tag{2.10}$$

where n_c is the number of scales per in. of chip

r is the radius of the workpiece

Experimental investigation by Bickel [20] showed that the circular frequency ω_f and the dimensionless quantity ε depend on the feed of the machine tool slide and are plotted

as shown in Figure 15. These curves indicate that ω_f increases as the cutting speed V_1 is increased and as the feed f is decreased.

Using the theory of mechanics of oblique metal cutting [25], the instantaneous mean value of the dynamic cutting force F_s is calculated as in Appendix II and is given by:

$$F_s = [\ F_1 - F_2 \frac{dz}{dt}\ ] \tag{2.11}$$

where

$$F_1 = (b_o f \cos\psi)\ [K_q \cos(\gamma-\psi) - K_r \sin(\gamma-\psi)]$$

$$F_2 = (b_o/n)\ [\cos(\gamma-\psi)][K_q \cos(\gamma-\psi) - K_r \sin(\gamma-\psi)]$$

Combining equations (2.9) and (2.11), the dynamic cutting force F_d can be written as:

$$F_d = [\ F_1 - F_2 \frac{dz}{dt}\ ]\ [\ 1 + \varepsilon \sin\omega_f t\ ] \tag{2.12}$$

It is seen from equation (2.12) that the dynamic cutting force F_d depends on the velocity response of the system and it has an effect equivalent to that of a viscous

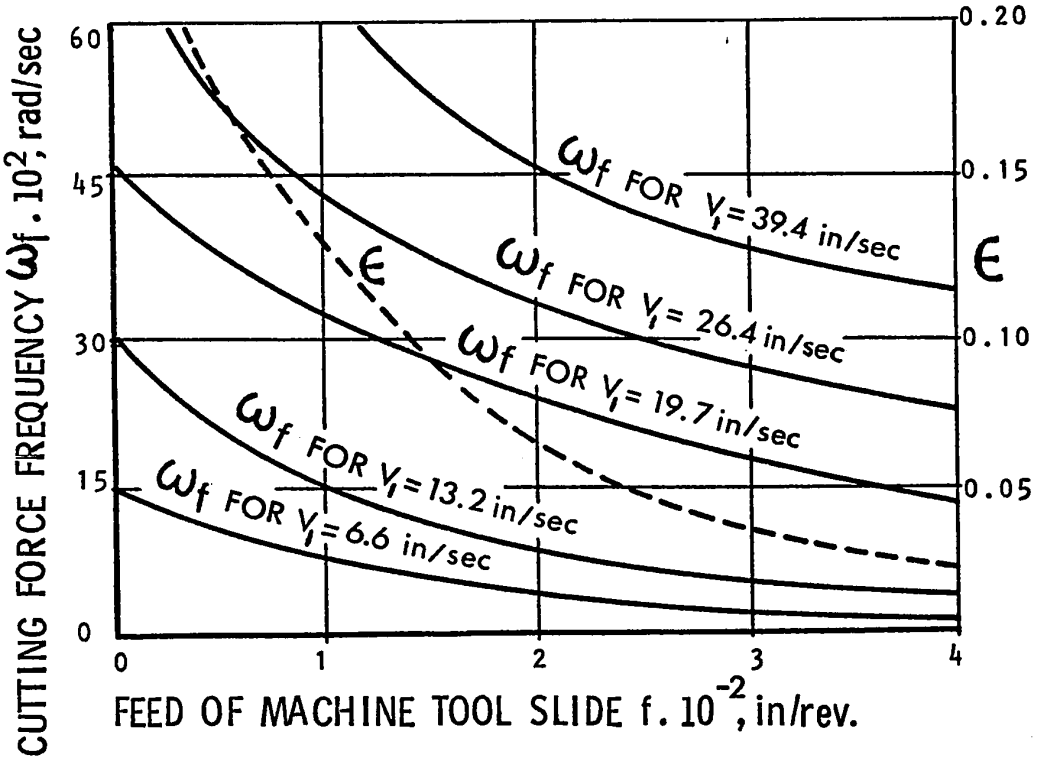

FIGURE 15 EFFECT OF FEED ON ω_f AND ϵ FOR STEEL CK60

friction in the system. Thus the dynamic cutting force introduces an additional damping when the copying system is under operation.

The equation governing the dynamic behavior of the control valve can be written from an equivalent spring, mass and damper system shown in Figure 16 and is given by:

$$m_s \frac{d^2y}{dt^2} + C_s\left(\frac{dy}{dt} - \frac{dz}{dt}\right) + K_s(y-z) + F_k + F_f = F \qquad (2.13)$$

This equation takes into account the flow forces acting on the control valve. These flow forces are due to the fluid momentum transfer in the valves and always have two component forces, axial and lateral. The lateral forces are balanced by providing symmetrical ports on the spool lands just opposite to the orifice edges in the spools. But the axial force is made up of transient and steady state forces. The transient flow force behaves like a viscous damping in the valves. By assuming matched and symmetrical valving orifices and neglecting the pressure derivatives, the damping coefficient can be calculated as:

$$C_s = (L_2-L_1)\ C_d\ W\ [\rho\{(P_s-P_e) - (P_1-P_2)\}]^{\frac{1}{2}} \qquad (2.14)$$

where L_1 and L_2 are the damping lengths shown schematically in Figure 17.

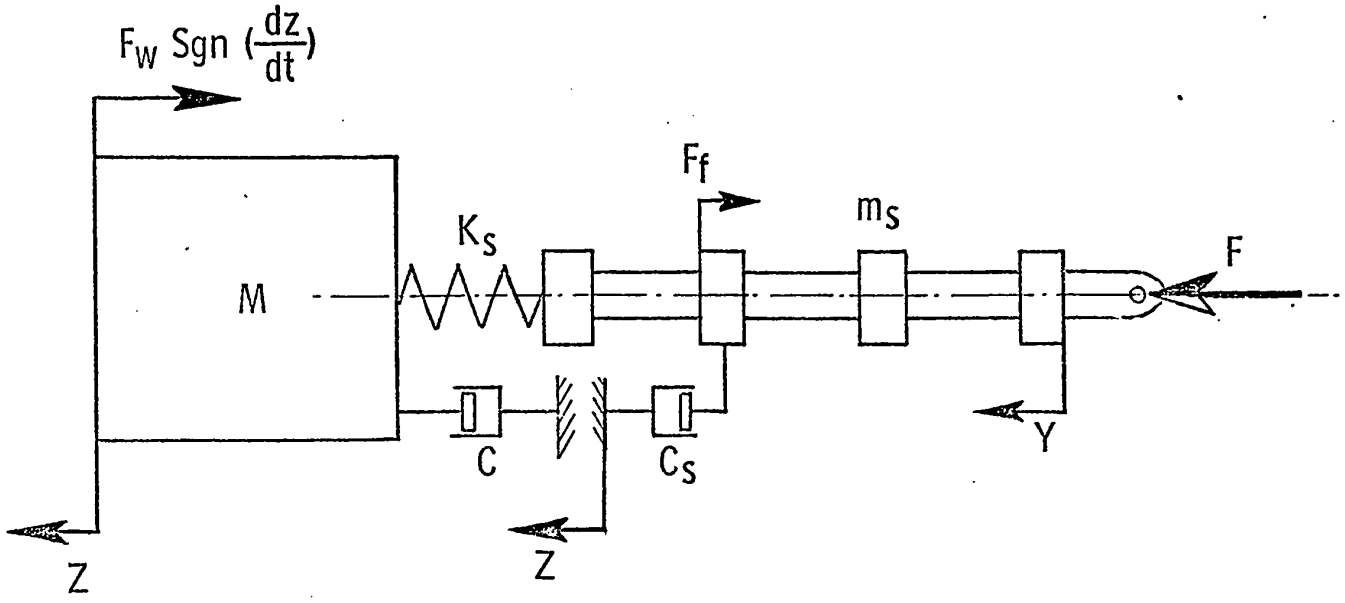

FIGURE 16 AN EQUIVALENT SPRING, MASS AND DAMPER SYSTEM FOR THE COPYING SYSTEM

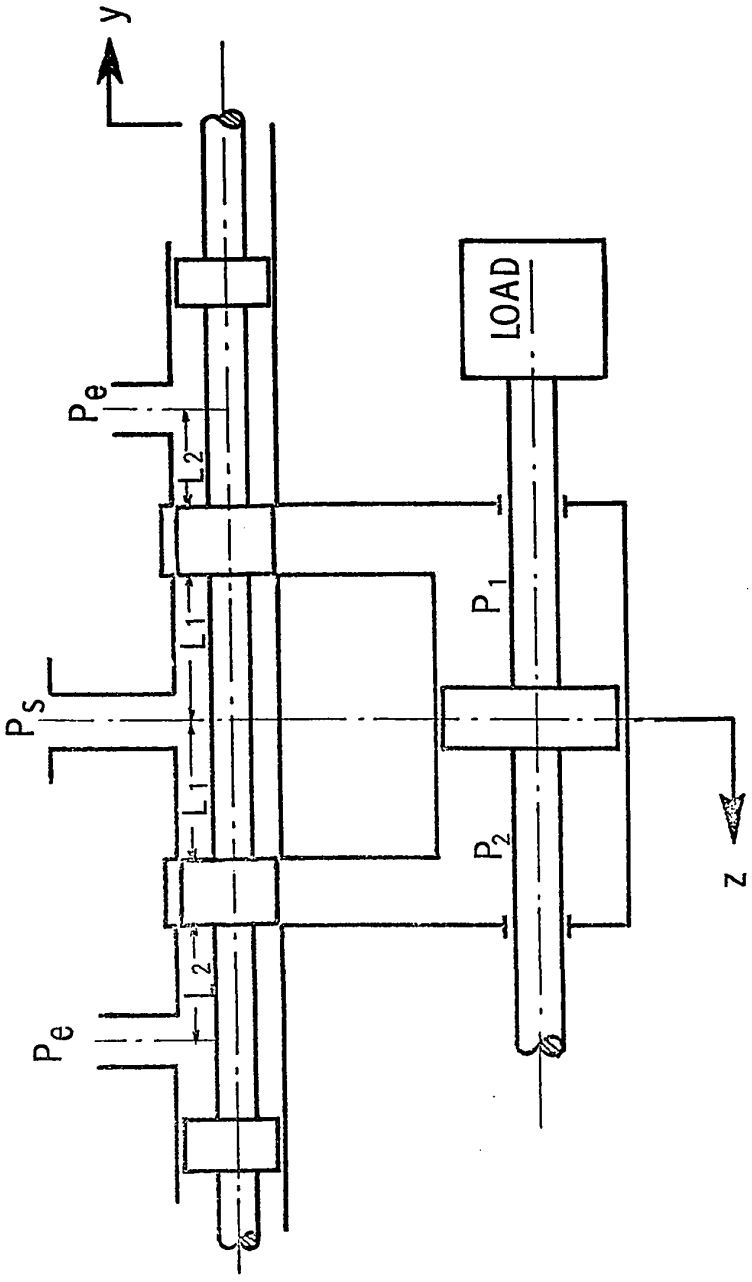

FIGURE 17 SCHEMATIC DIAGRAM OF A HYDRAULIC SERVOMOTOR

If the damping length $L_2 < L_1$, the transient flow force is negative and may cause valve instability. Therefore such a valve should be designed so that $L_2 \geq L_1$ to prevent this possibility. When the valve area gradient W is small, this transient flow force has limited potential to be considered as a damping [26].

The steady state flow force F_f always acts in a direction to close the valve opening and can be considered as a centering spring on the valve. With negligible radial clearance, the value of this force is calculated to be [26]:

$$F_f = 0.43\ W\ (y-z)\ [(P_s-P_e) - (P_1-P_2)] \qquad (2.15)$$

In order to obtain the effects of the mass moment of inertia of the stylus and its compliance on the dynamic accuracy and stability, one has to consider the dynamics of the stylus motion. In an actual operation as the stylus moves over the template, it is possible to have a certain deformation either in the template surface or in the stylus. Such elastic deformations often affect the accuracy and stability of copying systems [27]. By assuming a contact spring of stiffness K_m as shown in Figure 18, the equation of motion of the stylus can be written as:

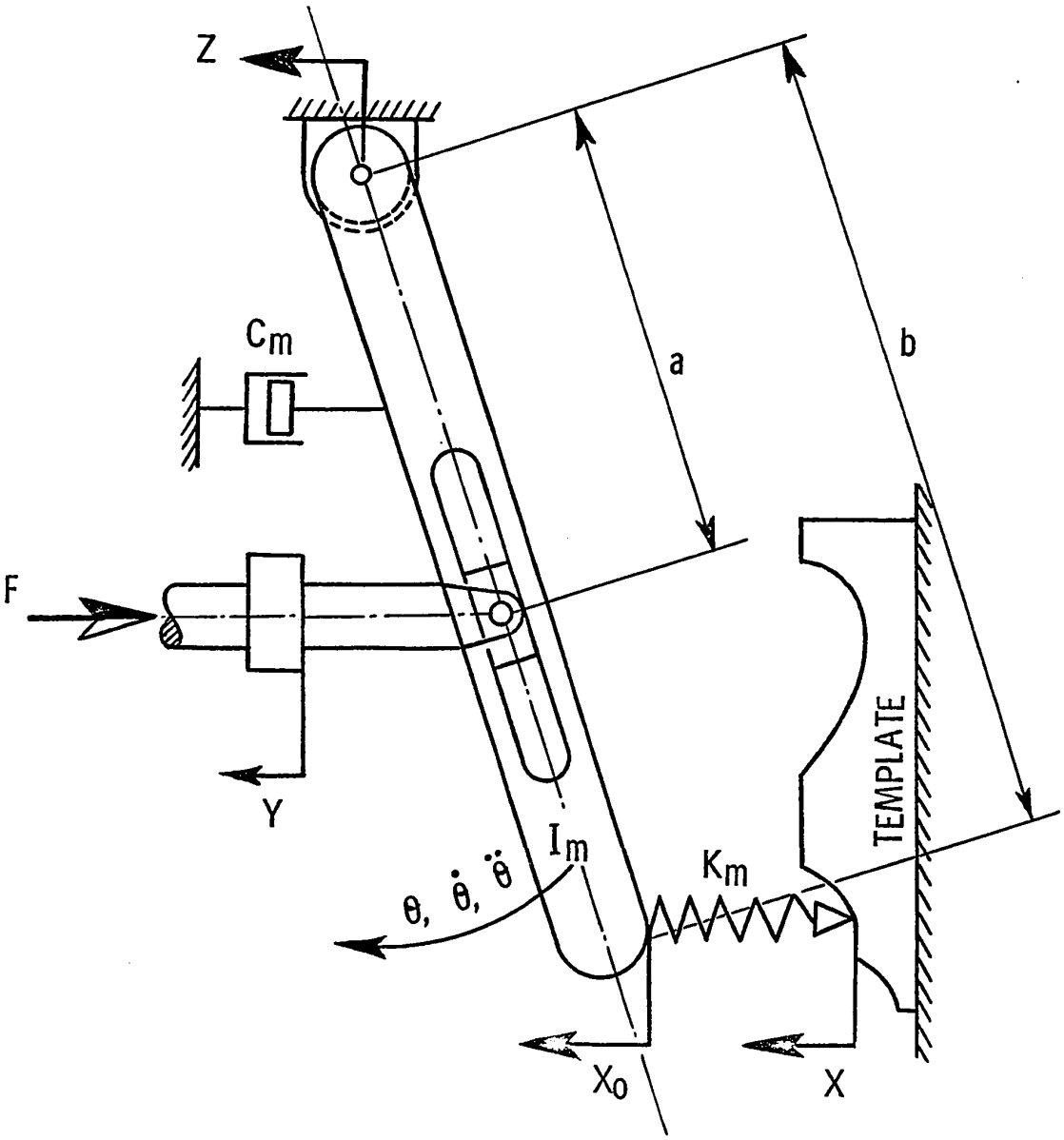

FIGURE 18 A SCHEMATIC DIAGRAM FOR THE STYLUS SYSTEM

$$I_m \frac{d^2\theta}{dt^2} + C_m \frac{d\theta}{dt} + (a \cos\theta)F = (b \cos\theta)\ [K_m(x-x_o) + F_{km}] \qquad (2.16)$$

where I_m is the mass moment of inertia of the stylus

C_m is the effective damping

Since the value of θ is always small, cos θ can be assumed to be unity and the equation (2.16) can be rewritten as:

$$I_m \frac{d^2\theta}{dt^2} + C_m \frac{d\theta}{dt} + aF = b[K_m(x-x_o) + F_{km}] \qquad (2.17)$$

The relationship of x_o and y with θ can be obtained from the kinematic motion of the stylus and are given by:

$$x_o = z + b\theta \qquad (2.18)$$

$$y = z + a\theta \qquad (2.19)$$

Considering the flow through each of the metering edges to be an orifice-type flow with negligible viscous effects, the flow characteristic equations through the valve ports are given by:

$$Q_1 = C_d W(y-z) \quad [\frac{2}{\rho} (P_s-P_1)]^{\frac{1}{2}} \tag{2.20}$$

$$Q_2 = C_d W(y-z) \quad [\frac{2}{\rho} (P_2-P_e)]^{\frac{1}{2}} \tag{2.21}$$

for $(y-z) > 0$

and

$$Q_1 = C_d W(y-z) \quad [\frac{2}{\rho} (P_1-P_e)]^{\frac{1}{2}} \tag{2.22}$$

$$Q_2 = C_d W(y-z) \quad [\frac{2}{\rho} (P_s-P_2)]^{\frac{1}{2}} \tag{2.23}$$

for $(y-z) < 0$

Hydraulic behavior of the control is characterized by the flow continuity equations. These equations express the fact that the sum of the mass of flow into the control volume plus the time rate of change of mass within the control volume must be equal to the mass of flow out of the control volume. Assuming that the connecting passages between the control valve and the cylinder chambers are thicker and shorter to eliminate the fluid inertance, and the frictional losses in the passages to be negligible, the set of equations

governing the continuity characteristics of the system are given as:

$$Q_1 = A\frac{dz}{dt} + \frac{1}{B}\left(\frac{V}{2} + Az\right)\frac{dP_1}{dt} + C_l(P_1-P_2) \tag{2.24}$$

$$Q_2 = A\frac{dz}{dt} - \frac{1}{B}\left(\frac{V}{2} - Az\right)\frac{dP_2}{dt} + C_l(P_1-P_2) \tag{2.25}$$

These continuity equations also take into account the dynamic compressibility of the fluid in the cylinder chambers and the laminar leakage flow past the cylinder piston.

The above set of equations (2.8) - (2.25) completely describe the behavior of the copying system.

2.4 Stylus Motion in Time Domain

2.4.1 Introduction

In previous studies on the accuracy of hydraulic copying systems [28,29], the response of the system is evaluated to an arbitrary input such as a step or a ramp function. Such a method of analysis can give only a qualitative estimate on the actual response and thus on the accuracy in copying a given profile. In order to obtain a closer estimate of the copying accuracy, the displacement input of the system should represent the actual motion of the stylus over the template profile. Hence, if the actual input function of the copying

system is known, the response can be evaluated from which a good estimate on the accuracy of the system can be obtained.

2.4.2 Transformation of Template Profile in Time Domain

In the actual operation of hydraulic copying systems, the stylus is forced to move over the template profile due to the constant feed of the machine-tool slide. Hence, the motion of the stylus depends on the template configuration and on the feed rate of the machine tool slide. Since the stylus movement depends on the feed rate, the motion of the stylus is a time-dependent quantity. Hence, if the displacement of the stylus can be expressed as a function of time from the known geometry of the template and the feed rate of the machine-tool slide, the input function of the copying system is exactly defined. The response of the copying system to this input describes the shape of the produced workpiece in the time domain.

Consider a template with a profile as shown in Figure 19. Let $\bar{x}$ and $\bar{y}$ be the two coordinate axes. Let v be the velocity of the machine tool slide and $\dot{x}$ be the velocity of the stylus along the copying axis. Let the stylus move from a point A_1 to a point A_2 along the profile. Then, from the velocity diagram in Figure 19, it can be written [30]:

$$\frac{\dot{x}}{\sin \bar{\alpha}_0} = \frac{v_a}{\sin \gamma} = \frac{v}{\sin (\gamma+\bar{\alpha}_0)} \qquad (2.26)$$

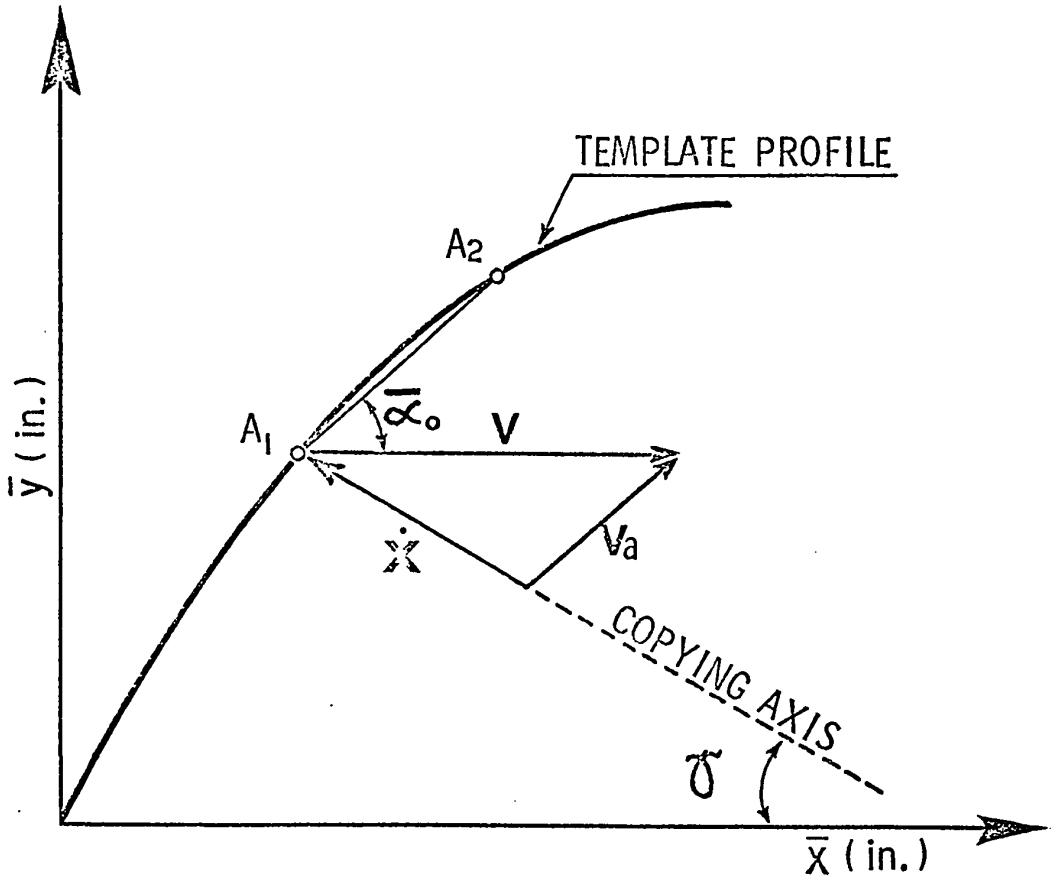

FIGURE 19 VELOCITY DIAGRAM FOR STYLUS MOTION

where $\tan \bar{\alpha}_0$ is the slope of the profile

v_a is the velocity of the stylus along the profile.

Rewriting equation (2.26) gives:

$$\dot{x} = \frac{v \cdot \sin \bar{\alpha}_0}{\sin (\gamma+\bar{\alpha}_0)} \tag{2.27}$$

$$v_a = \frac{v \cdot \sin \gamma}{\sin (\gamma+\bar{\alpha}_0)} \tag{2.28}$$

Since $\dot{x} = \frac{dx}{dt}$

and $v_a = \frac{ds}{dt}$

where dx is the elemental displacement of the stylus along the copying axis

ds is the elemental displacement of the stylus along the profile

dt is the elemental increment of the independent variable, time.

Equations (2.27) and (2.28) can be written as

$$dx = \frac{\left(\frac{d\bar{y}}{d\bar{x}}\right) \cdot v \cdot dt}{\left[\sin\gamma + \frac{d\bar{y}}{d\bar{x}} \cos\gamma\right]} \tag{2.29}$$

$$dt = \left(\frac{ds}{v}\right) \left[\frac{\sin(\gamma + \bar{\alpha}_o)}{\sin\gamma}\right] \tag{2.30}$$

$$\text{where } \frac{d\bar{y}}{d\bar{x}} = \tan\bar{\alpha}_o$$

Equations (2.29) and (2.30) completely describe the motion of the stylus in the time domain as a function of the shape of the profile and the velocity of the machine tool slide. In the case of a template profile having a surface at right angles to the workpiece axis, the motion of the stylus in time domain can be obtained from equations (2.29) and (2.30) as:

$$dx = \frac{v \cdot dt}{\cos\gamma} \tag{2.31}$$

$$dt = \frac{ds}{v} \tag{2.32}$$

C H A P T E R III

STABILITY OF HYDRAULIC COPYING SYSTEMS

3.1 General

Stability is an important factor in assessing the performance of hydraulic copying systems. It has been experienced that alterations in the design stage or selection of completely new sets of parameters based on experience, lead to the origin of self-excited vibration and dynamic instability in the system [31,32]. To study quantitatively the aspect of stability in hydraulic copying systems, an explicit theoretical investigation or a computer simulation may be carried out. Since the governing equations of the copying systems are non-linear, a theoretical investigation may be carried out by linearizing approximations as outlined in the following paragraphs.

3.2 Stability Analysis Using Linearization Method

In linearization method, the system equations are linearized using the small perturbation technique [1] and the stability of the systems is analyzed for small movements about an operating point. The concept of this technique is to perturb the system variables about the operating point and to expand the non-linear system functions using Tylor's series expansion. As an example, consider the following non-linear

function.

$$Q = f(X,P) \tag{3.1}$$

where $f(\cdot)$ is a non-linear function

Let Q_o, X_o and P_o be the system variables at the operating point and the corresponding perturbed variables be q, x and p. Then the perturbed equation is given by:

$$Q_o + q = f(X_o+x, P_o+p) \tag{3.2}$$

Now, expanding the non-linear function $f(\cdot)$ by Taylor's series and neglecting terms higher than second order, the equation (3.2) becomes

$$Q_o + q = f(X_o,P_o) + \frac{\delta f}{\delta X_o} x + \frac{\delta f}{\delta P_o} p \tag{3.3}$$

Rewriting equation (3.3) gives:

$$q = \frac{\delta f}{\delta X_o} x + \frac{\delta f}{\delta P_o} p \tag{3.4}$$

Hence, equation (3.4) gives the perturbed equation

corresponding to the original equation (3.1).

In the absence of the dynamic behavior of the control valve and the stylus, and neglecting the presence of dry friction in the copying slide, the governing equations of the hydraulic copying system outlined in Chapter II can be rewritten as:

$$M\frac{d^2z}{dt^2} + C\frac{dz}{dt} + K_s(z-y) = A(P_1-P_2) + F_k + F_d \tag{3.5}$$

$$Q_1 = A\frac{dz}{dt} + \frac{1}{B}\left(\frac{V}{2} + Az\right)\frac{dP_1}{dt} + C_l(P_1-P_2) \tag{3.6}$$

$$Q_2 = A\frac{dz}{dt} - \frac{1}{B}\left(\frac{V}{2} - Az\right)\frac{dP_2}{dt} + C_l(P_1-P_2) \tag{3.7}$$

$$Q_1 = f(e,P_1) \tag{3.8}$$

$$Q_2 = f(e,P_2) \tag{3.9}$$

$$e = (y-z) = \frac{a}{b}(x-z) \tag{3.10}$$

where $f(\cdot)$ is a non-linear function

Now, assuming the cutting force F_d to be a constant and using the small perturbation technique [1], the above set of equations (3.5) - (3.10) become

$$M\frac{d^2z}{dt^2} + C\frac{dz}{dt} - K_s e = A(p_1-p_2) + F_k + F_d \tag{3.11}$$

$$q_1 = A\frac{dz}{dt} + \frac{1}{B}\left(\frac{V}{2} + Az\right)\frac{dp_1}{dt} + C_l(p_1-p_2) \tag{3.12}$$

$$q_2 = A\frac{dz}{dt} - \frac{1}{B}\left(\frac{V}{2} - Az\right)\frac{dp_2}{dt} + C_l(p_1-p_2) \tag{3.13}$$

$$q_1 = \frac{\delta Q_1}{\delta e}\, e + \frac{\delta Q_1}{\delta P_1}\, p_1 \tag{3.14}$$

$$q_2 = \frac{\delta Q_2}{\delta e}\, e + \frac{\delta Q_2}{\delta P_2}\, p_2 \tag{3.15}$$

$$e = \frac{a}{b}(x-z) \tag{3.16}$$

where the italic letter represents the perturbed values of the corresponding system variables

These equations (3.11) - (3.16) are linear, although the coefficients $\frac{\delta Q_1}{\delta e}$, $\frac{\delta Q_2}{\delta e}$, $\frac{\delta Q_1}{\delta P_1}$, $\frac{\delta Q_2}{\delta P_2}$ are functions of the steady state operating point at which the system is analyzed. In the steady state condition the flows into and out of the cylinder chambers will be equal and, in general for the symmetrical valve porting

$$\frac{\delta Q_1}{\delta e} = \frac{\delta Q_2}{\delta e} = C_e, \text{ say}$$

and

$$-\frac{\delta Q_1}{\delta P_1} = \frac{\delta Q_2}{\delta P_2} = C_p, \text{ say.}$$

Then, from equations (3.12) and (3.14)

$$C_e\, e - C_p\, p_1 = A\frac{dz}{dt} + \frac{1}{B}\left(\frac{V}{2} + Az\right)\frac{dp_1}{dt} + C_l(p_1-p_2) \qquad (3.17)$$

and from equations (3.13) and (3.15)

$$C_e\, e + C_p\, p_2 = A\frac{dz}{dt} - \frac{1}{B}\left(\frac{V}{2} - Az\right)\frac{dp_2}{dt} + C_l(p_1-p_2) \qquad (3.18)$$

Adding equations (3.17) and (3.18) gives

$$2C_e e - C_p(p_1-p_2) = \frac{V}{2B}\frac{d}{dt}(p_1-p_2) + 2A\frac{dz}{dt} + 2C_l(p_1-p_2) \qquad (3.19)$$

Combining equations (3.11), (3.16) and (3.19) and rearranging gives:

$$a_3 \frac{d^3z}{dt^3} + a_2 \frac{d^2z}{dt^2} + a_1 \frac{dz}{dt} + a_0 z = a_0 x + b_0 \dot{x} + b_1 \qquad (3.20)$$

where

$$a_3 = \frac{MV}{4B}$$

$$a_2 = (\frac{1}{4B}) \quad [VC + 2MB(C_p + 2C_l)]$$

$$a_1 = (\frac{1}{4B}) \quad [\frac{VK_s a}{b} + 4BA^2 + 2BC(C_p + 2C_l)]$$

$$a_0 = (\frac{1}{2B}) \quad [2AC_e a + K_s a(C_p + 2C_l)]$$

$$b_0 = \frac{VK_s a}{4Bb}$$

$$b_1 = (\frac{1}{2}) \quad [(C_p + 2C_l)\ (F_k + F_d)]$$

To find the absolute stability of the system, consider the characteristic equation of the system and use the Routh Hurwitz Criterion [33]. Then, the conditions on the absolute stability of the system are given by:

$$a_3 > 0$$

$$a_2 > 0$$

$$a_0 > 0$$

$$a_2 a_1 > a_3 a_0$$

For the acceptable range of system parameters, the first three conditions are always satisfied. Hence, the stability condition for a copying system under linearizing approximation is given by:

$$\frac{a_2 a_1}{a_3 a_0} > 1$$

Using the above mentioned method, only the absolute stability of the system can be analyzed. If the relative stability of the hydraulic copying systems has to be analyzed, then the Nyquist stability criterion [34] or the root-locus method [35] may be adopted as described in [17,36].

3.3 Stability Analysis Using Matrix Theory

In analyzing stability using perturbation technique, the cutting force F_d is assumed to be a constant. But, if the cutting force is considered to be dynamic as described by equation (2.12), then the coefficients a_2 and a_1 become

periodic and the linearized equation describing the system is:

$$a_3\dddot{z} + a_2\ddot{z} + a_1\dot{z} + a_0 z = a_0 x + b_0\dot{x} + b_1 + b_2 \qquad (2.21)$$

where

$$a_3 = M$$

$$a_2 = C + F_2(1 + \varepsilon \sin\omega_f t) + 2MB(C_p + 2C_\ell) \;/\; V$$

$$a_1 = \frac{K_s a}{b} + F_2\, \varepsilon \cos\omega_f t + 4\left(\frac{B}{V}\right)A^2$$

$$+ \left[\left(\frac{2B}{V}\right)(C_p + 2C_\ell)\right]\left[C + F_2(1 + \varepsilon\sin\omega_f t)\right]$$

$$a_0 = \left(\frac{1}{Vb}\right)\left[4BAC_e a + 2BaK_s(C_p + 2C_\ell)\right]$$

$$b_0 = \frac{K_s a}{b}$$

$$b_1 = \left(\frac{2B}{V}\right)(C_p + 2C_\ell)F_k$$

$$b_2 = \left(\frac{F_1}{V}\right)\left[\varepsilon V\omega_f \cos\omega_f t + 2B(C_p + 2C_\ell)(1 + \varepsilon\sin\omega_f t)\right]$$

and a dot denotes differentiation with respect to t.

The conditions for stability of a periodic differential equation governing a system has been discussed [29] and

the procedure is outlined as follows:

Consider the force free system given by the equation

$$a_3\dddot{z} + a_2(t)\ddot{z} + a_1(t)\dot{z} + a_0 z = 0 \tag{3.22}$$

Define the variables

$$z_1 = z$$

$$z_2 = \dot{z}_1 = \dot{z}$$

$$z_3 = \dot{z}_2 = \ddot{z}$$

Then the state representation of equation (3.22) is given by:

$$\begin{bmatrix} \dot{z}_1 \\ \dot{z}_2 \\ \dot{z}_3 \end{bmatrix} = \begin{bmatrix} 0 & 1 & 0 \\ 0 & 0 & 1 \\ -\frac{a_0}{a_3} & -\frac{a_1}{a_3} & -\frac{a_2}{a_3} \end{bmatrix} \begin{bmatrix} z_1 \\ z_2 \\ z_3 \end{bmatrix} \tag{3.23}$$

$$\text{i.e., } \underline{\dot{Z}} = [A]\ \underline{Z} \tag{3.24}$$

where a bar underneath the letters represents a vector and a letter enclosed inside square brackets is a matrix.

In equation (3.24), [A] is a periodic matrix with period 2π.

$$\text{i.e.,} \quad [A_{2\pi}] = [A]$$

where a subscript 2π represents the argument is periodic with period 2π.

Let $\underline{Z}^{(1)}$, $\underline{Z}^{(2)}$, and $\underline{Z}^{(3)}$ be the fundamental set of solutions of equation (3.24). Then, a fundamental matrix can be defined as:

$$[Z] = [\, \underline{Z}^{(1)}; \underline{Z}^{(2)}; \underline{Z}^{(3)} \,]$$

Then [Z] satisfies

$$[\dot{Z}] = [A]\,[Z] \tag{3.25}$$

The state transition matrix $[\phi(t,t_o)]$ of equation (3.24) can be shown to satisfy [37],

$$\det\,[\phi(t,t_o)] = \exp\,[\int_{t_o}^{t} \text{tr}[A]\,dt]$$

and hence

$$\det [Z] = \det [Z_0] \cdot \exp \left[\int_0^t \operatorname{tr} [A]\, dt\right]$$

where $[Z_0]$ is the value of the matrix at $t = 0$

Hence if $\det [Z_0] \neq 0$, then $\det [Z] \neq 0$ for all t. Since [A] has a period 2π, $[Z_{2\pi}]$ is also a solution of equation (3.25), and in fact a fundamental solution. This means that the columns of $[Z_{2\pi}]$ can be expressed in terms of the columns of [Z]

$$[Z_{2\pi}] = [Z]\ [G]$$

where [G] is a matrix relating $[Z_{2\pi}]$ to [Z].

Let $\underline{Z}$ be any solution of equation (3.24). Then it can be expressed in terms of the columns of [Z]

$$\underline{Z} = [Z]\ \underline{b}$$

and

$$\underline{Z_{2\pi}} = [Z_{2\pi}]\ \underline{b} = [Z]\ [G]\ \underline{b}$$

If $\underline{Z}$ satisfies

$$\underline{Z}_{2\pi} = \lambda \underline{Z}$$

then

$$[Z]\ [G]\ \underline{b} = \lambda\ [Z]\ \underline{b}$$

or $$[Z]([G] - \lambda[I])\ \underline{b} = 0$$

Since det $[Z] \neq 0$, hence

$$([G] - \lambda[I])\ \underline{b} = 0$$

Therefore, λ must be the eigenvalue of [G]. Hence, if λ_j is a simple eigenvalue of [G] then there exists a vector $\underline{b}_j$ that satisfies

$$[G]\ \underline{b}_j = \lambda_j\ \underline{b}_j$$

So that

$$\underline{Z} = [Z]\ \underline{b}_j$$

and

$$\underline{Z}_{2\pi} = [Z_{2\pi}]\underline{b}_j = [Z][G]\underline{b}_j = \lambda_j[Z]\underline{b}_j = \lambda_j\underline{Z}$$

Let $\lambda = e^{j2\pi\sigma}$ and $\underline{Z} = e^{j\sigma t}\ \underline{f}$

Hence

$$e^{j\sigma(t+2\pi)}\ f_{2\pi} = e^{j2\pi\sigma}\ \underline{f}\ e^{j\sigma t}$$

or

$$\underline{f}_{2\pi} = \underline{f}$$

Thus any solution of $\underline{Z}$ of equation (3.24), where $\underline{Z}_{2\pi} = \lambda\underline{Z}$, has the form $\underline{Z} = e^{j\sigma t}\ \underline{f}$ where $\underline{f}_{2\pi} = \underline{f}$ and $\lambda = e^{j2\pi\sigma}$ is an eigenvalue of the matrix [G].

For a given set of initial conditions [Z], one can solve equation (3.25) numerically to obtain $[Z_{2\pi}]$. Let $[Z_{2\pi}]$ and [Z] be related by [D] such that:

$$[Z_{2\pi}] = [D][Z]$$

With the proper choice of [Z], one can obtain the fundamental set of solutions such that:

$$[Z_{2\pi}] = [Z][G] = [Z][G][Z]^{-1}[Z]$$

and [D] has the same eigenvalue as [G]. A fundamental set of solutions can be obtained if the initial conditions for [Z] is chosen to be identical to [I], which gives

$$[D] = [Z_{2\pi}]$$

Thus the solution of equation (3.24) will be stable if the eigenvalues of [D] are distinct and less than 1 in modulus. Figure 20 gives the flow diagram which can be used for the stability analysis.

3.4 Stability Analysis Using Simulation Procedures

The equations governing the behavior of the hydraulic copying system outlined in Chapter II are non-linear and a pure mathematical analysis of stability is rather complex. In order to make an explicit stability analysis, the system may be simulated on an analog computer. A decaying or an increasing transients in the response determines a stable or an unstable nature of the system. A copying system can be defined to be at its stability border when it executes a

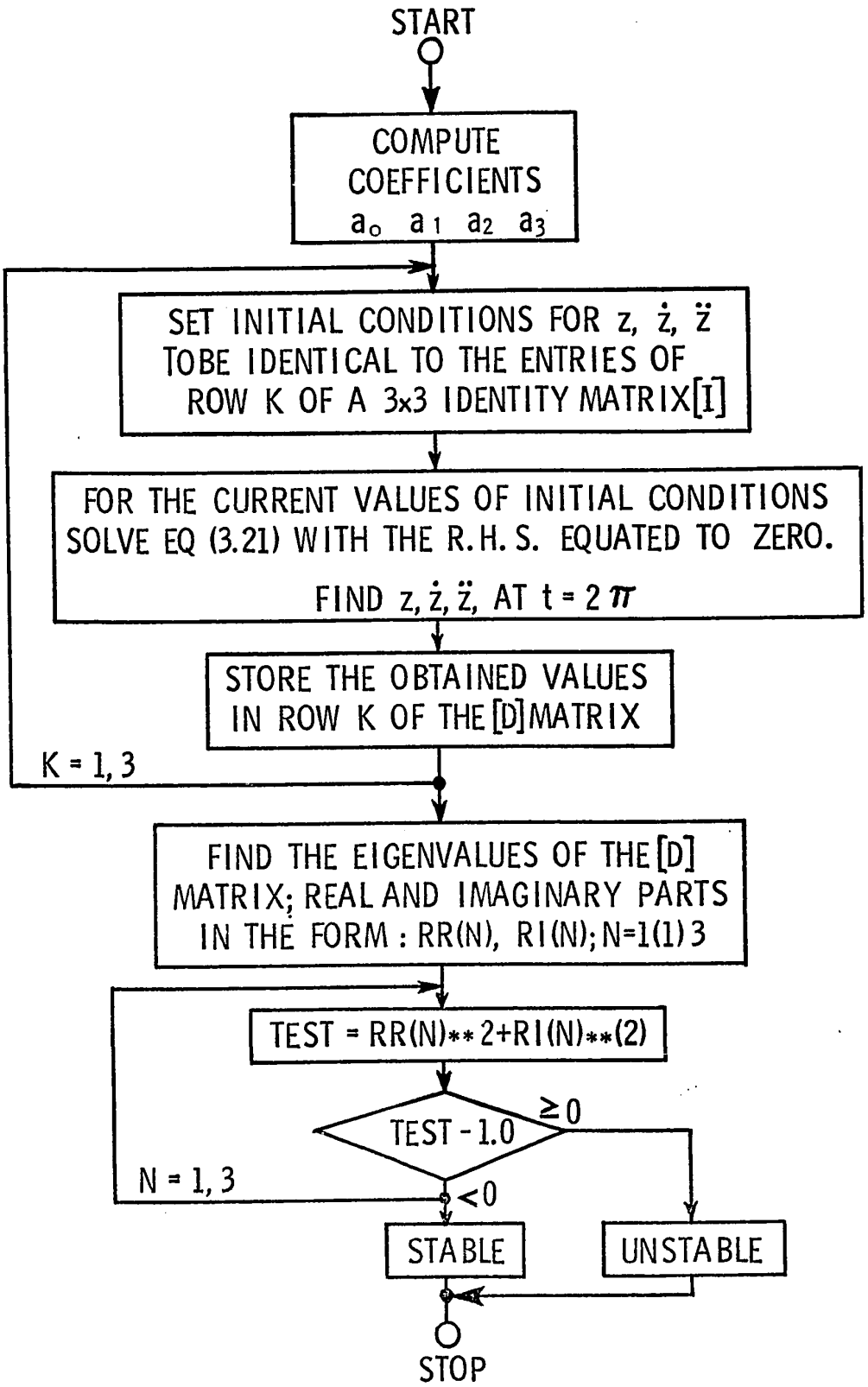

FIGURE 20 FLOW CHART FOR STABILITY ANALYSIS

transient phenomenon with constant amplitude. Considering one of the system parameters to be a stabilizing parameter, the simulation is carried out. The response of the system is obtained and whether it is damped or not is controlled by varying the stabilizing parameter and the value of this stabilizing parameter is determined.

C H A P T E R IV

DYNAMIC ACCURACY OF HYDRAULIC COPYING SYSTEMS

4.1 General

Accuracy is one of the major requirements of any hydraulic copying system. The accuracy of a hydraulic copying system depends on the type of disturbing action and the characteristics of the system. According to the type of disturbing action, the accuracy can be classified as static and kinematic accuracies. The static accuracy in a copying system gives the steady state positional error in the system due to an instantaneous disturbance. The kinematic accuracy gives the error in the system due to a constant velocity of the driving and driven members. These accuracies do not include the error due to the transients in the response, which especially occur due to changes in the shape of the template profile. Thus, an error due to the transients can be defined to give the local error of overshoot. Hence the performance of a hydraulic copying system can be described by giving the individual accuracies or errors.

4.2 Dynamic Accuracy Criterion for Hydraulic Copying Systems

In order to define the performance of copying systems by a single merit index, a dynamic accuracy criterion

which includes the static, kinematic and transient errors can be defined. To obtain the dynamic accuracy criterion consider an actual operation of a hydraulic copying system. The shape and size of the workpiece to be machined is known. Now if the workpiece is produced using a hydraulic copying system, the machined part is accepted or rejected depending on whether the dimensions of the produced part lie within the specified manufacturing tolerance zone. In other words, the deviation of the response from its input should always be less than the specified tolerance zone. Based on this, a dynamic accuracy criterion for copying systems can be derived as follows [30].

Consider the time domain model of the input and the response of a copying system as shown in Figure 21a. Δ_1 and Δ_2 represent the error limits and are given by:

$$\Delta_1 = [\, x(t) - z(t) \,]_{t=t_1} \tag{4.1}$$

$$\Delta_2 = [\, z(t) - x(t) \,]_{t=t_2} \tag{4.2}$$

where t_1 and t_2 represent the time during which the response $z(t)$ has a maximum deviation from the input $x(t)$ on either side of the input function. Thus the total error zone in a copying system is given by:

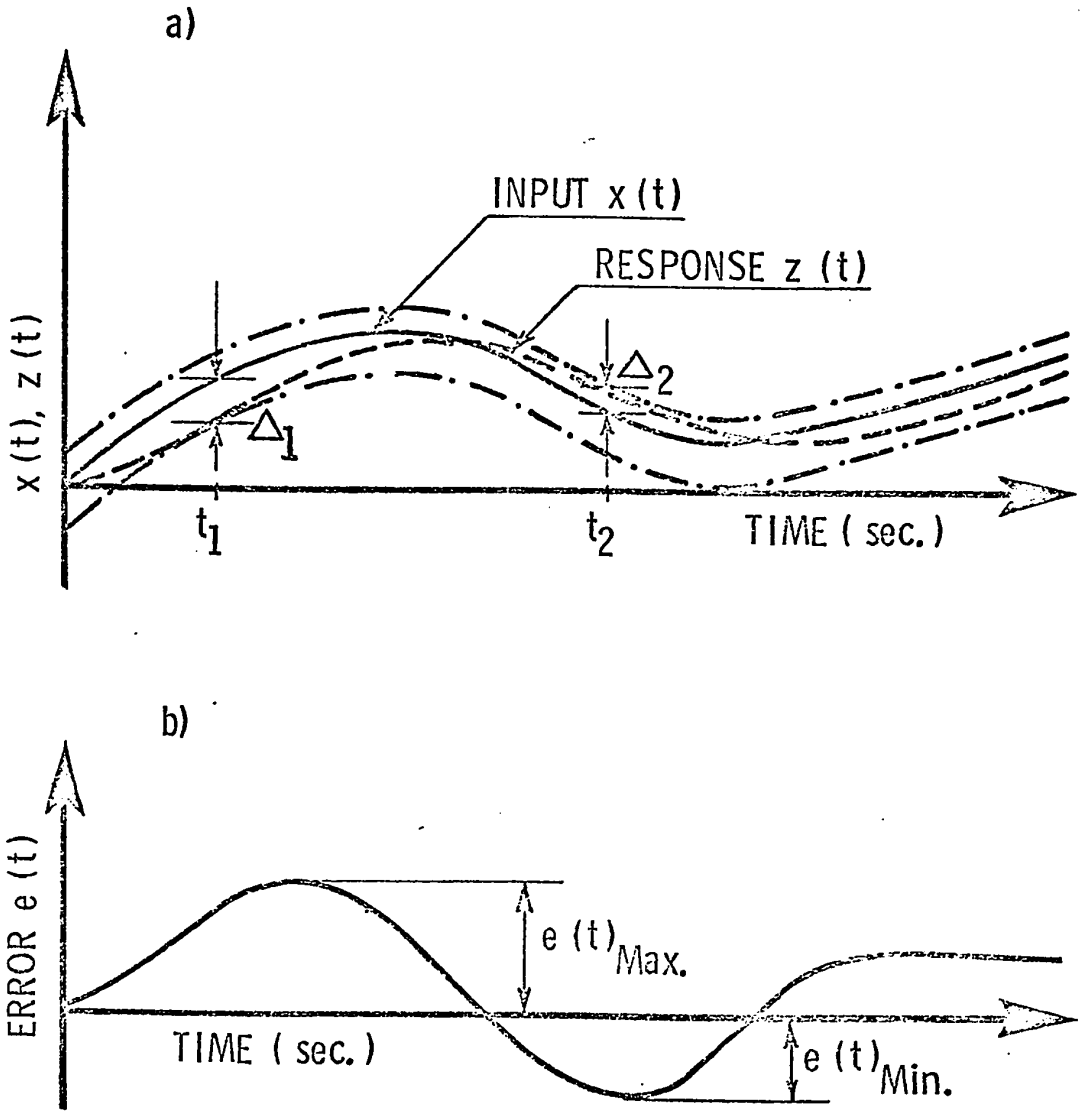

FIGURE 21 SCHEMATIC INPUT AND ERROR FUNCTION OF THE COPYING SYSTEM

$$\Delta_e = \Delta_1 + \Delta_2 \tag{4.3}$$

Therefore, the total error zone in the workpiece diameter can be written as:

$$\Delta_d = 2\Delta_e \sin \gamma \tag{4.4}$$

where γ is the angle between the copying slide and the workpiece axis

From a practical standpoint, Δ_d should always be less than the specified manufacturing tolerance of the workpiece. Since Δ_d takes into account static, kinematic and transient errors, it is in fact a valid dynamic accuracy criterion for the system. Since Δ_d and Δ_e are related by a constant value, Δ_e can be considered as the single merit index of the system.

Since the response of the system can be obtained by analysis, the total error zone Δ_e can be directly evaluated by plotting the error e(t) of the system. A typical plot of the error function e(t) is shown in Figure 21b. From this plot, the total error zone in the system along the copying axis can be given as:

$$\Delta_e = |e(t)_{max}| + |e(t)_{min}| \qquad (4.5)$$

Thus the dynamic accuracy of a system can be examined directly by knowing the total tolerance zone from the error plot of the system. It is seen from equation (4.4) that for a maximum copying accuracy, the total error zone in the system should be kept to a minimum.

Since the dynamic stability is also a major factor in assessing the dynamic accuracy of the system, this dynamic accuracy criterion should include conditions on stability. Hence, for this purpose, the dynamic accuracy criterion is determined only at its stability border (marginal stability). Since the dynamic response of the system is evaluated using simulation procedures, a stable or an unstable nature of the system is determined from a decaying or an increasing transience in the response.

C H A P T E R V

SIMULATION OF HYDRAULIC COPYING SYSTEM FOR DYNAMIC ACCURACY AND STABILITY

5.1 General

To investigate the dynamic accuracy and stability of hydraulic copying systems, the governing equations (2.8) - (2.25) which describe the dynamic behavior of the system should be solved to obtain the response. Since the governing equations are non-linear, an analytical investigation will be rather complex and hence an analog simulation procedure is adopted. In order to decrease the parametric complexity in simulation and to increase the generality, the governing equations are non-dimensionalized.

5.2 Non-Dimensionalization of System Equations

The first step in the non-dimensionalization procedure is to select reference values for flow, frequency and length.

Let

Reference flow $\hat{Q}$ = $C_d W u [2P_s/\rho]^{\frac{1}{2}}$

Reference length u = arbitrary

Reference frequency $\hat{\omega}$ = arbitrary

Then, define the following quantities

$$z^* = \frac{z}{u} \quad ; \quad y^* = \frac{y}{u} \quad ; \quad x^* = \frac{x}{u} \quad ;$$

$$x_0^* = \frac{x_0}{u} \quad ; \quad P_1^* = \frac{P_1}{P_s} \quad ; \quad P_2^* = \frac{P_2}{P_s} \quad ;$$

$$P_e^* = \frac{P_e}{P_s} \quad ; \quad \hat{L} = \frac{\hat{Q}}{A\omega_n} \quad ; \quad u^* = \frac{u}{\hat{L}} \quad ;$$

$$\tau = \hat{\omega}t$$

where ω_n is the natural frequency of the oil column and the mass

τ is the non-dimensional time

P_s is the supply pressure

Therefore

$$\frac{dz}{dt} = \frac{dz}{d\tau} \cdot \frac{d\tau}{dt} = \hat{\omega}\, u\, \frac{dz^*}{d\tau}$$

and

$$\frac{d^2z}{dt^2} = \hat{\omega}^2 u\, \frac{d^2z^*}{d\tau^2}$$

Let

$$\frac{dz^*}{d\tau} = \dot{z}^*$$

and

$$\frac{d^2z^*}{d\tau^2} = \ddot{z}^*$$

Then

$$\frac{dz}{dt} = \hat{\omega}\, u\, \dot{z}^*$$

and

$$\frac{d^2z}{dt^2} = \hat{\omega}^2 u\, \ddot{z}^*$$

Dynamic behavior of the copying slide:

To non-dimensionalize the equation governing the dynamic behavior of the copying slide, divide throughout the equation (2.8) by P_sA and using the dimensionless parameters as described above, rearrange the equation. Then it becomes:

$$\frac{Mu\hat{\omega}^2}{P_sA}\ddot{z}^* + \frac{Cu\hat{\omega}}{P_sA}\dot{z}^* + \frac{K_su}{P_sA}(z^*-y^*) + \frac{F_w}{P_sA}\,\mathrm{sgn}(\dot{z}^*)$$

$$= \frac{A(P_1-P_2)}{P_sA} + \frac{F_k}{P_sA} + \left[\frac{F_1}{P_sA} - \frac{F_2u\hat{\omega}}{P_sA}\dot{z}^*\right]\left[1 + \varepsilon\sin\frac{\omega_f\tau}{\hat{\omega}}\right] \qquad (5.1)$$

Let

$$\alpha = \frac{\hat{MQ}\omega_n}{P_sA^2}, \quad \text{the inertia parameter}$$

$$\nu = \frac{\hat{CQ}}{P_sA^2}, \quad \text{the viscous friction factor}$$

$$\mu_s = \frac{K_s\hat{Q}}{P_sA^2\omega_n}, \quad \text{the spring stiffness parameter}$$

$$\sigma = \frac{F_w}{P_sA}, \quad \text{the dry friction factor}$$

$$\lambda_k = \frac{F_k}{P_sA}, \quad \text{the initial spring force parameter}$$

$$\sigma_c = \frac{F_1}{P_sA}, \quad \text{cutting force parameter}$$

$$\nu_c = \frac{F_2\hat{Q}}{P_sA^2}, \quad \text{cutting force friction parameter}$$

$$\omega_f^* = \frac{\omega_f}{\hat{\omega}}$$

$$\omega^* = \frac{\hat{\omega}}{\omega_n}$$

Using the above non-dimensional parameter and rearranging equation (5.1), gives:

$$\alpha\omega^{*2}\ddot{z}^* + \nu\omega^*\dot{z}^* + \mu_s(z^*-y^*) + \frac{\sigma}{u^*}\,\mathrm{sgn}(\dot{z}^*) = \frac{P_1^*-P_2^*}{u^*} + \frac{\lambda_k}{u^*} + \left[\frac{\sigma_c}{u^*} - \nu_c\omega^*\dot{z}^*\right]\left[1+\varepsilon\sin\omega_f^*\tau\right] \tag{5.2}$$

Dynamic behavior of the control valve:

The dynamic behavior of the control valve can be non-dimensionalized by dividing throughout equation (2.13) by P_sA and using dimensionless parameters it becomes:

$$\frac{m_s u\hat{\omega}^2}{P_sA}\ddot{y}^* + \frac{C_s u\hat{\omega}}{P_sA}(\dot{y}^*-\dot{z}^*) + \frac{K_s u}{P_sA}(y^*-z^*) + \frac{F_k}{P_sA} + \frac{F_f}{P_sA} = \frac{F}{P_sA} \tag{5.3}$$

Let

$$\alpha_s = \frac{m_s \hat{Q} \omega_n}{P_s A^2}$$

$$\lambda_k = \frac{F_k}{P_s A}$$

$$F^* = \frac{F}{P_s A}$$

Assuming the transient flow forces to be negligible, and substituting for the value of the steady state flow force F_f from equation (2.15), the equation (5.3) becomes:

$$\alpha_s \omega^{*2} \ddot{y}^* + \mu_s (y^*-z^*) + \frac{\lambda_k}{u^*} + k(y^*-z^*) [(1-P_e^*) - (P_1^*-P_2^*)] = \frac{F^*}{u^*} \tag{5.4}$$

where

$$k = 0.43 \, Wu/A$$

Dynamic behavior of the stylus:

To non-dimensionalize the equation relating the motion of the stylus, divide throughout equation (2.17) by $P_s Aa$ and define the following parameters:

$$I_m^* = \frac{I_m \omega_n^3}{P_s \hat{Q}} \quad \text{, non-dimensional mass moment of inertia of stylus}$$

$$C_m^* = \frac{C_m \omega_n^2}{P_s \hat{Q}} \quad \text{, friction parameter in the stylus}$$

$$\mu_{km} = \frac{K_m \hat{Q}}{P_s A^2 \omega_n} \quad \text{, contact spring stiffness parameter}$$

$$\lambda_{km} = \frac{F_{km}}{P_s A} \quad \text{, the initial spring force parameter}$$

$$a^* = \frac{a}{u}$$

$$b^* = \frac{b}{u}$$

Now, using the above dimensionless parameters and rearranging gives:

$$I_m^* \omega^{*2} \ddot{\theta} + C_m^* \omega^* \dot{\theta} + F^* a^* u^* = b^* u^* [\mu_{km} u^* (x^* - x_0^*) + F_{km}^*] \qquad (5.5)$$

Equations (2.18) and (2.19) are non-dimensionalized by dividing by u and are given by:

$$x_0^* = z^* + b^*\theta \tag{5.6}$$

$$y^* = z^* + a^*\theta \tag{5.7}$$

Flow characteristic equations:

To non-dimensionalize the flow characteristic equations, divide throughout equations (2.20) - (2.23) by $\hat{Q}$; then they become:

$$\begin{aligned} Q_1^* &= [y^*-z^*]\ [1-P_1^*] \\ Q_2^* &= [y^*-z^*]\ [P_2^*-P_e^*] \end{aligned} \tag{5.8}$$

for $(y^*-z^*) > 0$

and

$$\begin{aligned} Q_1^* &= [y^*-z^*]\ [P_1^*-P_e^*] \\ Q_2^* &= [y^*-z^*]\ [1-P_2^*] \end{aligned} \tag{5.9}$$

for $(y^*-z^*) < 0$

Flow continuity equations:

The flow continuity equations (2.24) - (2.25) are

non-dimensionalized by dividing throughout the equation by $\hat{Q}$ and are evaluated as:

$$\frac{Q_1}{\hat{Q}} = \frac{Au\hat{\omega}}{\hat{Q}}\dot{z}^* + \frac{1}{B}\left[\frac{V}{2\hat{Q}} + \frac{Az^*u}{\hat{Q}}\right] P_s\hat{\omega}\dot{P}_1^* + \frac{C_l P_s}{\hat{Q}}(P_1^*-P_2^*) \qquad (5.10)$$

Let

$$\phi = \frac{C_l P_s}{\hat{Q}} \quad , \text{ leakage parameter}$$

$$\beta = \frac{B}{P_s} \quad , \text{ bulkmodulus parameter}$$

Then rearranging equation (5.10) becomes

$$Q_1^* = u^*\omega^*\dot{z}^* + \left(\frac{2\omega^*}{\alpha} + \beta u^*\omega^* z^*\right)\dot{P}_1^* + \phi\,(P_1^* - P_2^*) \qquad (5.11)$$

Similarly

$$Q_2^* = u^*\omega^*\dot{z}^* - \left(\frac{2\omega^*}{\alpha} - \beta u^*\omega^* z^*\right)\dot{P}_2^* + \phi\,(P_1^* - P_2^*) \qquad (5.12)$$

Substituting equation (5.4) in equation (5.5) and combining with equation (5.7), the equations relating the dynamic behavior of the control valve and the stylus can be combined to give:

$$K\ddot{\theta} + K_1\dot{\theta} + \mu_s u^*a^*\theta + ku^*a^*\theta[(1-P_e^*) - (P_1^*-P_2^*)]$$

$$+ \alpha_s\omega^{*2}u^*\ddot{z}^* + \lambda_k = \frac{\mu_{km}u^*b^*}{a^*}(x^*-x_o^*) + \frac{b^*}{a^*}\lambda_{km} \qquad (5.13)$$

where $K = (I_m^*\omega^{*2} + \alpha_s\omega^{*2}u^{*2}a^{*2}) / a^*u^*$

$K_1 = C_m^*\omega^* / a^*u^*$

At initial starting point

$$a^*\lambda_k = b^*\lambda_{km}$$

Then, equation (5.13) can be simplified to give

$$K\ddot{\theta} + K_1\dot{\theta} + \mu_s u^*a^*\theta + ku^*a^*\theta[(1-P_e^*) - (P_1^*-P_2^*)]$$

$$+ \alpha_s\omega^{*2}u^*z^* = \frac{\mu_{km}u^*b^*}{a^*}(x^*-x_o^*) \qquad (5.14)$$

5.3 Simulation of Governing Equations

The above non-dimensionalized equations which describe the behavior of the hydraulic copying system are simulated on an Analog computer, manufactured by the Electronic Associates, Inc., Model 680, and the unscaled analog circuit diagram is shown in Figure 22. Amplitude and time scaling are carried out directly on the unscaled computer diagram and the procedure is outlined in Appendix III.

A template profile as shown in Figure 23a is chosen for the simulation. Since the actual input function for the simulation should represent the stylus motion in time domain, it must be evaluated separately using the method outlined in Chapter II. A computer program that is used to calculate this time domain configuration of the input is shown in Appendix IV and the calculated input function is plotted as shown in Figure 23b. A variable diode function generator which allows the generation of arbitrary continuous non-linear functions is used to generate this time domain input function on an analog computer for the simulation.

In order to test the validity of the analysis, commercial machine-tool hydraulic copying systems manufactured by Duplomatic, Oerlikon-Bührle and True-Trace are simulated on the analog computer and the simulation was carried out

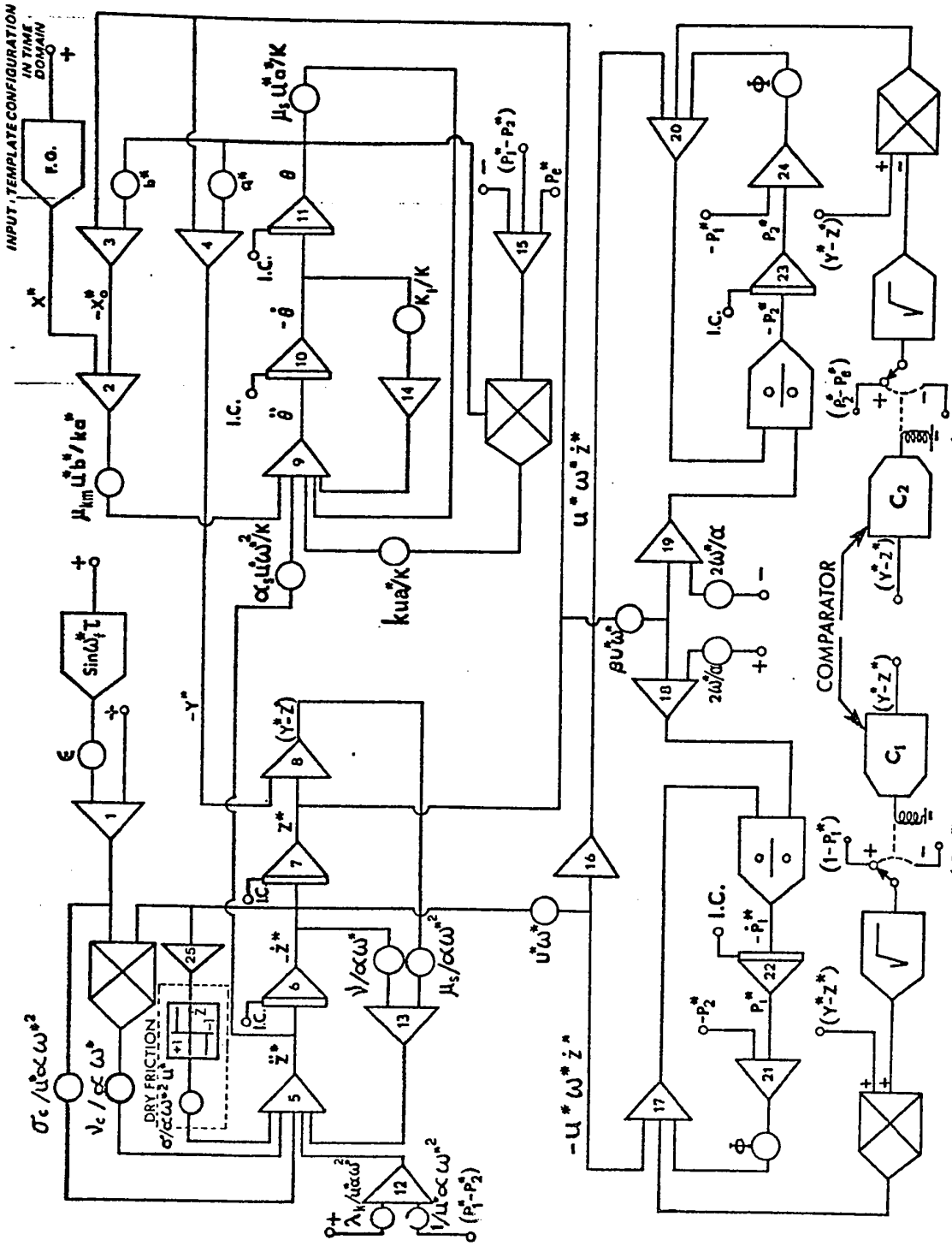

FIGURE 22 ANALOG CIRCUIT DIAGRAM OF THE COPYING SYSTEM

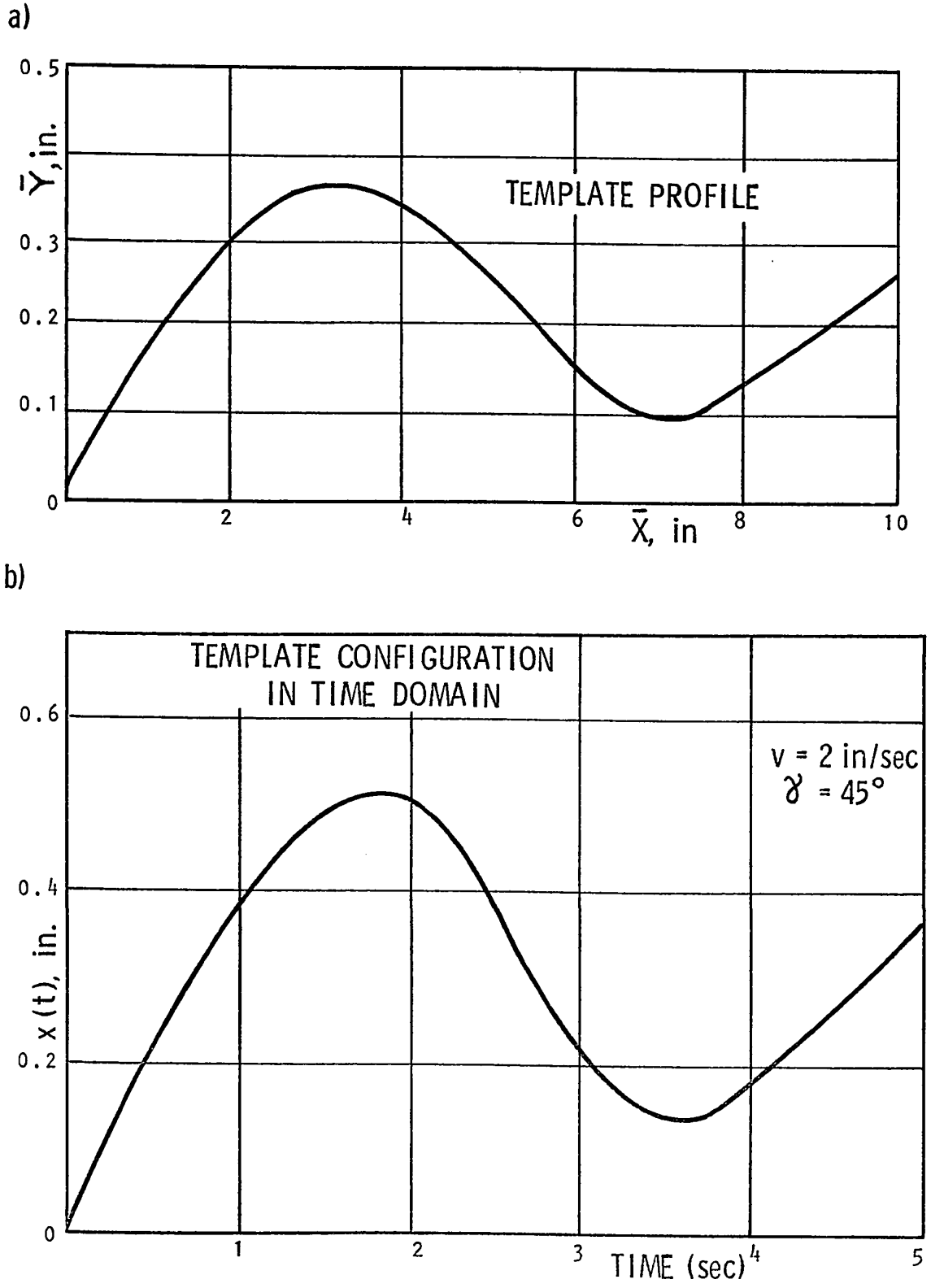

FIGURE 23 TEMPLATE PROFILE AND ITS CONFIGURATION IN TIME DOMAIN

for both finishing and roughing parallel turning operations. The simulation results show that the copying system performs under stable conditions and that the total error zone in the workpiece diameter Δ_d is less than 5×10^{-4} in. for finishing operation and less than 1×10^{-3} in. for roughing operation. These results agree with the data supplied by the manufacturer which confirms the validity of the analysis.

C H A P T E R VI

SYSTEM PARAMETER ANALYSIS AND CASE STUDIES

6.1 General

To investigate the relative effects of various system parameters on the dynamic accuracy and stability, a commercial copying system manufactured by Oerlikon-Bührle, model HKv, with parameters as outlined in Appendix V is simulated on the analog computer. The simulation is carried out with the time domain input function as shown in Figure 23 and the response of the system is obtained. The error between the time domain input and the response of the copying system is evaluated and is plotted as shown in Figure 24. It is seen from the error plot that the steady state error in the system is the major source of error and it increases the total error zone Δ_e in copying. The total error zone in the workpiece diameter Δ_d can be calculated from the equation (4.4) and the error plot to be 8.9×10^{-3} in. This shows that the hydraulic copying system with the given system parameters as in Appendix V can produce workpiece with a diametrical tolerance of 0.0089 in. in following a template as shown in Figure 23.

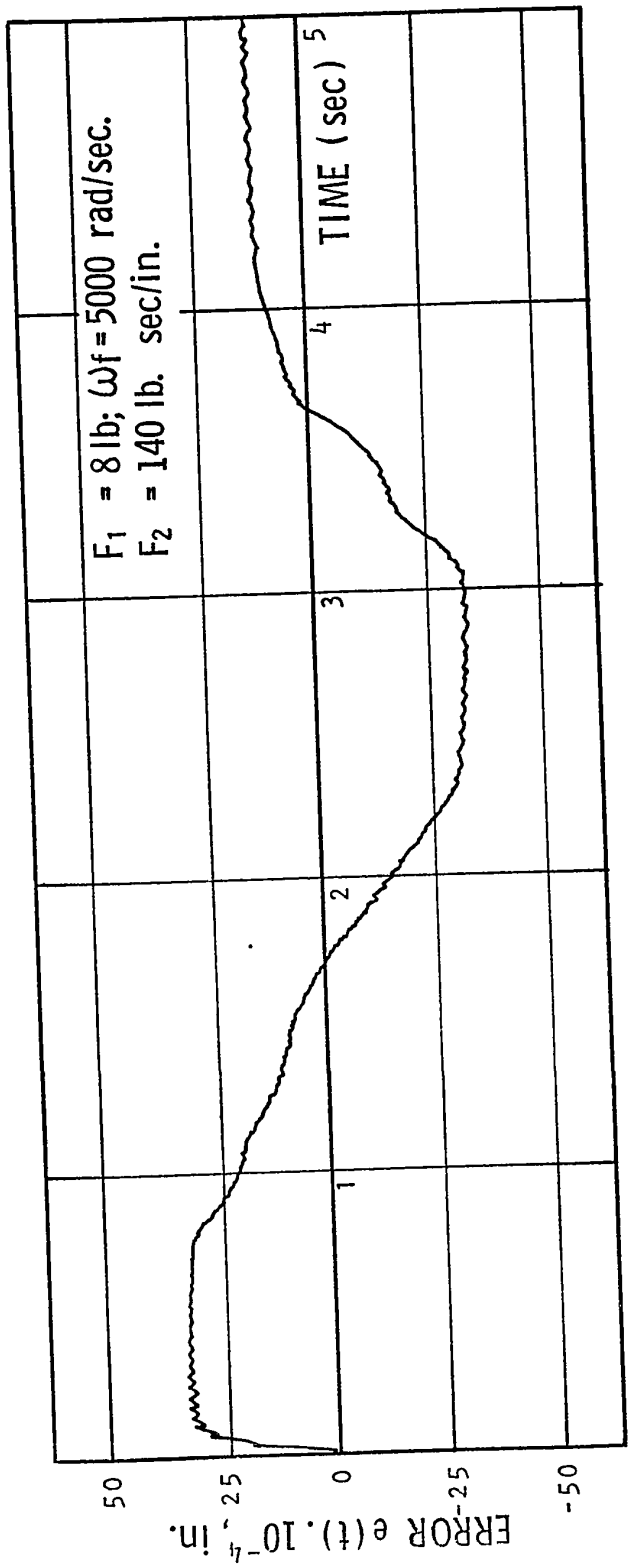

FIGURE 24 TYPICAL ERROR FUNCTION OF THE COPYING SYSTEM

6.2 Effects of System Parameters on the Dynamic Accuracy and Stability

In order to study the effects of system parameters on the dynamic accuracy and stability, each of the parameters is varied and the analog simulation is carried out. The error plots are obtained for stable operations and the total error zone Δ_e is calculated. Since the total error zone Δ_e is considered as the index of performance, the variation of Δ_e for different values of the system parameters are plotted and discussed.

6.2.1 Effect of Dry Friction

The simulation results show that the presence of dry friction decreases the dynamic accuracy of the system. Figure 25 shows the dependence of the total error zone Δ_e for variations in the amount of dry friction in the system. It can be seen from the plot that an increase in the amount of dry friction increases the total error zone and thus decreases the dynamic accuracy. This phenomenon is due to the fact that an increase in the value of dry friction increases the dead zone in the system as described by equation (2.6) and hence decreases the dynamic accuracy. The simulation results also show that the dry friction has a positive effect on the stability of the system. The stabilizing effect of dry friction can be seen from the error plots in Figure 26,

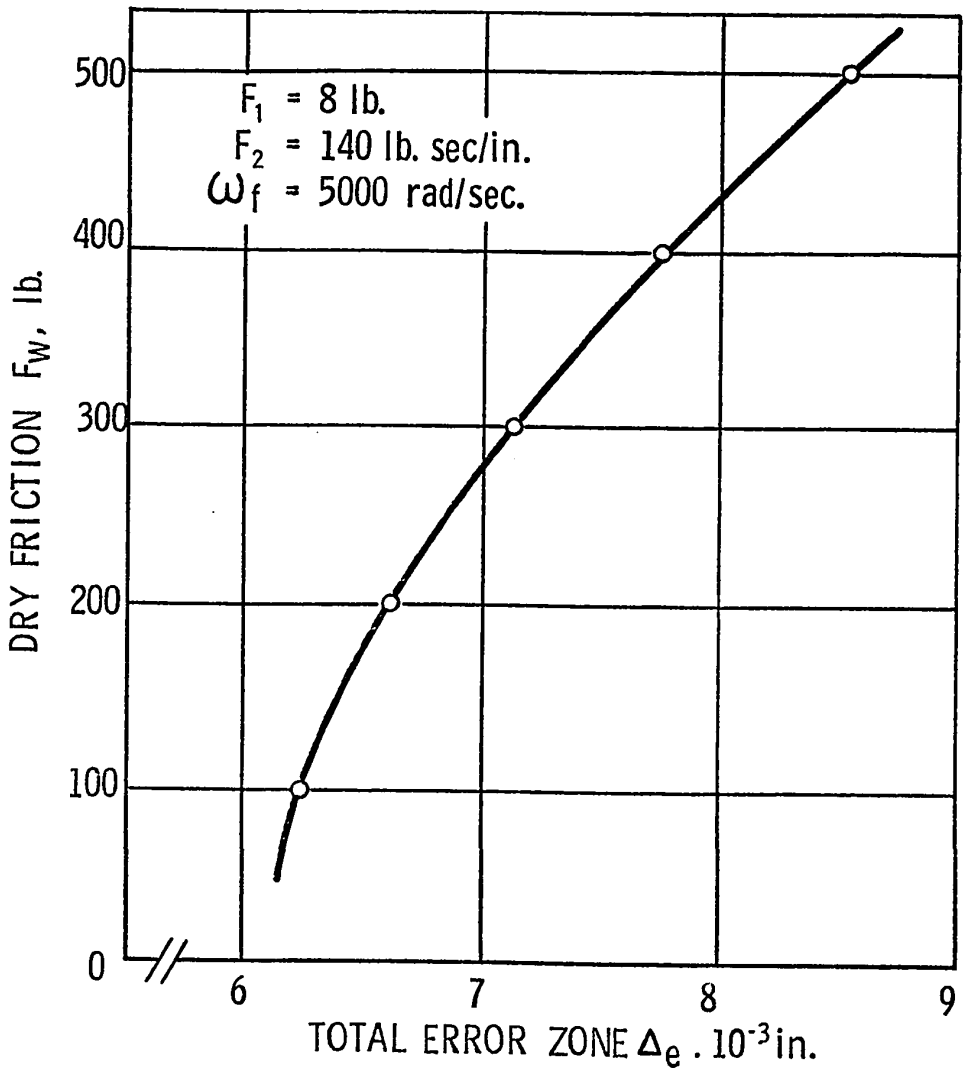

FIGURE 25 EFFECT OF DRY FRICTION ON THE TOTAL ERROR ZONE

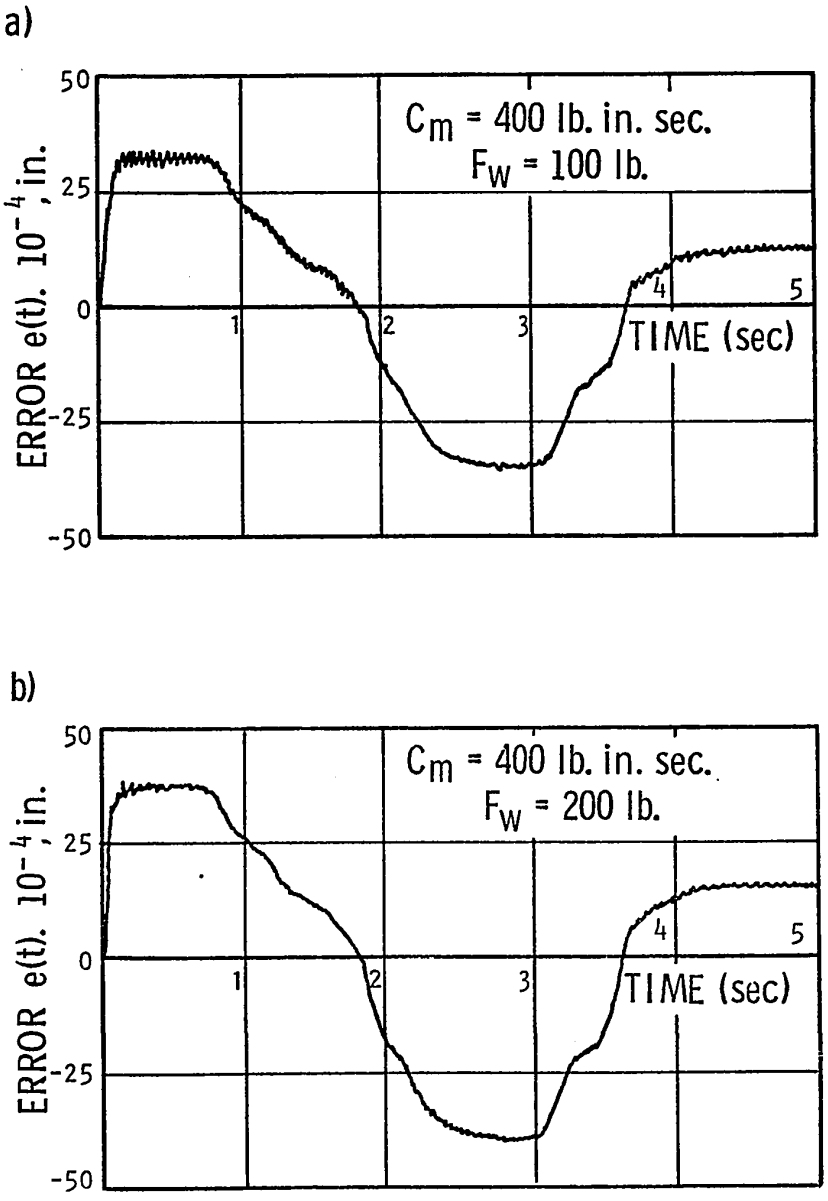

FIGURE 26 STABILIZING EFFECT OF DRY FRICTION

in which the system is stabilized by increasing the amount of dry friction. Hence, it can be concluded that the dry friction in the system can be used as a stabilizing parameter at the cost of a decrease in the dynamic accuracy.

6.2.2 Effect of Cross-Sectional Area of the Piston

The cross-sectional area of the piston is found to have a greater influence on both the dynamic accuracy and the stability of the system. The simulation shows that a decrease in the cross-sectional area of the piston increases the stability and decreases the dynamic accuracy. It is also seen that for large values of the cross-sectional area, the system becomes unstable. The above phenomena result from the dependency of the cross-sectional area of the piston on the hydro-mechanical stiffness of the system. The relationship between the cross-sectional area of the Piston A and the hydro-mechanical stiffness C_h is given in Appendix VI. It is seen from this relation that a decrease in the cross-sectional area of the piston decreases the value of C_h. Since a decrease in C_h increases the total error according to equation (2.6), the dynamic accuracy is decreased. For a stable system, it is shown in Appendix VI that the hydro-mechanical stiffness should be less than the product of the reciprocal of the kinematic gain and the hydraulic stiffness. Hence, a decrease in the cross-sectional area increases the

system stability.

By increasing the cross-sectional area, the value of C_h increases and hence the dynamic accuracy of the system increases. From the stability point of view, the system will be stable for an increase in the cross-sectional area until the condition $C_h < (\frac{1}{K_g})C_o$ is satisfied, but becomes unstable for those values of the cross-sectional area for which the above condition is violated. In the case of instability due to the above phenomenon, it is found that the system can be stabilized by increasing the dry friction. Figure 27 shows the value of the total error zone Δ_e and the amount of dry friction F_w at the stability border for changes in the cross-sectional area of the piston. It is seen that, however, the system can be stabilized by increasing dry friction, the damped transients in the response diminish only by increasing the damping in the stylus system. Error plots describing the above phenomenon are shown in Figure 28.

6.2.3 Effect of Inertia of the Stylus

The simulation results show that the mass moment of inertia of the stylus affects both the dynamic accuracy and the stability of the system. It is found that a decrease in the value of the mass moment of inertia I_m increases the dynamic accuracy and stability. This is due to the fact that decreasing I_m decreases the amplitude of the stylus

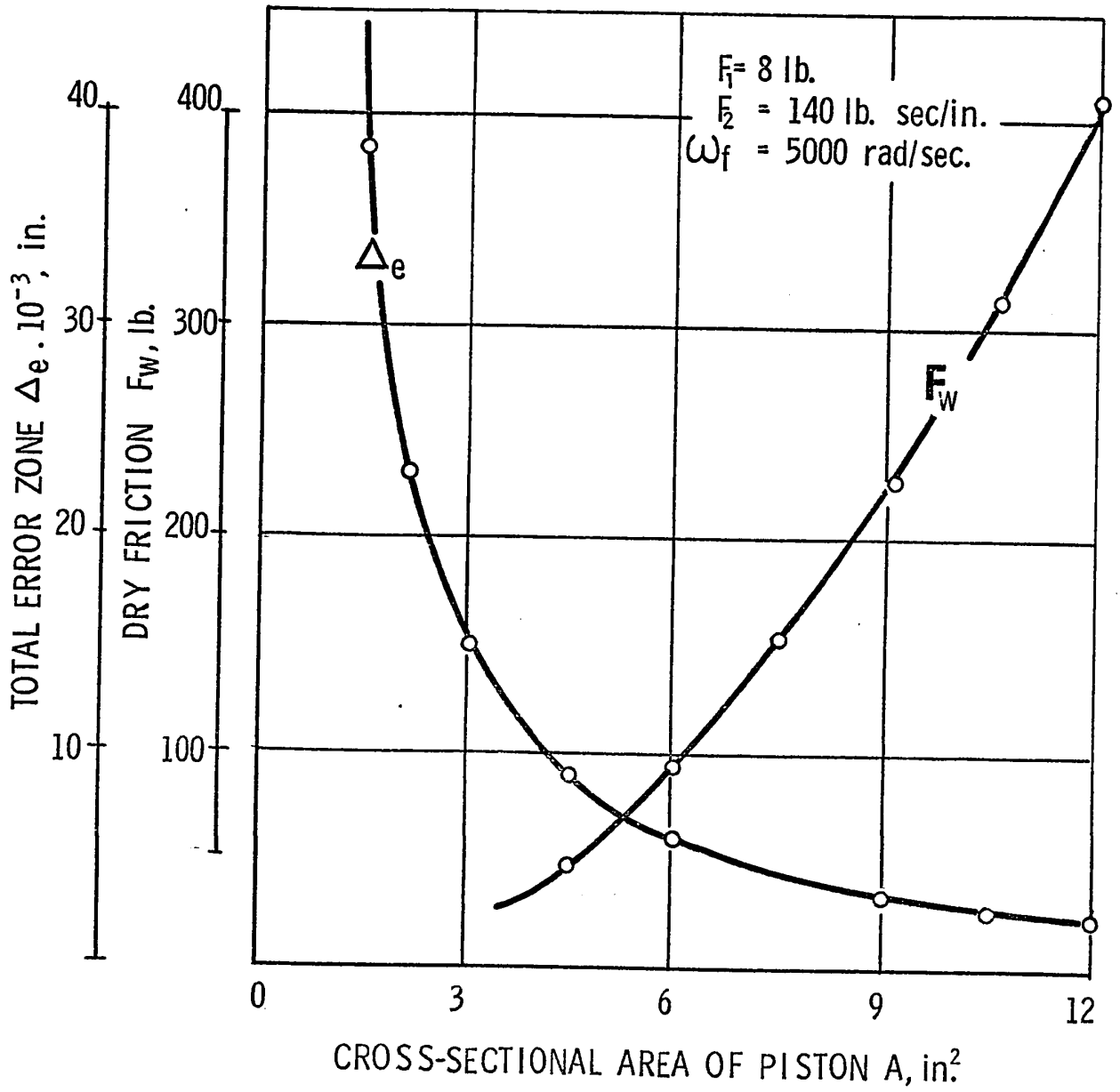

FIGURE 27 EFFECT OF CROSS-SECTIONAL AREA OF PISTON A ON Δ_e AND F_w

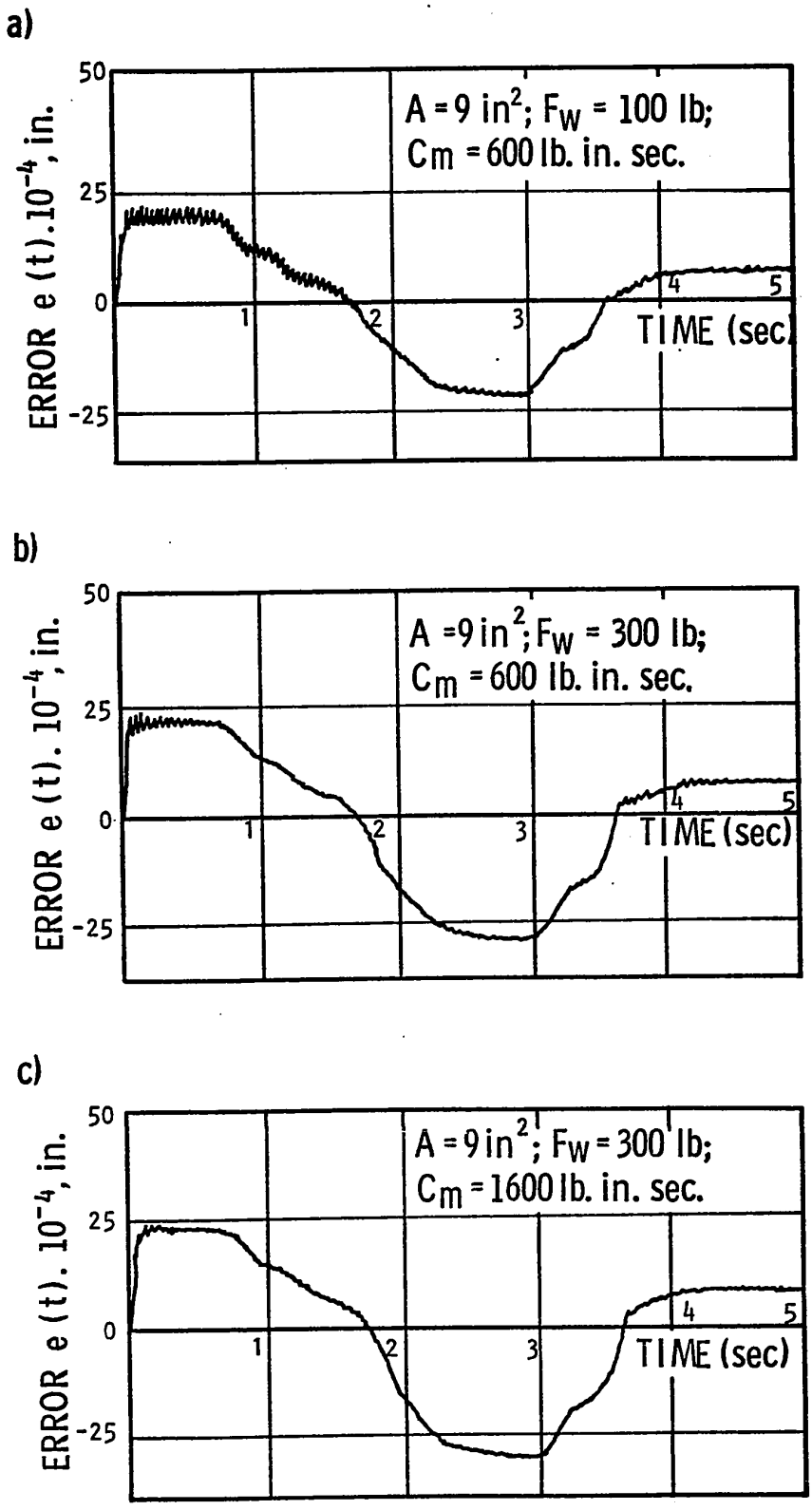

FIGURE 28 ERROR PLOTS FOR THE CROSS-SECTIONAL AREA OF THE PISTON A=9 in^2

oscillation and increases the natural frequency of the stylus system. In the case of a large value for I_m, the natural frequency of the stylus system decreases and the system becomes unstable. But the system is found to be stabilized by increasing the dry friction. Figure 29 shows the value of the total error zone Δ_e and the amount of dry friction at the stability border for any changes in the value of I_m.

6.2.4 Effect of Contact Spring in the Stylus System

To study the effect of the contact spring K_m on the dynamic accuracy and stability, the value of K_m is varied and the simulation is carried out. It is found that as the value of K_m decreases, large overshoots appear in the response due to a decrease in the value of the natural frequency of the stylus system. It is also seen that neither the dry friction nor the damping in the stylus system have any effect on these overshoots. Figure 30 shows an error plot of the system with large overshoots when the value of K_m is decreased to 4×10^4 lb/in. When the value of K_m is increased both the dynamic accuracy and the stability increases and the plot relating the total error zone Δ_e and the value of the stiffness K_m is shown in Figure 31.

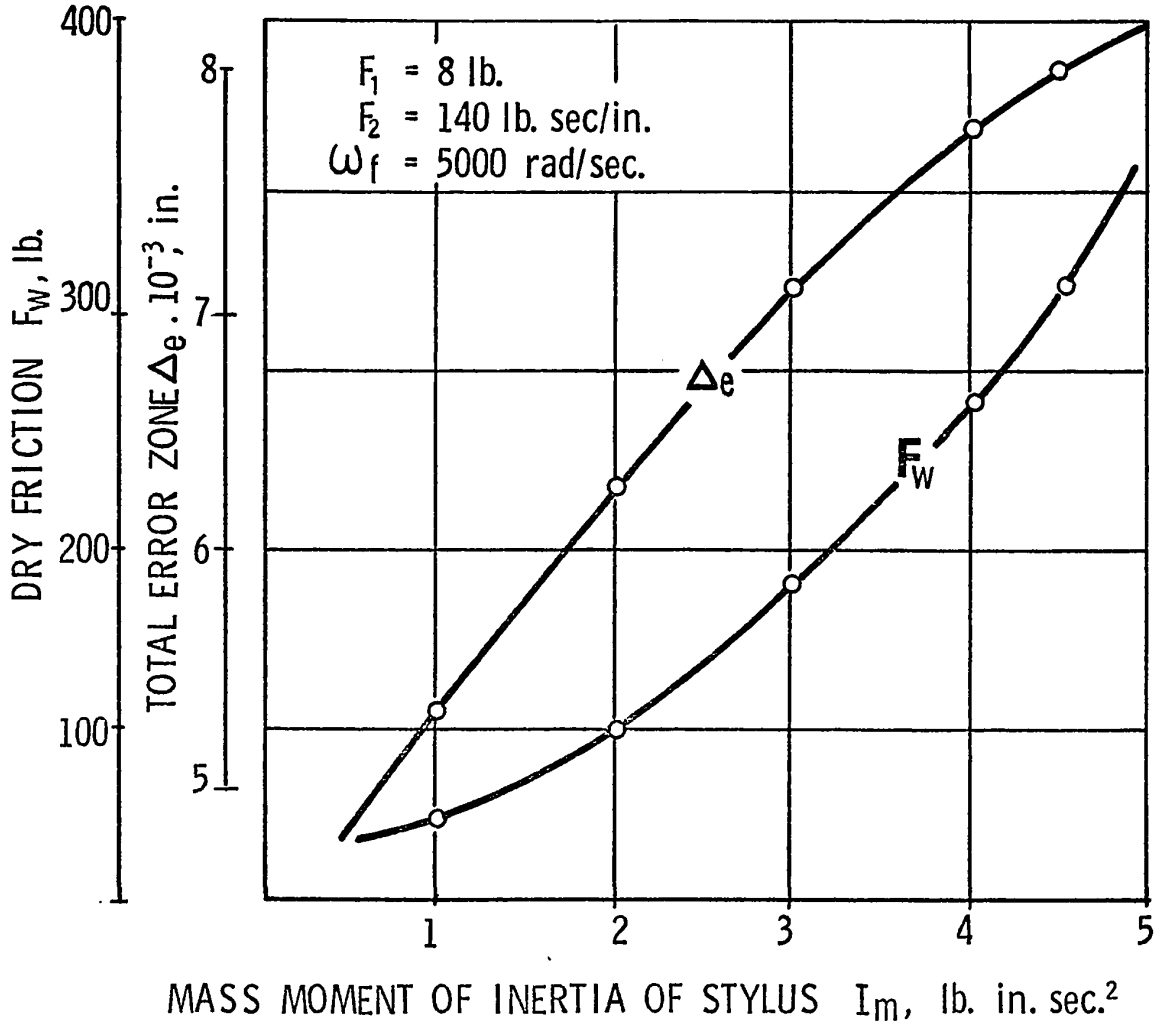

FIGURE 29 EFFECT OF MASS MOMENT OF INERTIA OF STYLUS I_m ON Δ_e AND F_W

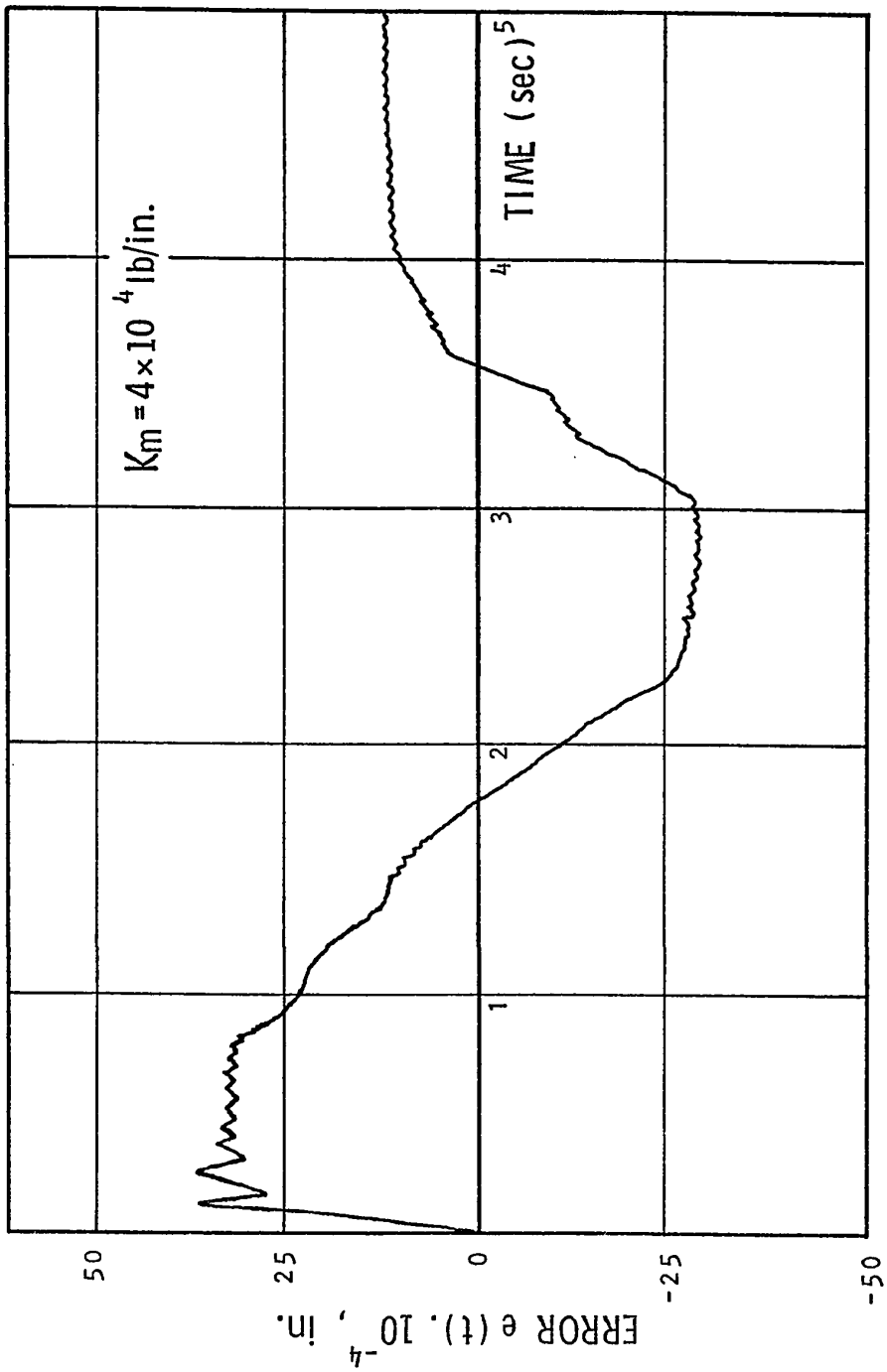

FIGURE 30 ERROR PLOTS FOR THE CONTACT SPRING STIFFNESS $K_m = 4 \times 10^4$ lb/in.

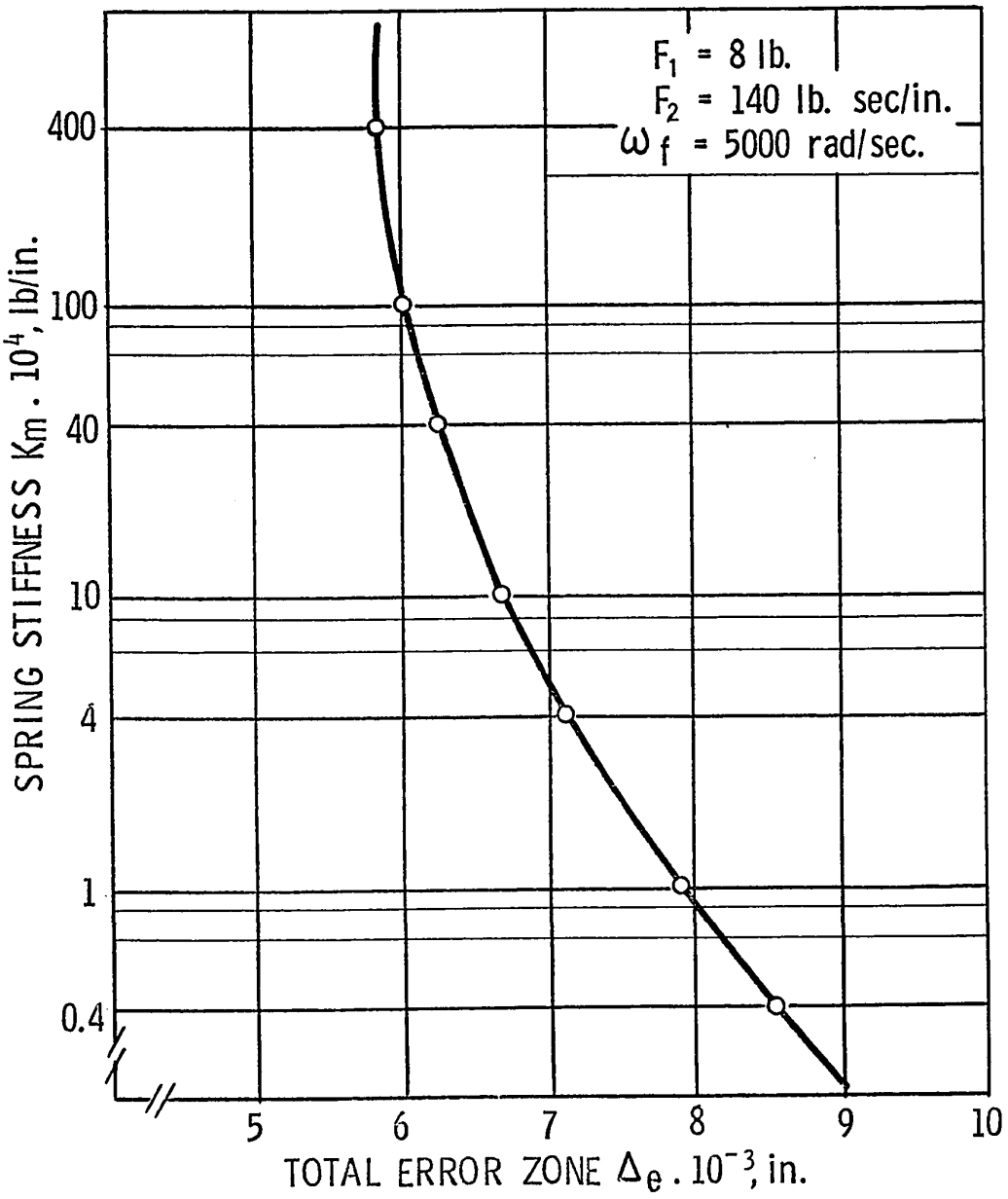

FIGURE 31 EFFECT OF SPRING STIFFNESS K_m ON THE TOTAL ERROR ZONE Δ_e

6.2.5 Effect of Spring Stiffness K_s

Analog computer simulation shows that the stiffness K_s of the spring between the spool valve and the slide has very little effect on the dynamic accuracy. However, it is noticed that for large values of K_s ($K_s > 10^3$ lb/in. , small amplitude limit cycle oscillations of the order of 10^{-4} in. are introduced in the response. But it is found that by increasing the dry friction by a small amount (F_w = 100 lb. to F_w = 120 lb.), these oscillations disappear. Hence, it can be concluded that both the dynamic accuracy and stability of the system decrease by a small amount at large values of K_s and has negligible effect while K_s is small.

6.2.6 Effect of Initial Spring Force λ_k

The response of the system from the simulation shows that the initial spring force λ_k has no influence on the stability and on the total error zone Δ_e of the system. However, it is noted from the error plots of the system that an increase in the initial spring force λ_k decreases the steady state error in copying an up-profile (cutting tool moves away from workpiece) and increases the steady state error while copying a down-profile (cutting tool moves towards the workpiece axis). This can be explained from the fact that the initial spring force aids the motion of the copying slide in copying an up-profile and opposes the motion

while copying a down-profile. Table 1 shows the steady-state errors Δ_1 and Δ_2 during copying an up- and a down-profile for different values of λ_k.

6.2.7 Effect of Kinematic Gain K_g

The simulation results show that the kinematic gain K_g influences both the dynamic accuracy and the stability of the system. It is found that the dynamic accuracy increases while increasing the kinematic gain but decreases the stability. In order to explain this phenomenon, describe the copying system as a feedback control system. Now to obtain the transfer function of the system, consider the linearized equation (3.20) in Chapter III and assume that the initial spring force and the cutting forces are negligible. Now divide throughout the equation by A^2; then it becomes

$$a'_3\frac{d^3z}{dt^3} + a'_2\frac{d^2z}{dt^2} + a'_1\frac{dz}{dt} + a'_0 z = a'x + b'_0\frac{dx}{dt} \qquad (6.1)$$

where

$$a'_3 = \frac{a_3}{A^2}$$

$$a'_2 = \frac{a_2}{A^2}$$

$$a'_1 = \frac{a_1}{A^2}$$

$$a'_o = \frac{a'_o}{A^2}$$

$$b'_o = \frac{b'_o}{A^2}$$

Now consider the coefficient b'_o:

$$b'_o = \frac{VK_s}{4BA^2} = \frac{K_s}{C_o}$$

where C_o = Hydraulic stiffness = $\frac{4BA^2}{V}$

(Appendix VI)

Since the hydraulic stiffness C_o is always very much greater than the restoring stiffness K_s, the term b'_o is much smaller than unity and hence can be neglected.

Now using the Laplace transform, the equation (6.1) becomes:

$$(a'_3 s^3 + a'_2 s^2 + a'_1 s + a'_0)\ z(s) = a'_0 x(s) \qquad (6.2)$$

where

$$z(s) = Lz(t) = \int_0^\infty e^{-st} z(t)\,dt$$

Rewriting equation (6.2),

$$x(s) - z(s) = \frac{s}{a'_o}(a'_3 s^2 + a'_2 s + a'_1) z(s)$$

Then the open loop transfer function is given by:

$$H_1(s) = \frac{z(s)}{x(s)-z(s)} = \frac{a'_{03}}{s(s^2+a'_{23}s+a'_{13})} \qquad (6.3)$$

where

$$a'_{03} = \frac{a'_0}{a'_3}$$

$$a'_{23} = \frac{a'_2}{a'_3}$$

$$a'_{13} = \frac{a'_1}{a'_3}$$

The closed loop transfer function of the copying system can be obtained from the open loop transfer function and is given by:

$$H(s) = \frac{z(s)}{x(s)} = \frac{H_1(s)}{1 + H_1(s)} \qquad (6.4)$$

$$= \frac{1}{1 + \frac{s}{a'_{03}}(s^2 + a'_{23} + a'_{13})}$$

Hence it can be seen from the open loop transfer function that an increase in the kinematic gain K_g increases the open loop gain a'_{03}. Since an increase in the open loop gain decreases the steady state error and the stability, it can be concluded that an increase in the kinematic gain increases the dynamic accuracy and decreases the stability. Figure 32 shows the relationship between the kinematic gain K_g and the total error zone Δ_e.

6.2.8 Effect of Leakage Coefficient

The leakage between the cylinder chambers in hydraulic copying systems acts like a damping and hence a reduction in the value of the leakage coefficient C_l below a certain value introduces instability in the system. But the use of the leakage path across the cylinder chambers, as a damping technique, introduces a large power loss through this leakage path. This power loss can result in undesirable trends, such as the introduction of seal friction in the cylinder which causes a magnification of the

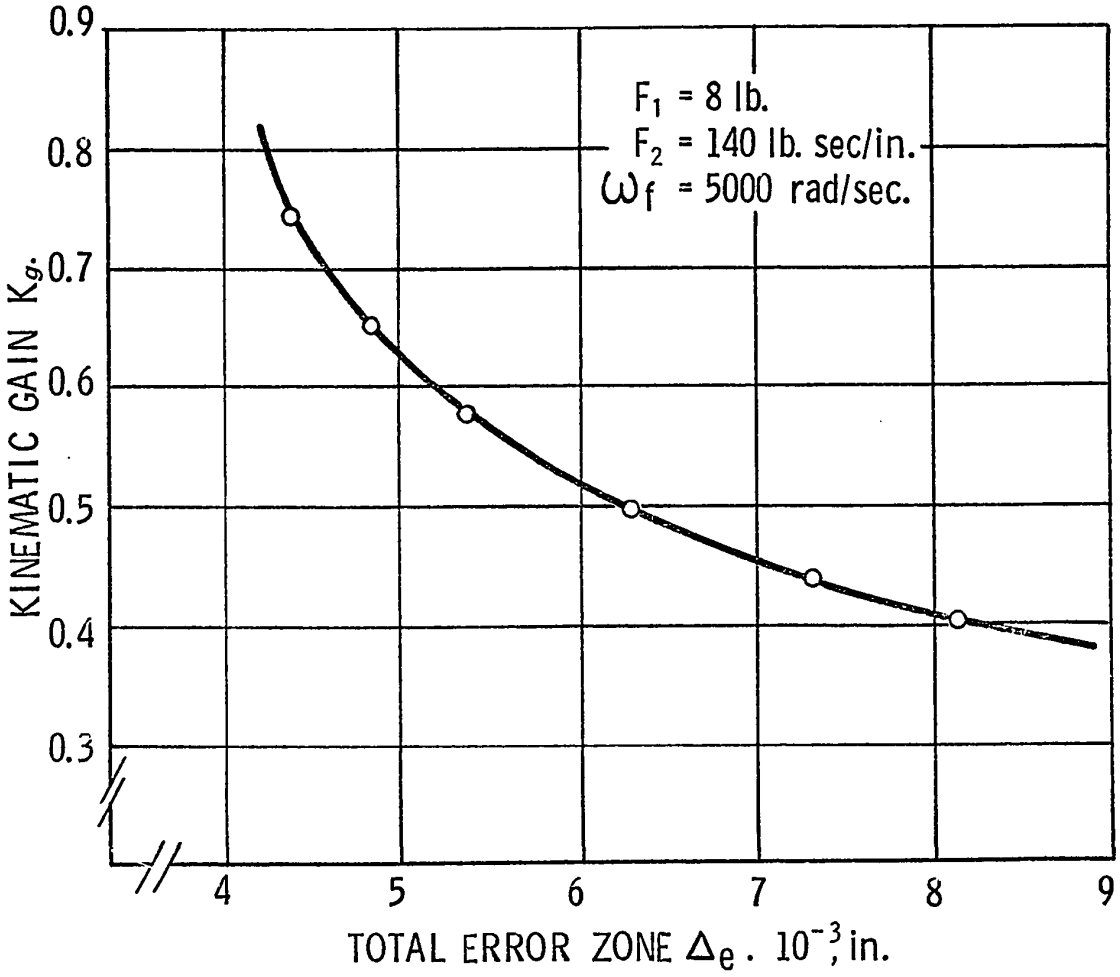

FIGURE 32 EFFECT OF KINEMATIC GAIN ON THE TOTAL ERROR ZONE

dead zone in the system and thus decreases the dynamic accuracy. Hence, an increase in the value of the laminar leakage coefficient C_l decreases the dynamic accuracy. Figure 33 shows the variation in the total error zone Δ_e for different values of C_l.

6.2.9 Effect of Supply and Exhaust Pressures

Both supply and exhaust pressures in a hydraulic copying system influence the dynamic accuracy and stability of the system. It is found that an increase in the supply pressure increases the dynamic accuracy but decreases the stability of the system. This can be explained from the relationship between the supply pressure and the hydro-mechanical stiffness C_h. It can be seen that the value of C_h increases for an increase in the supply pressure and hence increases the dynamic accuracy and decreases the system stability. Since the hydro-mechanical stiffness increases only for a decrease in the exhaust pressure, both the total error zone and the stability increase for an increase in the exhaust pressure. Figure 34 shows the variation in the total error zone Δ_e for different values of supply and exhaust pressures. From this plot it can be seen that the influence of supply pressure on the dynamic accuracy is more than that of exhaust pressure.

In hydraulic servosystems, the fluid is supplied

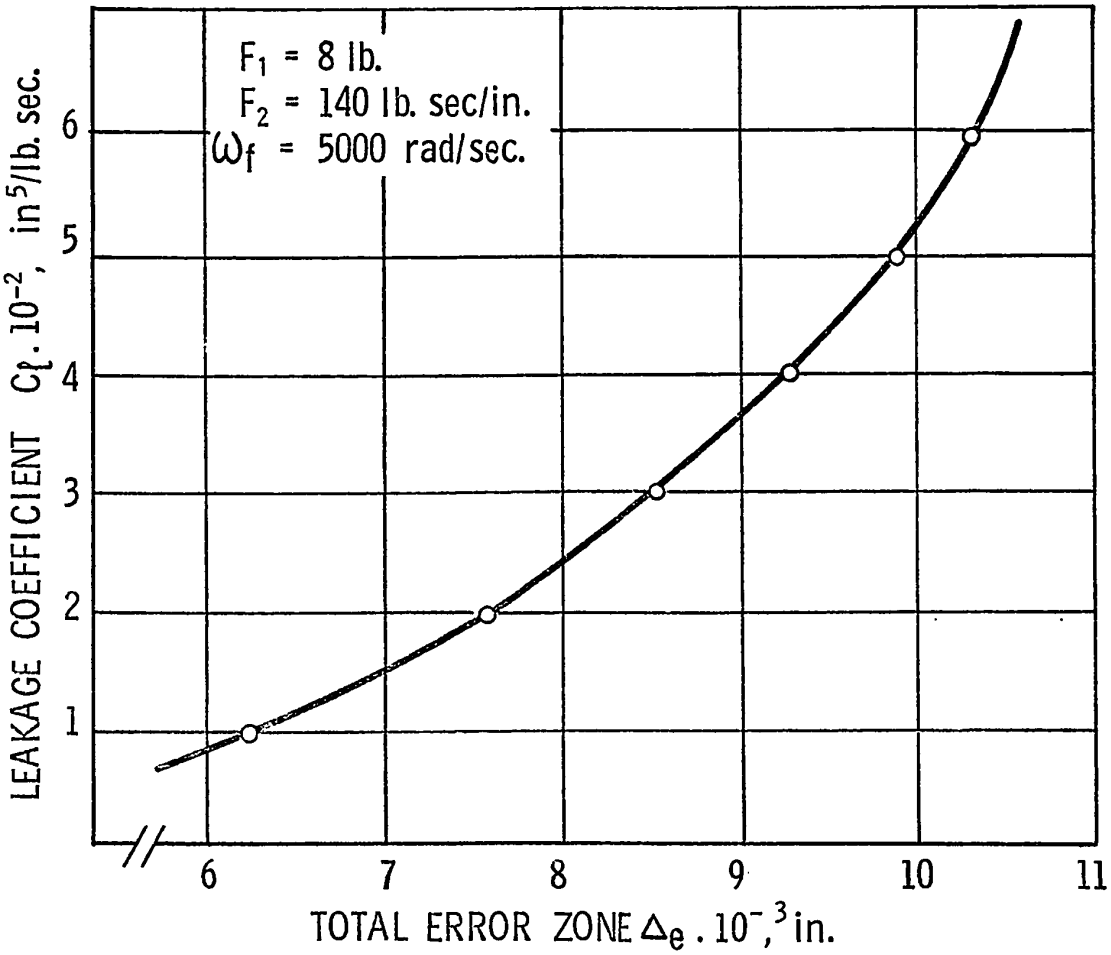

FIGURE 33 EFFECT OF LEAKAGE COEFFICIENT ON THE TOTAL ERROR ZONE

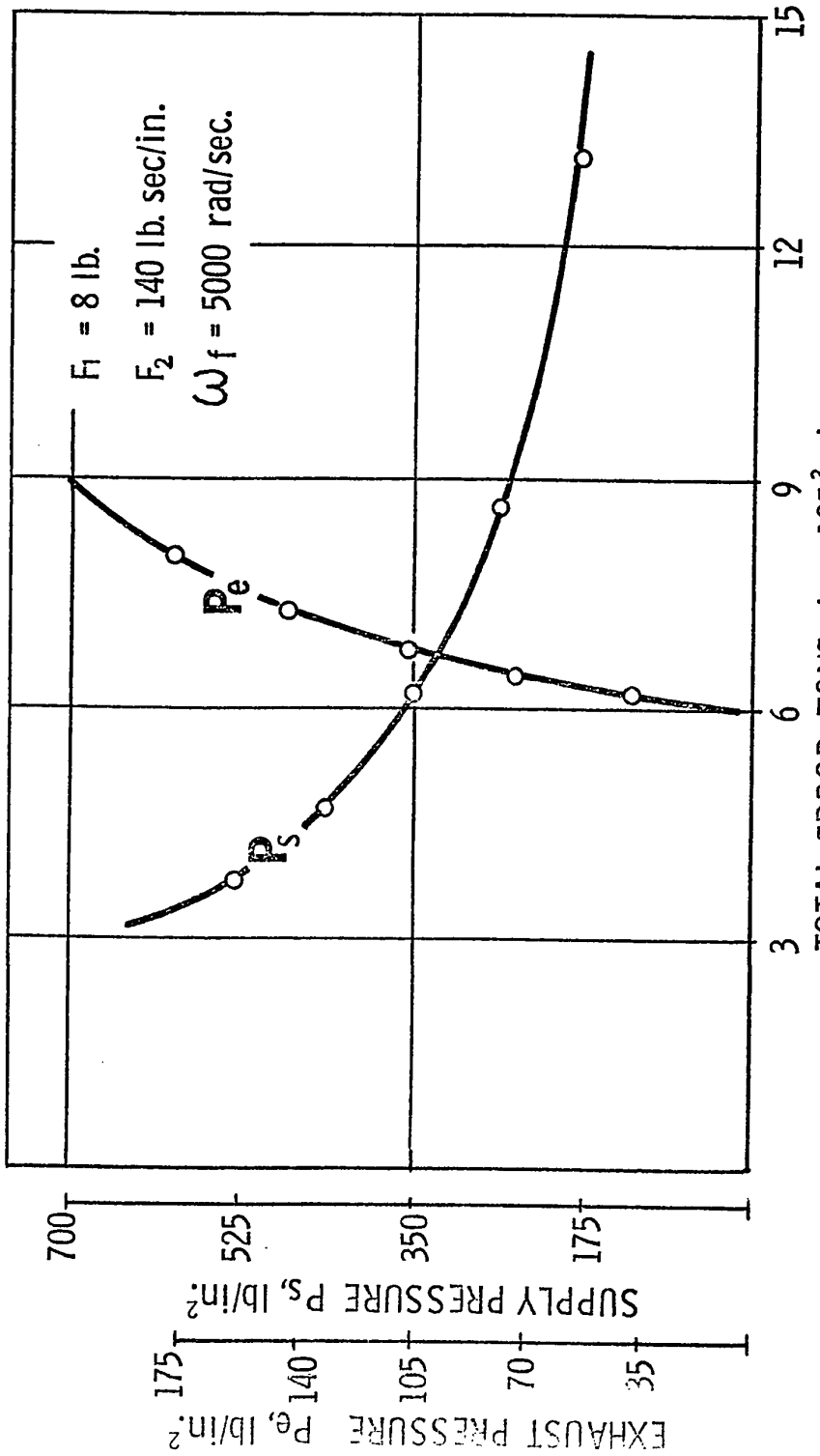

FIGURE 34 EFFECT OF SUPPLY AND EXHAUST PRESSURES ON THE TOTAL ERROR ZONE

usually by a gear, vane or piston pumps. In most hydraulic copying systems, only a gear pump is used. It consists of two meshing external gears and run inside an oil-tight casing to supply fluid up to 1500 lb/in^2 pressure. The delivery of oil with straight-toothed gears is not entirely uniform or pulsation-free. This shortcoming, however, is small as compared to a vane or a piston pump. Hence, in order to study the effects of these pulsating delivery on the reproduction of the workpiece in hydraulic copying systems, a sinusoidal signal with frequency ω_{f_o} superimposed over a mean supply pressure P_s is chosen to represent the pulsating delivery pressure. Under this assumption, the pulsating delivery pressure P_p is defined as:

$$P_p = P_s(1 + \varepsilon_o \sin\omega_{f_o} t) \tag{6.5}$$

where ω_{f_o} is the fluctuating frequency of the pulsating delivery pressure

ε_o is the non-dimensional ratio of the magnitude of the fluctuating pressure to the mean value.

The simulation of the hydraulic copying system with this pulsating delivery pressure show that at higher frequencies ($\omega_{f_o} > 500$ rad/sec) the coefficient ε_o has negligible

effect on both the dynamic accuracy and the stability of the system. But it is found that at lower frequencies ($\omega_{f_o} < 500$ rad/sec), both the stability and the dynamic accuracy are affected even for small values of ε_o. Figure 35 shows the error plots of the system for supply pressure pulsation over a range of three decades of frequency. It can be seen from these plots that both the dynamic accuracy and stability decrease as the fluctuating frequency is decreased.

6.2.10 Influence of Other System Parameters

The simulation results also show that the mass of the spool valve m_s has very little influence on the stability of the system. An increase in the value of m_s decreases the dynamic accuracy by a small amount and further increases of the mass have no influence on the accuracy. Table 2 shows the variation in the total error zone Δ_e for an increase in the mass of the spool valve.

It is also noted from the simulation that the effective damping in the stylus system influences only the stability and has negligible influence on the dynamic accuracy. For small values of the damping, the response of the copying system is found to have large oscillations and sometimes even becomes unstable. Figures 24 and 26a show the error plots for stable and unstable response of

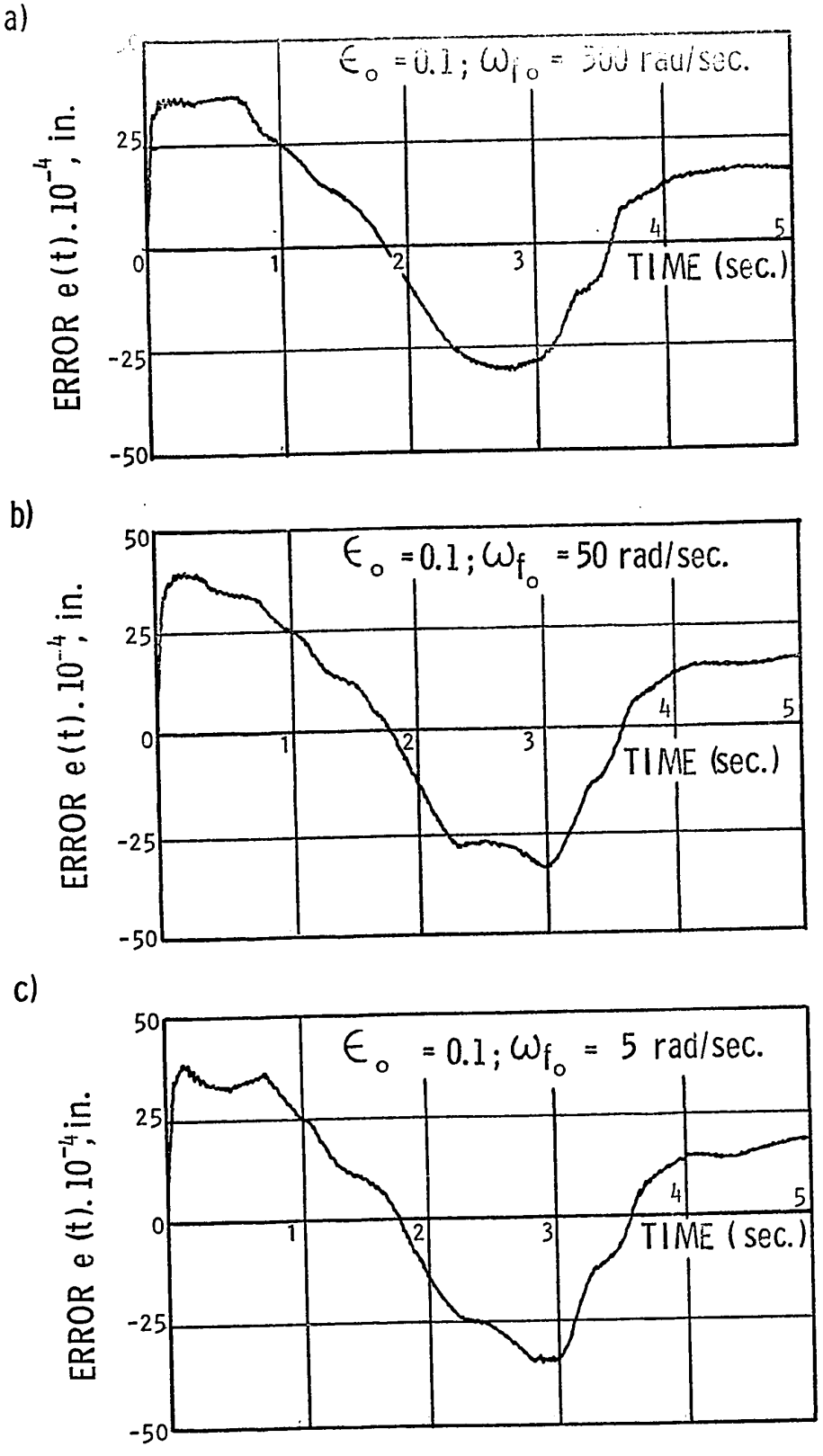

FIGURE 35 EFFECT OF SUPPLY PRESSURE PULSATION

the system when the damping coefficient C_m = 600 lb.in.sec (damping ratio ζ = 0.33) and C_m = 400 lb.in.sec (ζ = 0.22).

6.3 Effect of Dynamic Cutting Force

To simulate the actual cutting process in copying, the magnitude of the cutting forces should be properly selected. A particular cutting condition is determined by selecting proper values for F_1 and F_2; low values of F_1 and F_2 correspond to finishing operation and large values correspond to roughing operation. Figure 36 shows the effect of F_1 and F_2 on the stability of the system and the corresponding total error zone Δ_e. It can be seen that at lower values of F_1 and F_2, the system can be stabilized by increasing the dry friction F_w. This gives rise to the need of a higher value of dry friction F_w for finishing operation. Since a higher value of F_w introduces a larger total error zone Δ_e, careful selection of the amount of dry friction F_w is required.

6.4 Effect of Cutting Force Fluctuation Frequency and the Coefficient ε

To study the effect of the cutting force fluctuating frequency ω_f on the dynamic accuracy of the copying system, different values of ω_f are simulated and the error plots

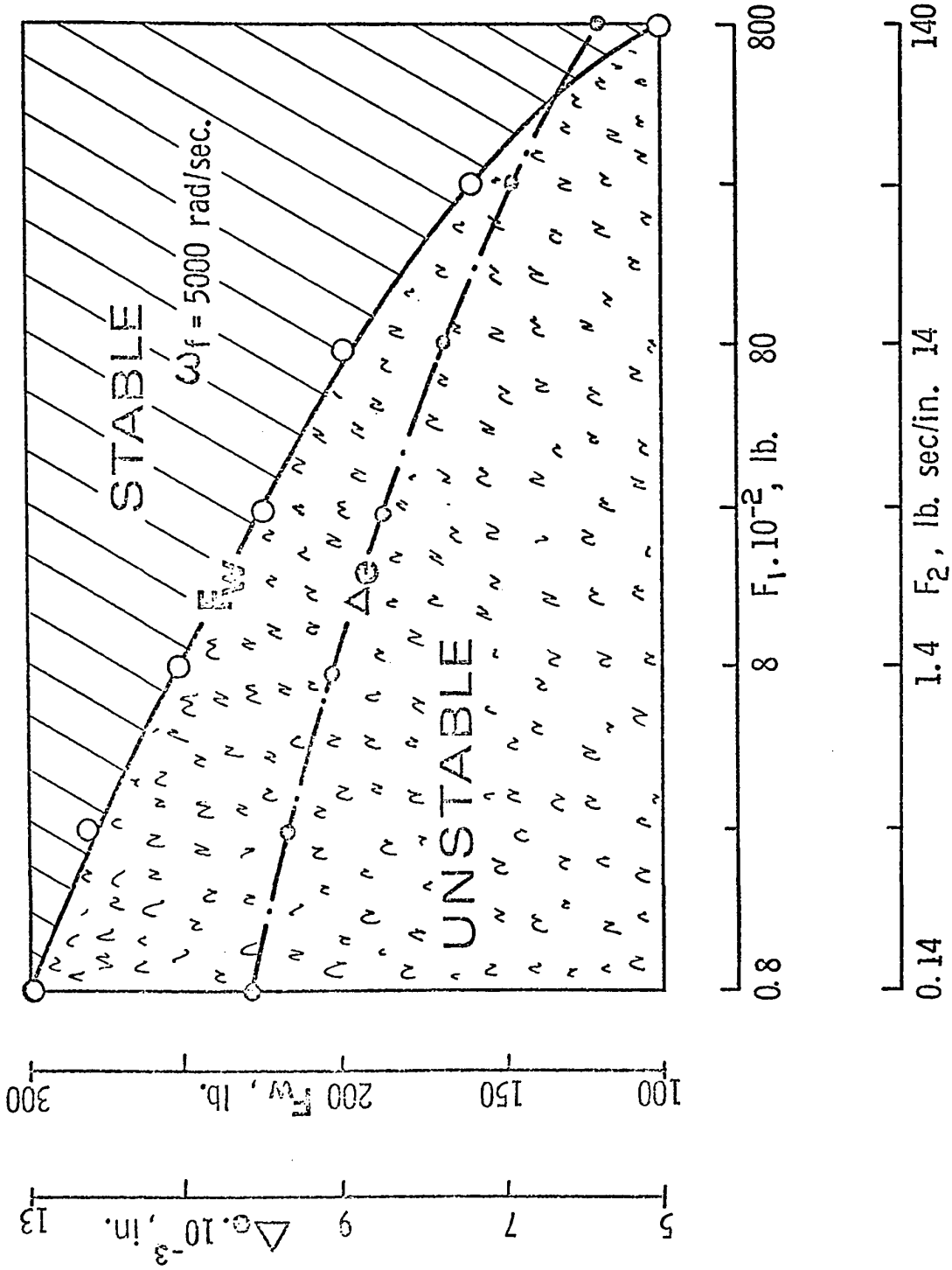

FIGURE 36 EFFECTS OF F_1 AND F_2 ON F_w AND Δ_e

for these different values are obtained as shown in Figure 37. These plots indicate that as the value of ω_f decreases, sustained oscillations are detected and a further reduction induced instability in the system. Since ω_f depends on the feed and the cutting speed in a cutting process, it can be concluded that a finishing process characterized by low feed and high cutting speed, will have a higher value of ω_f and hence the chances of instability in the finishing process due to ω_f are minimal.

Further simulution results show that the non-dimensional ratio of the magnitude of the fluctuating force to the mean value ε has negligible influence on both the stability and the dynamic accuracy of the system.

6.5 Effect of Velocity v and Angle γ

The velocity of the machine-tool slide and the angle γ between the copying and the workpiece axes influence the movement of the stylus in a hydraulic copying system. Since, in the analysis of this investigation, the input function corresponds to an actual movement of the stylus, both the velocity v and the angle γ affect the shape of the input function as seen from equation (2.29) and (2.30).

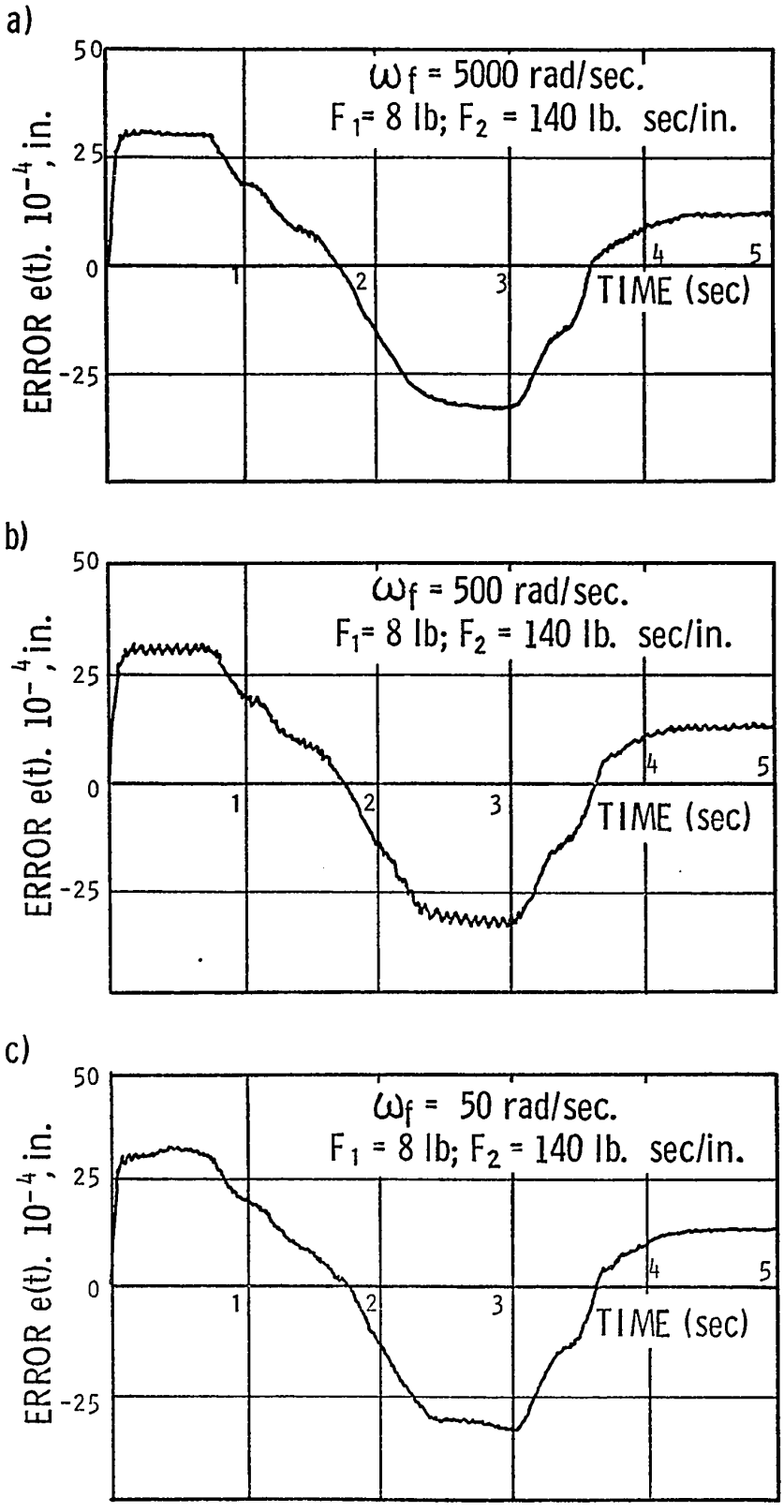

FIGURE 37 EFFECT OF ω_f ON THE ERROR FUNCTION

In order to obtain the relative effects of the velocity v and the angle γ on the stylus motion, the displacement of the stylus in time domain for various values of v and γ are evaluated and are shown in Figures 38 and 39. It can be seen that as the value of the velocity v increases, the time required for the stylus to traverse the template profile decreases, but the shape of the profile remains unaltered with the same maximum and minimum amplitudes for the stylus displacement. In the case of an increase in the value of γ, the amplitude of displacement of the stylus decreases and in addition, the traverse time also decreases. It can also be noted that the rate of change of stylus displacement decreases as the value of γ increases or the velocity v decreases.

The simulation results show that the total error zone Δ_e increases for an increase in the velocity v and for a decrease in the angle γ. Figure 40 shows the effect of the velocity v on the total error zone Δ_e for variations in the angle γ. Since, the total error zone in the workpiece diameter Δ_d depends on the angle γ as seen from equation (4.4), the effect of γ on the total error zone Δ_d is calculated and is shown in Table 3. It is seen from this table that the increase in the value of Δ_d for a decrease in γ is smaller than that of an increase in the

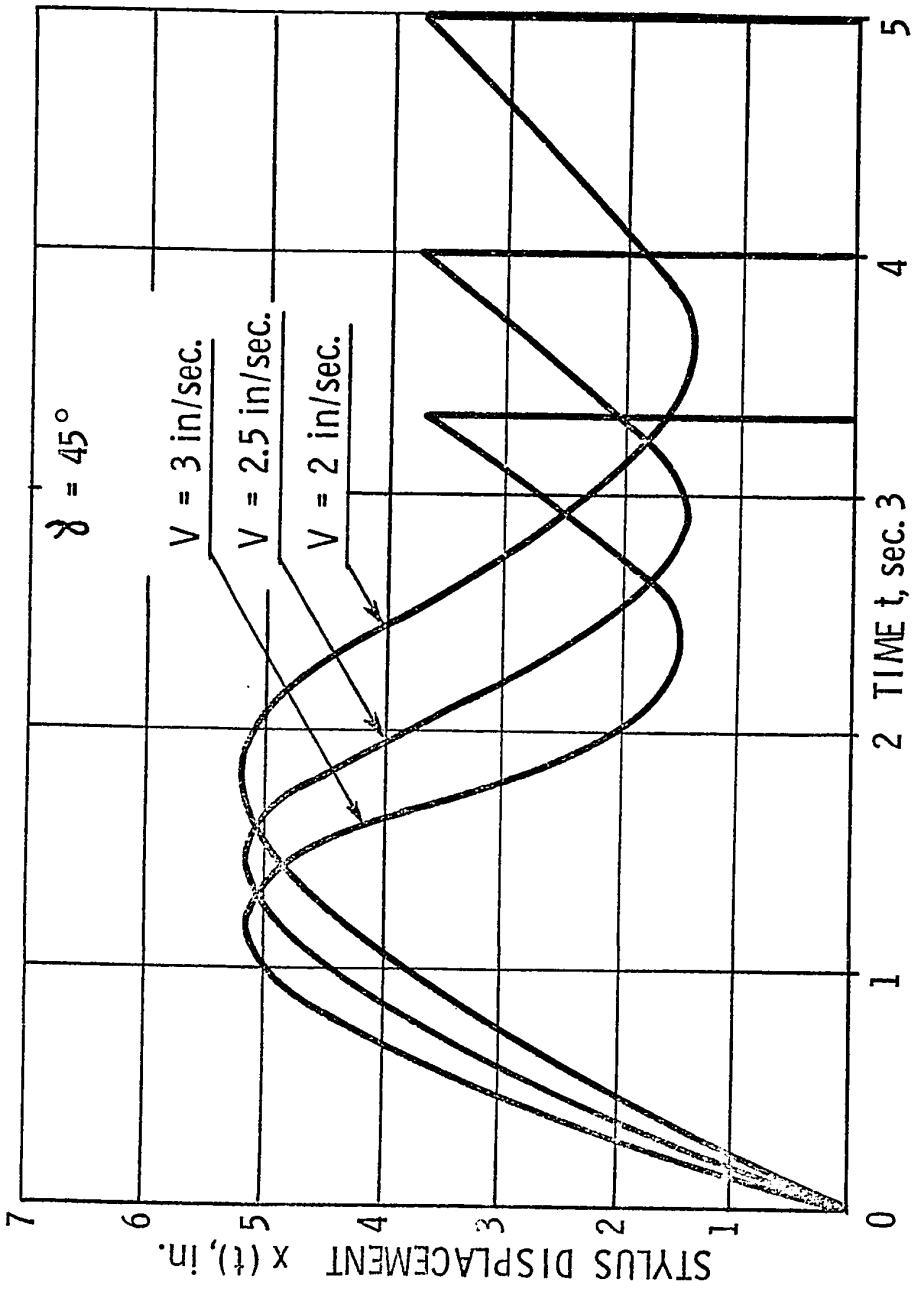

FIGURE 38 EFFECT OF VELOCITY OF SLIDE ON THE STYLUS DISPLACEMENT

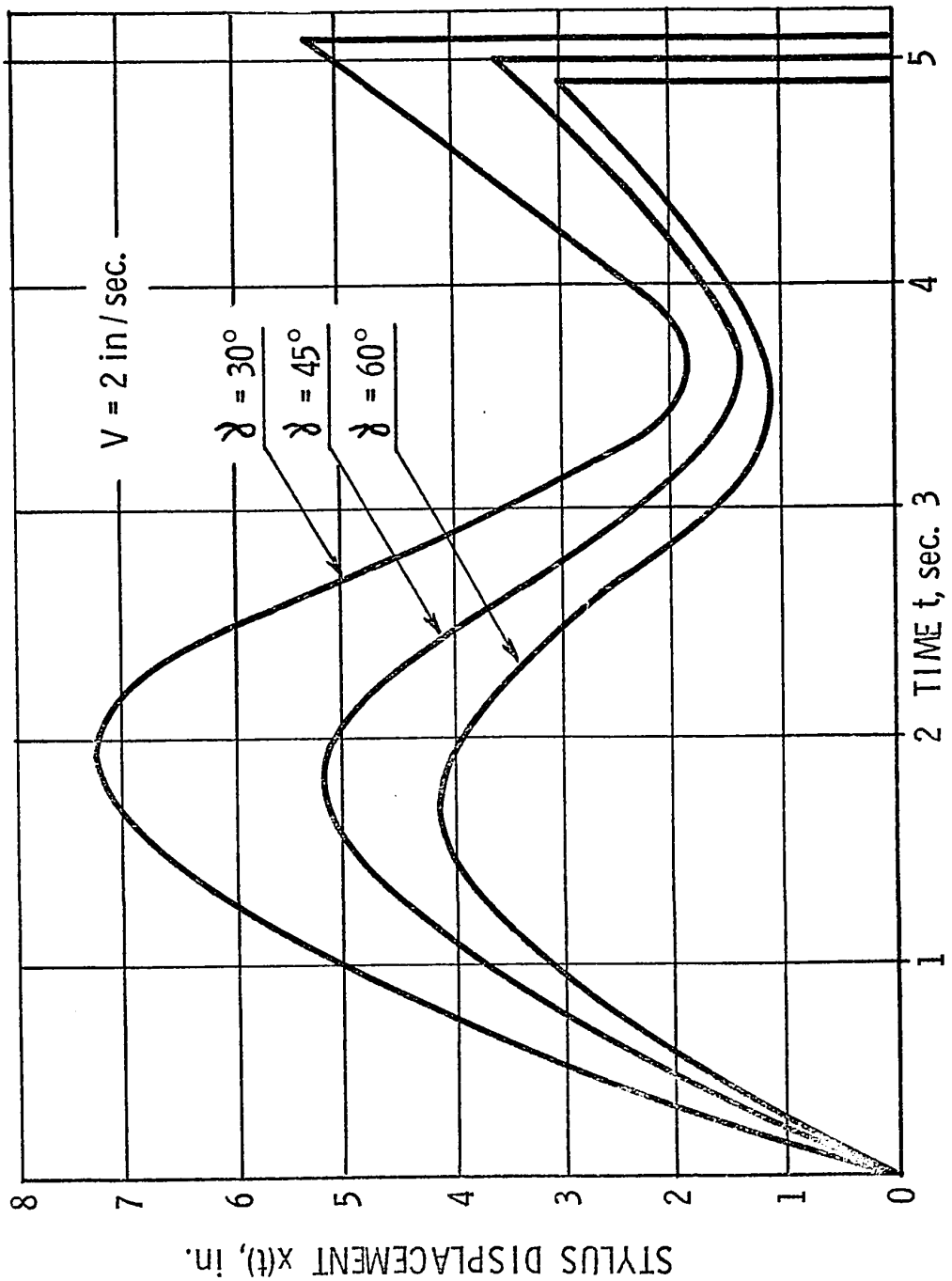

FIGURE 39 EFFECT OF ANGLE ϑ ON THE STYLUS DISPLACEMENT

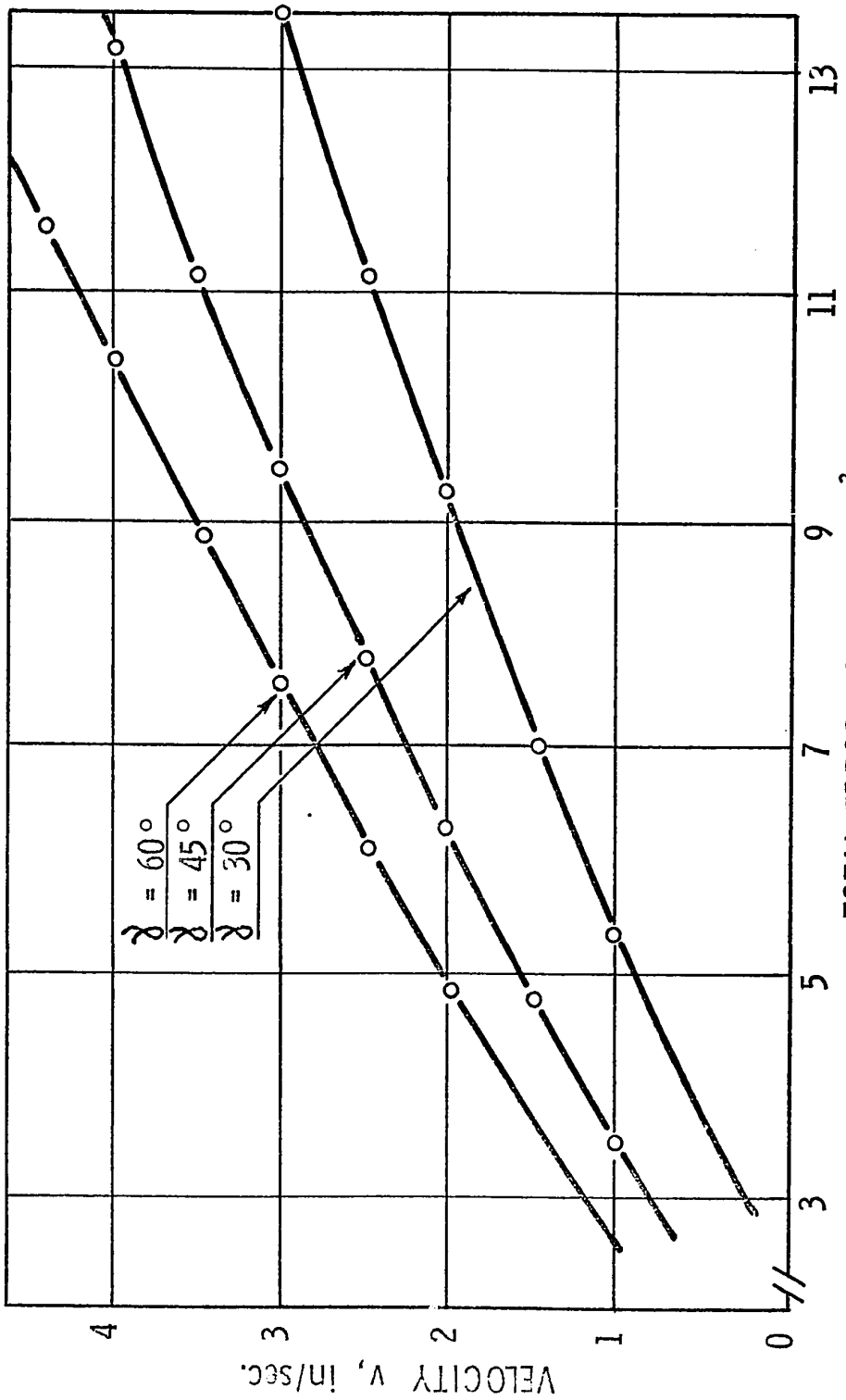

FIGURE 40 EFFECT OF VELOCITY OF SLIDE ON THE TOTAL ERROR ZONE

value of Δ_e.

6.6 Effect of Leakage Flow

The leakage flow between the cylinder chambers has been used in the past [1,12] to stabilize hydraulic servo-systems. These leakage flows are incorporated by introducing an orifice either across the piston or between the connecting passages. The flow through the orifice may be either laminar or turbulent depending on which the leakage is termed: laminar or turbulent.

In order to study the effect of leakage flow on the performance of copying, these leakage flows are simulated on the analog computer. The continuity equations represented in Chapter II are no longer valid and can be rewritten in the presence of these leakage flows as:

$$Q_1 - Q_l = A\frac{dz}{dt} + \frac{1}{B}\left(\frac{V}{2} + Az\right)\frac{dP_1}{dt} + C_l(P_1-P_2)$$

$$Q_2 - Q_l = A\frac{dz}{dt} - \frac{1}{B}\left(\frac{V}{2} - Az\right)\frac{dP_2}{dt} + C_l(P_1-P_2)$$

where Q_l = the leakage flow

= $A_o(P_1-P_2)$, in the case of a laminar leakage flow

= $C_o'\,[|P_1-P_2|]^{\frac{1}{2}}\,\mathrm{sgn}(P_1-P_2)$, in the case of a turbulent leakage flow

The simulation results show that the leakage flow stabilizes the system at the cost of a decrease in the dynamic accuracy. Figures 41 and 42 show the stabilizing effect of these leakage flows for different cutting conditions and the resulting total error zone of the system at its stability border. It can also be noted that both laminar and turbulent leakage flows introduce an equal amount of error in copying the given profile under stable operation at different cutting conditions.

Although the leakage flow has a stabilizing effect, the results of simulation show that the leakage flow does not stabilize the system from instability due to high inertia or low stiffness of the stylus. Hence, it can be concluded that the leakage flow will not cure all types of instability, but only those which arise directly from the hydraulic effects inside the unit.

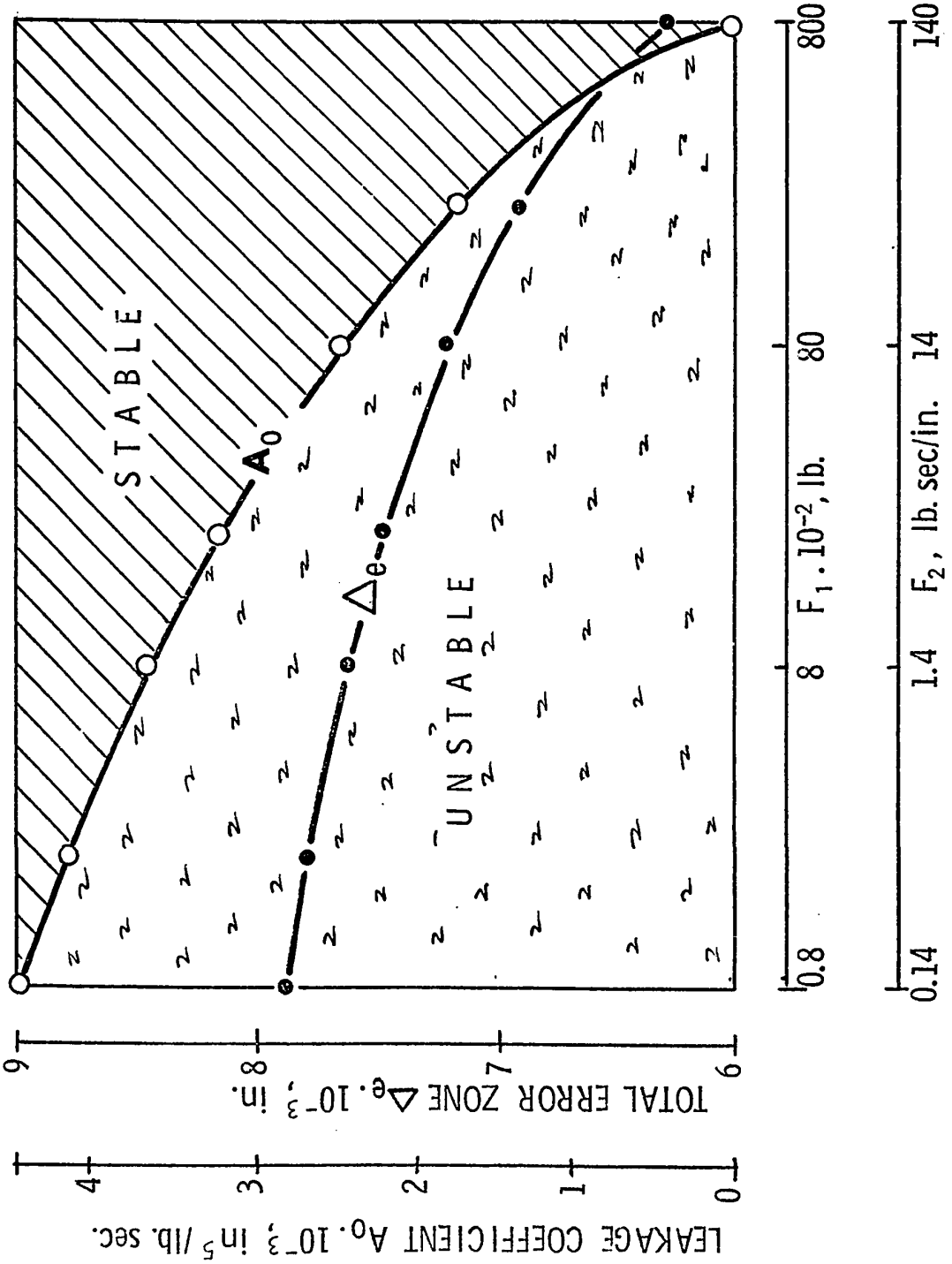

FIGURE 41 EFFECT OF LAMINAR LEAKAGE COEFFICIENT ON Δ_e AND F_w

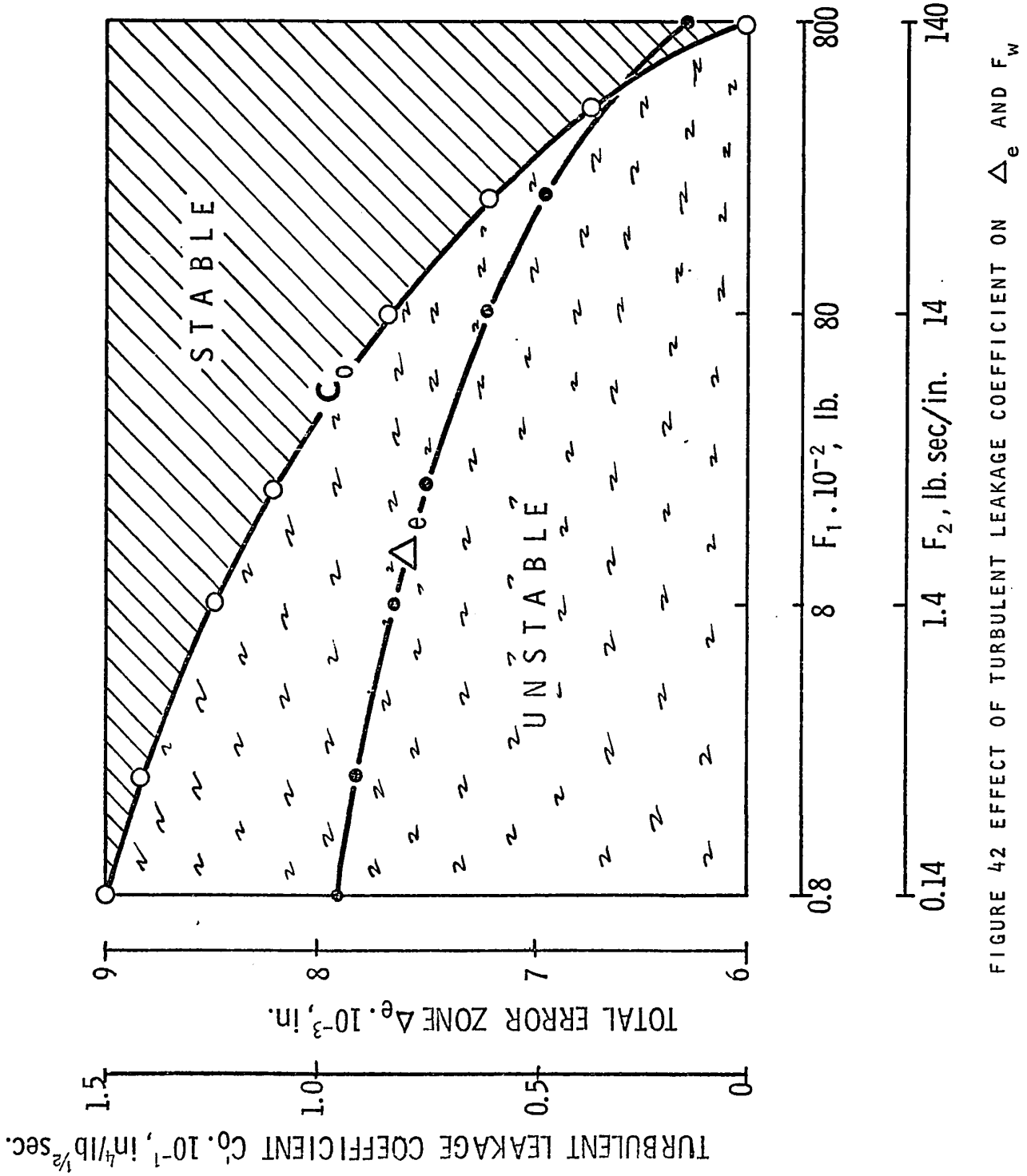

FIGURE 42 EFFECT OF TURBULENT LEAKAGE COEFFICIENT ON Δ_e AND F_w

C H A P T E R VII

CONCLUSIONS AND RECOMMENDATIONS FOR FUTURE WORK

The dynamic accuracy and stability of machine-tool hydraulic copying systems are investigated by formulating a dynamic accuracy criterion. Since the dynamic accuracy criterion is a function of the specified manufacturing tolerance of the produced workpiece, the proposed criterion gives a true account of the performance of the copying system when it is in actual operation. The dynamic accuracy is directly evaluated from the error plot of the copying system and can be easily evaluated by simulation procedures.

One of the main features of this investigation is the representation of the template configuration in the time domain which gives the actual motion of the stylus during copying. The response of the system to this input describes the shape of the produced workpiece in the time domain. This method of analysis is directly applicable in the design of any hydraulic copying system.

Based on the results of this investigation, the following conclusions can be drawn:

- stability of copying deponds to a great extent on the amount of dry friction, inertia, size, and

stiffness of the stylus, the supply pressure and the cross-sectional area of the piston.

- dry friction in the system increases the stability but decreases the dynamic accuracy.
- both dynamic accuracy and stability increase by decreasing the inertia and by increasing the stiffness of the stylus.
- increasing the supply pressure and the cross-sectional area of the piston increases the dynamic accuracy.
- dynamic accuracy increases by increasing the kinematic gain K_g but decreases the system stability.
- leakage flow increases the stability at the cost of a decrease in the dynamic accuracy.
- increasing the angle γ and decreasing the velocity v of the machine-tool slide increases the dynamic accuracy.
- decrease of the exhaust pressure increases the dynamic accuracy and decreases the stability.
- from the stability point of view, the dry friction in the system should be higher for finishing operation than for roughing operation.
- the stiffness K_s, the initial spring force λ_k and the mass of the spool valve have negligible influence on both dynamic accuracy and stability.

- dynamic accuracy and stability decrease for small values of the fluctuating frequency of the supply pressure ω_{f_o} and the cutting force fluctuating frequency ω_f.
- laminar and turbulent leakage flow will stabilize only those instability that arise directly from the hydraulic effects inside the system.

The results also provide some useful information on:

- control of stability of existing devices.
- optimization of existing copying devices for maximum dynamic accuracy under stable operation.

For future investigation in the area of hydraulic copying systems, the following suggestions are made:

- investigation to study the effects of fluid inertance and resistance in the flow passages and the effects of different kinds of control valves on the dynamic accuracy and stability.
- experimental investigation to study the parametric changes in the system and the practical implementation for controlling the amount of dry friction.
- investigation of dynamic accuracy and stability of hydraulic copying systems with hydrodynamic and hydrostatic lubrication in the slideways.
- investigation of dynamic accuracy and stability

of multi-dimensional copying systems with automatic feed control using the methods developed in this thesis.

- investigation to study the Stick-Slip phenomenon in the machine-tool slide.

TABLE 1

EFFECT OF INITIAL SPRING FORCE λ_k ON

THE STEADY STATE ERROR

INITIAL SPRING FORCE λ_k, lb	STEADY STATE ERROR	
	UP-PROFILE $\Delta_1 \cdot 10^{-3}$, in.	DOWN-PROFILE $\Delta_2 \cdot 10^{-3}$, in.
10	3.05	3.20
20	2.95	3.30
40	2.75	3.50
60	2.60	3.65
80	2.45	3.80

TABLE 2

EFFECT OF MASS OF SPOOL VALVE ON

THE TOTAL ERROR ZONE

MASS OF SPOOL VALVE $m_s \cdot 10^{-3}$, lb·sec²/in.	TOTAL ERROR ZONE $\Delta_e \cdot 10^{-3}$, in.
1.5	6.25
15	6.50
150	6.50
1500	6.50

TABLE 3

EFFECT OF ANGLE γ ON THE TOTAL

ERROR ZONE OF THE WORKPIECE DIAMETER

ANGLE γ, deg.	TOTAL ERROR ZONE $\Delta_d \times 10^{-3}$, in.
30	9.4
45	9.2
60	8.5

REFERENCES

1. Harpur, N.F., "Some Design Considerations of Hydraulic Servos of Jack Type," Proceedings of Conference on Hydraulic Servomechanisms, Institution of Mechanical Engineers, London, 1953.

2. Thomasson, R.K., "Stability of Jack Type Power Control," Aircraft Engineering, Vol. 34, July 1962, pp. 198-204.

3. Lambert, T.H., and Davies, R.M., "Investigation of the Response of a Hydraulic Servomechanism with Inertial Load," Journal of Mechanical Engineering Science, Vol. 5, No. 3, Sept. 1963.

4. Glaze, S.G., "Analog Technique of Non-Linear Jack Servomechanism," Proceedings of Symposium on Recent Mechanical Engineering Developments on Automatic Control, Institution of Mechanical Engineers, London, 1960, pp. 178-188.

5. Parnaby, J., "Electronic Analogue Computer Study of Non-Linear Effects in a Class of Hydraulic Servomechanism," Journal of Mechanical Engineering Science, Vol. 10, No. 4, 1968, pp. 346-359.

6. Royle, J.K., "Inherent Non-Linear Effects of Hydraulic Control Systems with Inertial Loading," Proceedings of the Institution of Mechanical Engineers, London, Vol. 173, No. 9, 1959.

7. Davies, R.M., "Analytical Design for Time Optimum Transient Response of Hydraulic Servomechanisms," Journal of Mechanical Engineering Science, Vol. 7, No. 1, 1965, pp. 8-14.

8. Urata, E., "The Ramp Response of a Loaded Hydraulic Servomechanism," Bulletin of the Japan Society of Mechanical Engineers, Vol. 13, No. 64, 1970, pp. 1172-1181.

9. Martin, K.F., "Stability and Step Response of Hydraulic Servo with Special Reference to Unsymmetrical Oil Volume Conditions," Journal of Mechanical Engineering Science, Vol. 12, No. 5, 1970, pp. 331-338.

10. Ito, T., Muto, T., Kano, S., and Hattori, M., "Study

on the Instability in a Loaded Hydraulic Servomechanism," Bulletin Japan Society of Mechanical Engineers, Vol. 13, No. 63, 1970, pp. 1066-1075.

11. McCloy, D., and Martin, H.R., "Some Effects of Cavitation and Flow Forces in the Electro-Hydraulic Servomechanism," Proceedings of the Institution of the Mechanical Engineers, London, Vol. 178, No. 21, 1963-64.

12. McCloy, D., "Some Effects of Oil Compressibility and Valve Lap on the Performance and Stability of the Hydraulic Servomechanism," Ph.D. Thesis, Queen's University, Belfast, 1964.

13. Montgomery, J., and Lichtarowicz, A., "Asymmetrical Lap and Other Non-Linearities in Valve-Controlled Hydraulic Actuators," Proceedings of the Institution of Mechanical Engineers, London, Vol. 183, No. 33, 1968-69.

14. Enyon, G.T., "Developments in High Performance Electro-Mechanical Servomechanisms at the Royal Aircraft Establishment, Farnborough," Proceedings of the Institution of Mechanical Engineers, London, No. 93, 1960.

15. Bell, R., and dePennington, A., "Active Compensation of Lightly Damped Electrohydraulic Cylinder Drives Using Derivative Signals," Proceedings of the Institution of Mechanical Engineers, London, Vol. 184, No. 4, 1969-70.

16. Davies, A.M., and Davies, R.M., "Nonlinear Behavior, Including Jump Resonance, of Hydraulic Servomechanisms," Journal of Mechanical Engineering Science, Vol. 11, No. 3, 1969, pp. 281-289.

17. Chiappulini, R., "Sur la Stabilité Dynamique des Hydrocopieurs avec Rétro-action et Appui de Faible Rigidité," Annals of the C.I.R.P., Vol. 15, 1967, pp. 129-135.

18. Chiappulini, R., "Équipements Hydrauliques de Copiage pour les Machines-Outils," La Technique Moderne, Vol. 49, 1957, pp. 1-8.

19. American Society of Tool and Manufacturing Engineers, Tool Engineers Hand Book, Second Edition, McGraw-Hill, Inc., New York, 1959, pp.20:16-20:23.

20. Bickel, E., "Die Wechselnden Kräfte bei der Spanbildung," Annals of the C.I.R.P., Vol. 12, 1963, pp. 205-212.

21. Rakhit, A.K., Osman, M.O.M., and Sankar, T.S., "The Effects of Stochastic Response of Machine-Tool-Workpiece System on the Formulation of Surface Texture in Turning," To be presented at the ASME Vibrations Conference, Cincinnati, Sept. 1973.

22. Zahor, I., "Copy-System on Czechoslovak Machine Tools," Czechoslovak Heavy Industry, No. 3, 1957, pp. 28-33.

23. Viersma, T.J., "Investigations into the Accuracy of Hydraulic Servomotors," Ph.D. Thesis, Technological University, Delft, April 1961.

24. Osman, M.O.M., "The Response of a Machine Tool Copying System to Dynamic Tool Loading," Technological Report 71-11, Sir George Williams University, Canada.

25. Brown, R.H., and Armarego, E.J., "Oblique Machining with a Single Cutting Edge," International Journal of Machine Tool Design and Research, Vol. 4, 1964, pp. 2-25.

26. Merritt, H.E., Hydraulic Control Systems, John Wiley & Sons, Inc., New York, 1967.

27. Khaimovich, E.M., Hydraulic Control of Machine Tools, Pergamon Press, London, 1965.

28. Lenssen, P., "The Influence of Dry Friction and Mechanical Parameters on the Stability and Accuracy of an Hydraulic Copying System," International Journal of Machine Tool Design and Research, Vol. 10, 1970, pp. 65-78.

29. Mansour, W.M., Osman, M.O.M., and Gladwell, G.M.L., "Stability and Kinematic Accuracy of Hydraulic Copying Mechanisms in Metal Cutting," Journal of Engineering for Industry, Trans. ASME, Series B (in press).

30. Sankar, S., and Osman, M.O.M., "On the Dynamic Accuracy of Machine-Tool Hydraulic Copying Systems," to be presented at the ASME Vibrations Conference, Cincinnati, Sept. 1973, and also to be published in ASME Transactions.

31. Zeleny, J., "Stability of Hydraulic Copying-Systems," Czechoslovak Heavy Industry, No. 1, 1955.

32. Optiz, H., and Backé, W., Über die Dynamische Stabilität Hydraulischer Steuerungen unter Berucksichtigung

der Strömungskräfte, Westdeutscher, Verlag, 1964.

33. Shinners, S.M., Modern Control System Theory and Application, Addison-Wesley, Inc., California, 1972.

34. Nyquist, N., "Regeneration Theory," Bell System Technical Journal, Vol. 11, 1932.

35. Evans, W.R. "Graphical Analysis of Control Systems," Transactions of AIEE, Vol. 67, 1948.

36. "The Analysis and Performance of Electro-Hydraulic Feed Drive," Proceedings of Conference on Electro-Hydraulic Feed Drives, University of Manchester Institute of Science and Technology, Manchester, Dec. 1970.

37. Willems, J.L., Stability Theory of Dynamical Systems, Thomas Nelson Ltd., London, 1970.

38. Merchent, M.E., "Mechanics of Metal Cutting Process in Orthogonal Cutting and a Type 2 Chip," Journal of Applied Physics, Vol. 16, No. 5, May 1945, pp. 267-275.

39. Levine, L., Methods for Solving Engineering Problems Using Analog Computers, McGraw Hill, Inc., New York, 1964.

40. Ulrich, H.J., "Some Factors Influencing the Natural Frequency of Linear Hydraulic Actuators," International Journal of Machine Tool Design and Research, Vol. 11, 1971, pp. 199-207.

A P P E N D I X I

MANUFACTURERS OF HYDRAULIC COPYING SYSTEMS

A P P E N D I X I

NO.	NAME OF THE MANUFACTURER	TYPE OF COPYING SYSTEM		
		HYDRO-MECHANICAL	ELECTRO-HYDRAULIC	NUMERICALLY CONTROLLED
1.	DUPLOMATIC, ITALY	X	X	
2.	EX-CELL-O, U.S.A	X	X	X
3.	GETTYS, U.S.A	X		
4.	HARRISON, U.K.	X	X	
5.	HEPWORTH, U.K.	X	X	
6.	HYRATECH, U.S.A	X		
7.	INGERSOLL, U.S.A.	X	X	
8.	JONES & LAMSON, U.S.A	X	X	
9.	LeBLOND, U.S.A			X
10.	MIMIK, CANADA	X		
11.	OERLIKON-BÜHRLE, SWITZERLAND	X	X	X
12.	PRATT & WHITNEY, U.S.A.		X	
13.	SCAN-O-MATIC, U.S.A	X	X	X
14.	SOUTHBEND-GALLICOP, U.S.A.	X		
15.	TRUE-TRACE, U.S.A	X	X	X
16.	TURCHEON, U.S.A	X		

A P P E N D I X II

CALCULATION OF THE CUTTING FORCE F_s

A P P E N D I X II

In oblique metal cutting operations, the cutting forces can be conveniently resolved along three mutually perpendicular axes: P, Q, and R. The P-axis is chosen parallel to the cutting velocity vector, the Q-axis normal to the finished workpiece and the R-axis is defined to be perpendicular to the plane formed by the previous two directions. Figure A.1 shows the representation of the cutting forces along the three axes. Assuming a uniform stress distribution on the shear plane and the ploughing forces on the tool tip to be non-existent, the cutting force components along P, Q, and R axes are given by [25]:

$$F_p = \frac{S_s b_0 S_0}{\sin \phi_0} \cdot \frac{\cos(\beta_0-\alpha_0) + \sin\beta_0 \tan\eta_0 \tan i_0}{[\cos^2(\beta_0+\phi_0-\alpha_0) + \tan^2\eta_0 \sin^2\beta_0]^{\frac{1}{2}}} \qquad (A.1)$$

$$F_q = \frac{S_s b_0 S_0}{\sin \phi_0} \cdot \frac{\sin(\beta_o-\alpha_o) \,/\, \cos i_o}{[\cos^2(\beta_0+\phi_0-\alpha_0) + \tan^2\eta_0 \sin^2\beta_0]^{\frac{1}{2}}} \qquad (A.2)$$

$$F_r = \frac{S_s b_0 S_0}{\sin \phi_0} \cdot \frac{\cos(\beta_0-\alpha_0)\tan i_0 - \sin\beta_0 \tan\eta_0}{[\cos^2(\beta_0+\phi_0-\alpha_0) + \tan^2\eta_0 \sin^2\beta_0]^{\frac{1}{2}}} \qquad (A.3)$$

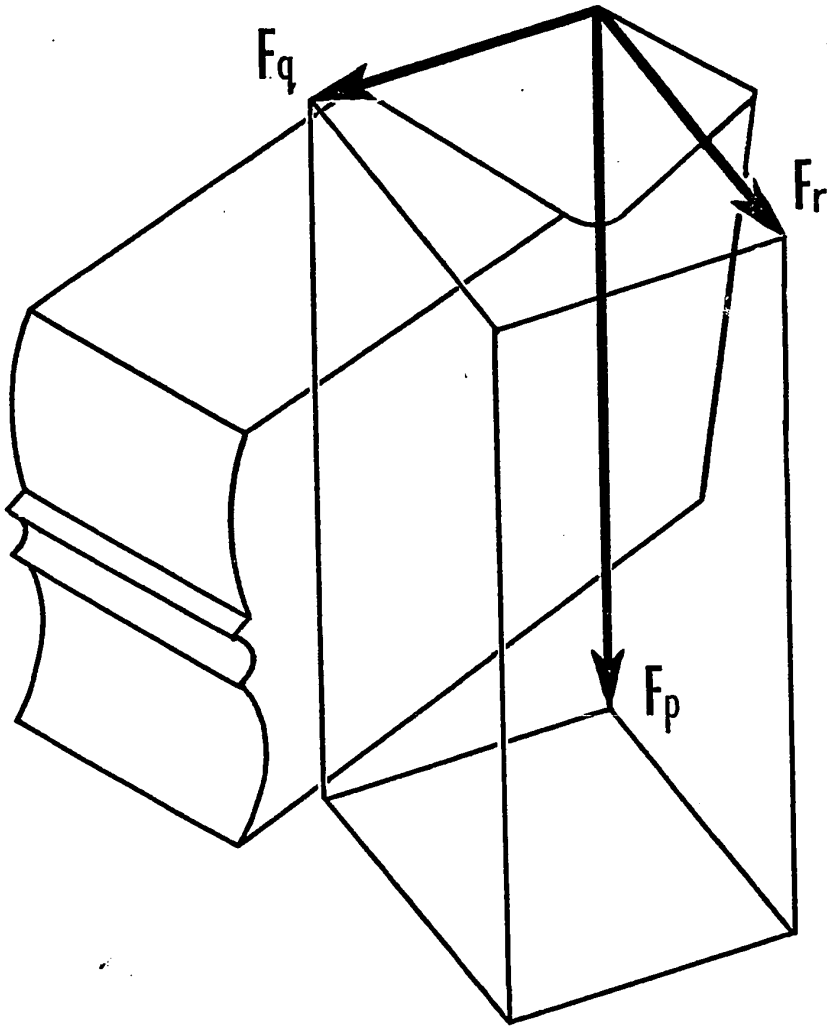

FIGURE A.1 REPRESENTATION OF CUTTING FORCE IN THREE MUTUALLY PERPENDICULAR AXES.

The shear stress S_s along the shear plane can be related to the shear strength of the material at zero normal stress S_n using Merchant's analysis [38], and be given as:

$$S_s = S_n \; / \; [1 - K_0 \tan (\beta_0 + \phi_0 - \alpha_0)] \tag{A.4}$$

where K_0 is a material constant and can be determined experimentally.

In equations (A.1) - (A.3), the angles α_0 and i_0 are usually measured from the operating conditions. It can also be assumed that $\eta_0 = i_0$ for turning operations [25]. The remaining angles β_0 and ϕ_0 can be related from the geometrical considerations of the tool and chip and are given by:

$$\tan (\beta_0+\phi_0) = \frac{\cos\alpha_0 \tan i_0}{\tan\eta_0 - \sin\phi_0 \tan i_0} \tag{A.5}$$

$$\tan \phi_0 = \frac{r_t \cos\alpha_0}{1 - r_t \sin \alpha_0} \tag{A.6}$$

where r_t is the ratio of the undeformed to the deformed chip thickness

Rewriting equations (A.1) - (A.3), the cutting forces along P, Q, and R are given by

$$F_p = K_p b_0 S_0$$

$$F_q = K_q b_0 S_0 \qquad \text{(A.7)}$$

$$F_r = K_r b_0 S_0$$

where

$$K_p = \frac{S_s}{\sin \phi_0} \cdot \frac{\cos(\beta_0-\alpha_0) + \sin\beta_0 \cdot \tan^2 i_0}{[\cos^2(\beta_0+\phi_0-\alpha_0) + \tan^2 i_0 \sin^2\beta_0]^{\frac{1}{2}}}$$

$$K_q = \frac{S_s}{\sin \phi_0} \cdot \frac{1}{\cos i_0} \frac{\sin(\beta_0-\alpha_0)}{[\cos^2(\beta_0+\phi_0-\alpha_0) + \tan^2 i_0 \sin^2\beta_0]^{\frac{1}{2}}} \qquad \text{(A.8)}$$

$$K_r = \frac{S_s}{\sin \phi_0} \cdot \frac{[\cos(\beta_0-\alpha_0) - \sin\beta_0] \tan i_0}{[\cos^2(\beta_0+\phi_0-\alpha_0) + \tan^2 i_0 \sin^2\beta_0]^{\frac{1}{2}}}$$

The instantaneous mean value of the dynamic cutting force F_s along the copying axis can be determined by resolving the three cutting force components and is calculated from Figure A.2 as:

$$F_s = F_q \cos(\gamma-\psi) - F_r \sin(\gamma-\psi) \qquad \text{(A.9)}$$

Combining equations (A.7) and (A.9) gives

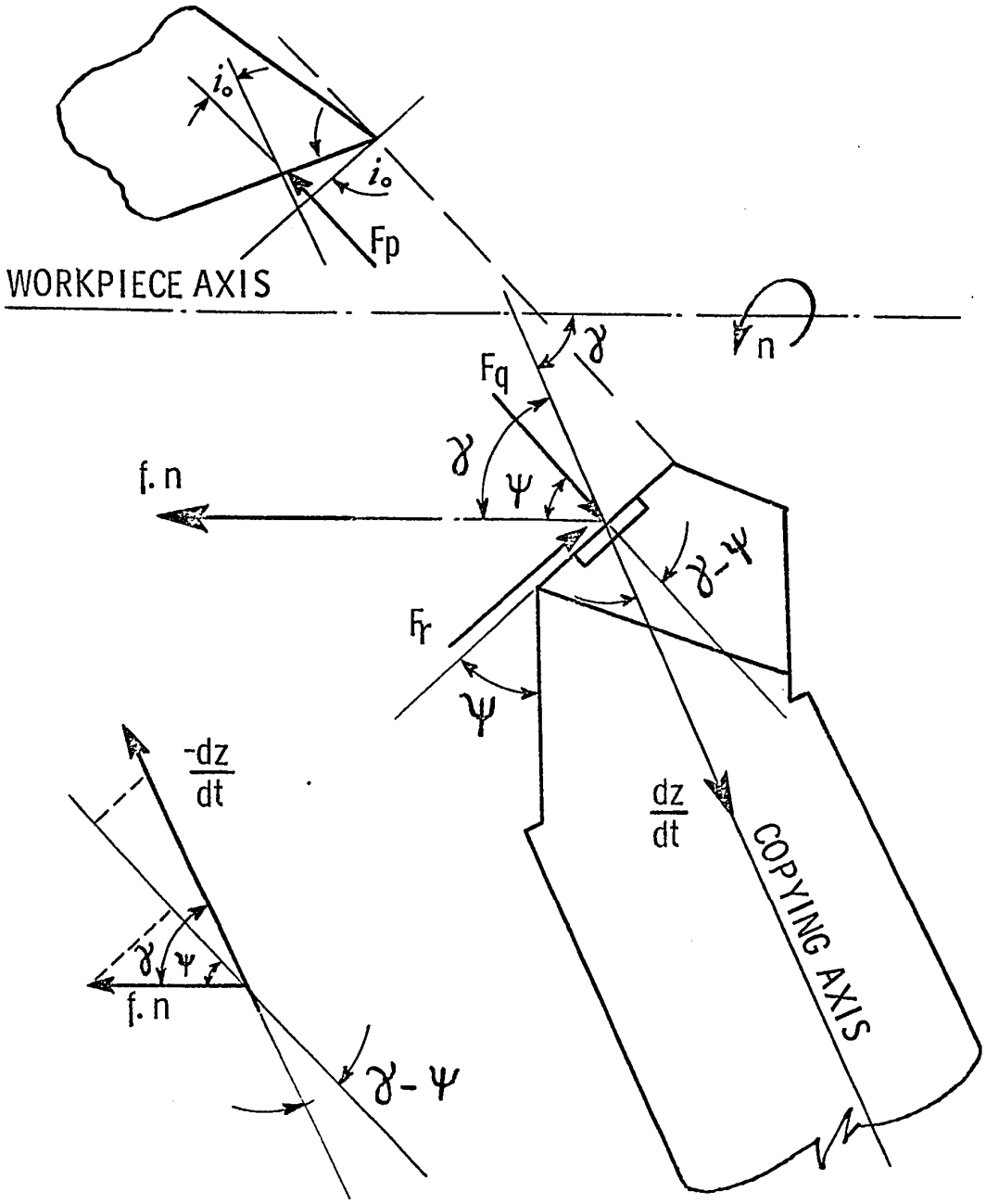

FIGURE A.2 CUTTING FORCES IN A HYDRAULIC COPYING SYSTEM

$$F_s = b_0 S_0 \left[K_q \cos(\gamma-\psi) - K_r \sin(\gamma-\psi)\right] \tag{A.10}$$

In hydraulic copying systems, the feed rate S_0 along the Q axis, depends not only on the feed rate of the machine tool slide ($f \cdot n$), but also on the velocity of the copying slide. Hence, S_0 can be written from the velocity diagram in Figure A.2 as:

$$S_0 = f \cdot \cos\psi - \frac{dz}{dt} \cos(\gamma-\psi) \;/\; n \tag{A.11}$$

Hence, combining equations (A.10) and (A.11) gives:

$$F_s = \left[F_1 - F_2 \frac{dz}{dt}\right] \tag{A.12}$$

where

$$F_1 = (b_o f) \cdot \cos\psi \cdot \left[K_p \cdot \cos(\gamma-\psi) - K_r \cdot \sin(\gamma-\psi)\right]$$

$$F_2 = (b_0/n) \left[\cos(\gamma-\psi)\right] \left[K_q \cos(\gamma-\psi) - K_r \sin(\gamma-\psi)\right] \tag{A.13}$$

Since for a given cutting operation, the workpiece material and the cutting tool geometry are known, F_1 and F_2 can be calculated from equation (A.13) and the procedure is outlined in the form of a flow chart in Figure A.3. Thus, a

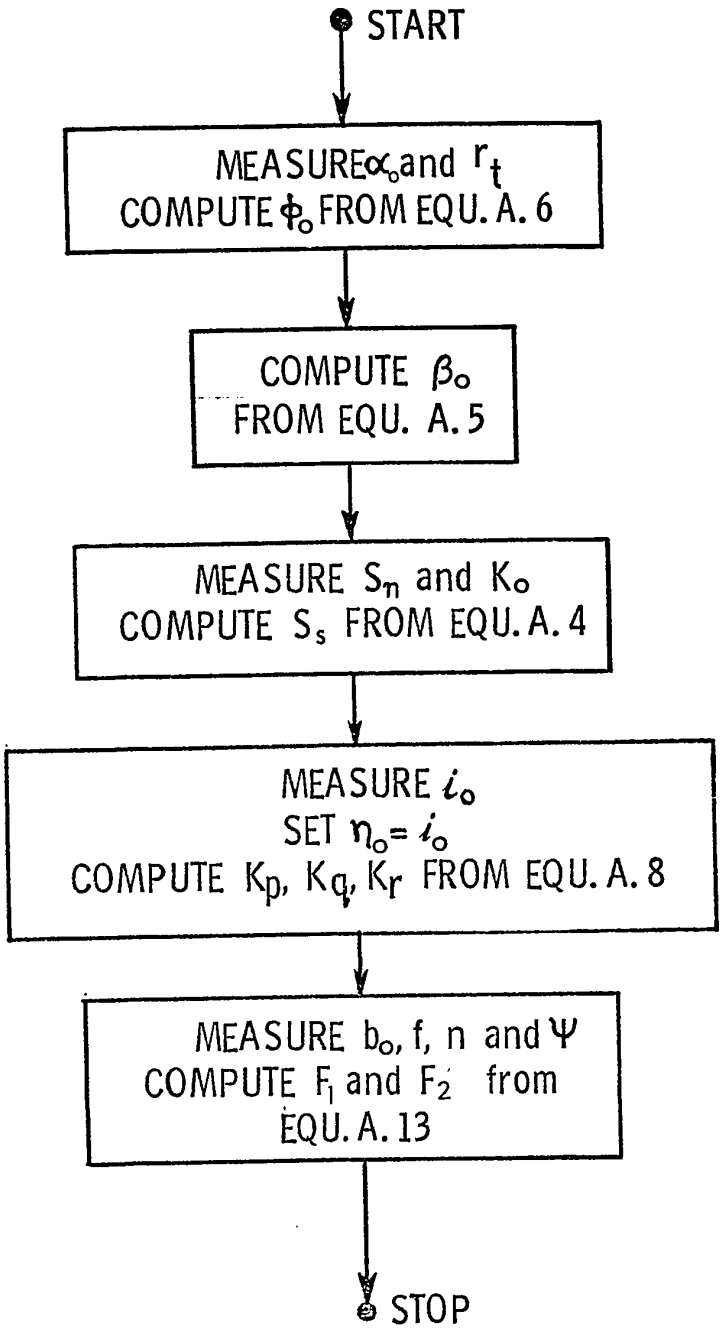

FIGURE A.3 FLOW CHART FOR COMPUTING F_1 AND F_2

particular cutting operation can be defined by determining the values of F_1 and F_2.

To acquire an appreciation for the magnitudes of F_1 and F_2 in a copying process, a wide range of geometrical configurations for the cutting operation is examined. Since F_1 and F_2 depend on the coefficients K_q and K_r, these coefficients are evaluated at first for different cutting operations. For this purpose, a workpiece of material steel 4340 with coefficients $K_0 = 0.175$ and $S_n = 69{,}000$ lb./in^2 [38] is chosen. The range of values for i_0, r_t and α_0 are selected as:

$$i_0 = [0^\circ \text{ to } 30^\circ]$$

$$\alpha_0 = [-40^\circ \text{ to } 40^\circ]$$

$$r_t = [0.1 \text{ to } 1.0]$$

A computer program as shown at the end of this Appendix is prepared to evaluate these coefficients. It is found from the computed values that the dependence of K_q on i_0 is less than 10 percent and hence K_q can be treated as independent of i_0. With this assumption, the variation of K_q for different values of r_t with α_0 as a parameter are

plotted and are shown in Figure A.4 . Since the dependence of K_r on r_t is less than 5 percent, K_r is considered independent of r_t and the plots K_r against α_0 with i_o as a parameter are obtained and are shown in Figure A.4. Now, using these plots and selecting the following parameters:

$$\gamma = 45^{\circ}$$

$$\psi = 15^{\circ}$$

$$b_0 = 0.04 \text{ in.}$$

$$f = 0.009 \text{ in / rev}$$

$$\text{and } n = 5 \text{ rps}$$

the values of F_1 and F_2 in a copying process (Steel 4340 as the workpiece material) are calculated to be 8 lb. and 140 lb.sec / in.

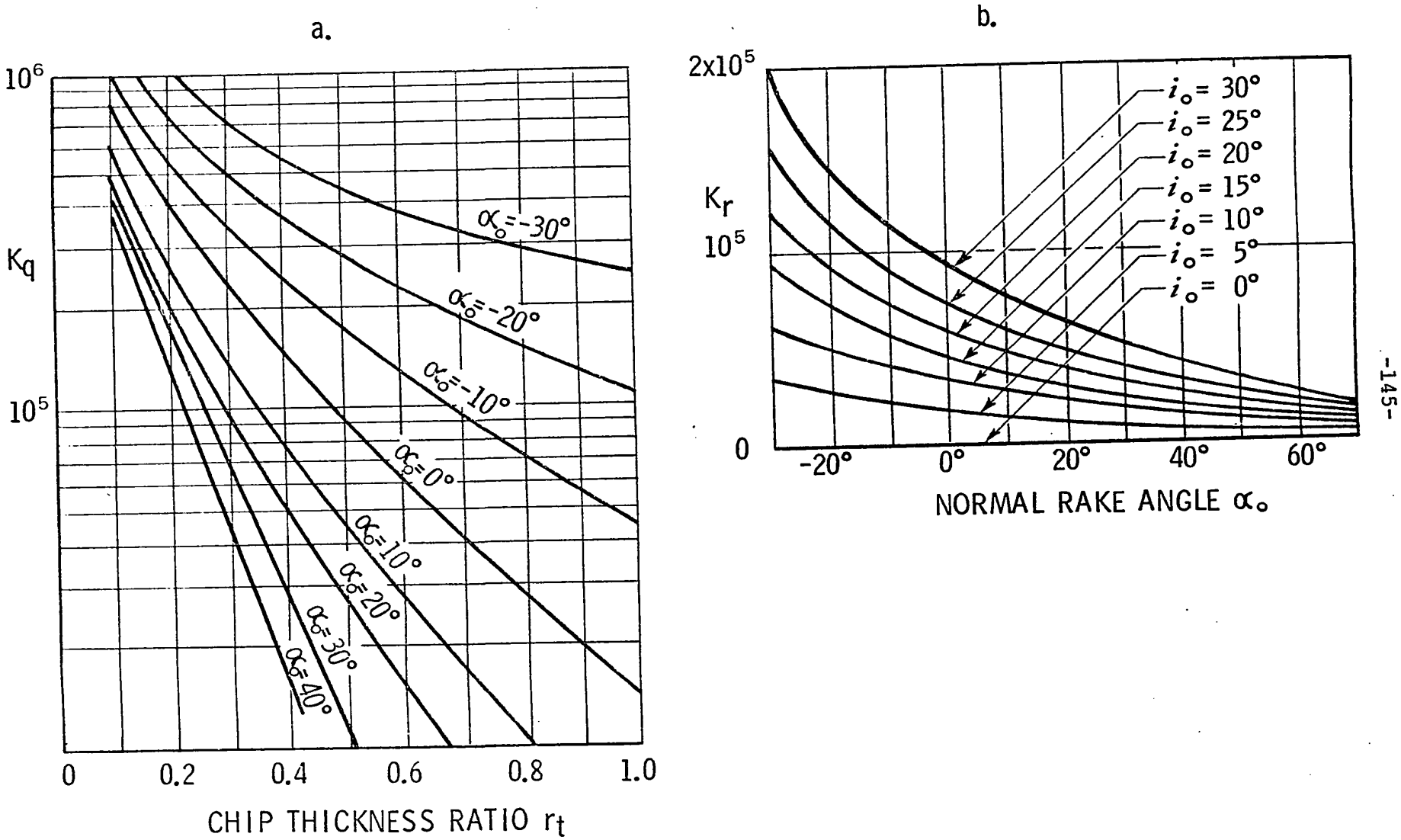

FIGURE A.4 THE COEFFICIENTS K_Q AND K_r FOR STEEL SAE 4340

```
      PROGRAM KPKQKR (INPUT,OUTPUT)
C     THIS PROGRAM IS USED TO CALCULATE VARIOUS CONSTANTS
C     KP,KQ,AND KR FROM THE KNOWN TOOL GEOMETRY.
C     KQ AND KR ARE DIRECTLY USEFUL IN CALCULATING THE
C     DYNAMIC CUTTING FORCES.
C     THE WORKPIECE MATERIAL IS SAE 4340.
C     SO- IS THE SHEAR STRESS OF MATERIAL AT ZERO
C     NORMAL STRESS IN CUTTING.
C     AK- IS THE MATERIAL CONSTANT DUE TO PLASTICITY.
C     ALPHA- IS THE NORMAL RAKE ANGLE OF THE TOOL.
C     AI- IS THE ANGLE OF OBLIQUITY
C     RT- IS THE CHIP THICKNESS RATIO.
      READ 1, SO,AK
    1 FORMAT (2F10.3)
      PRINT 2
    2 FORMAT (1H1,///,10X,12HSHEAR STRESS,10X,8HCONSTANT,//)
      PRINT 3,SO,AK
    3 FORMAT (2(10X,E10.4))
      PRINT 4
    4 FORMAT (///,10X,2HKP,10X,2HKQ,10X,2HKR,10X,5HALPHA,10X,2HRT,10X,
     11HI)
C     THE CALCULATIONS ARE DONE BY VARYING RT FROM ZERO TO UNITY
C     ALPHA FROM -40 DEGREES TO +40 DEGREES AND AI FROM ZERO DEGREE TO
C     +30 DEGREES
      ALPHA1=-40.
      RT1=0.0
      AI1=0.0
      PAI=3.14159
      DO 30 J=1,9
      AJ=J-1
      ALPHA2=ALPHA1+AJ*10.
      ALPHA=ALPHA2*PAI/180.
      DO 20 M=1,9
      AM=M
      RT=RT1+AM/10.0
      DO 10 N=1,4
      AP=N-1
      AI2=AI1+AP*10.
      AI=AI2*PAI/180.
      CALPHA=COS(ALPHA)
      SALPHA=SIN(ALPHA)
      APHI=ATAN(RT*CALPHA/(1.0-RT*SALPHA))
      B1=ATAN(CALPHA/(1.0-SALPHA))
      BETA=B1-APHI
      B2=BETA+APHI-ALPHA
      TB2=TAN(B2)
      SS=SO/(1.0-AK*TB2)
      CB2=COS(B2)
      SAPHI=SIN(APHI)
      B3=BETA-ALPHA
      CB3=COS(B3)
      SBETA=SIN(BETA)
      TAI=TAN(AI)
      SB3=SIN(B3)
      CAI=COS(AI)
```

```
      CC=SQRT(CB2**2.0+(TAI**2.0)*(SBETA**2.0))
      AKP=SS*(CB3+SBETA*TAI**2.0)/(SAPHI*CC)
      AKQ=SS*SB3/(SAPHI*CAI*CC)
      AKR=SS*(CB3-SBETA)*TAI/(SAPHI*CC)
60    PRINT 5, AKP,AKQ,AKR,ALPHA2,RT,AI2
    5 FORMAT (//,4X,3(2X,E10.4),3X,E10.4,4X,E10.4,2X,E10.4)
   10 CONTINUE
   20 CONTINUE
   30 CONTINUE
65    STOP
      END
```

A P P E N D I X III

AMPLITUDE AND TIME SCALING IN ANALOG COMPUTER

A P P E N D I X III

Amplitude and time scaling may be done directly on the computer diagram. The first step is to set up the computer diagram directly from the problem equation on a one-to-one amplitude and time scale as shown in Figure 22. Then, to change the time scale, observe the following rules [39]

Amplitude Scaling

1) Change the scale factor of the pertinent elements.
2) Insert gains which make the computer variable consistent with the scale factors in the diagram.
3) Add gains where needed so that all loop gains are the same as they were in the diagram with a one-to-one amplitude scale.
4) Relabel all computer diagram variables which have been changed as a result of the scaling. Two variables are related as the gain between them.

Time scaling

1) Choose $\tau_1 = \beta_t \tau$

where τ is the problem independent variable

τ_1 is the computer independent variable

and β_t is the scale factor

If $\beta_t > 1$, the problem is slowed down by β_t;

$\beta_t < 1$, the problem is sped up by β_t.

2) To scale by a factor of β_t, change all the inputs of each by the integrators by a factor of $\frac{1}{\beta_t}$.

3) Initial conditions on the integrators remain unchanged. The variable at the output of each integrator is the same as before scaling. However, β_t units of computer time τ_1 are equal to one unit of independent variable τ.

4) If the input function is a function of the problem-independent variable, then it must have the same time scale as the computer.

Using the above rules and choosing the maximum values for the problem variables as shown below:

$$Z^* = 10 \; ; \; \dot{Z}^* = 10^2 \; ; \; \ddot{Z}^* = 5\times10^3$$

$$\theta = 1 \; ; \; \dot{\theta} = 10 \; ; \; \ddot{\theta} = 10^2$$

$$P_1^* = 1 \; ; \; \dot{P}_1^* = 10^3$$

$$P_2^* = 1 \quad ; \quad \dot{P}_2^* = 10^3$$

and with a time scale factor $\beta_t = 10$, the scaling is carried out and the corresponding scaled computer diagram is shown in Figure A.5.

FIGURE A.5 AMPLITUDE AND TIME SCALED ANALOG CIRCUIT DIAGRAMS

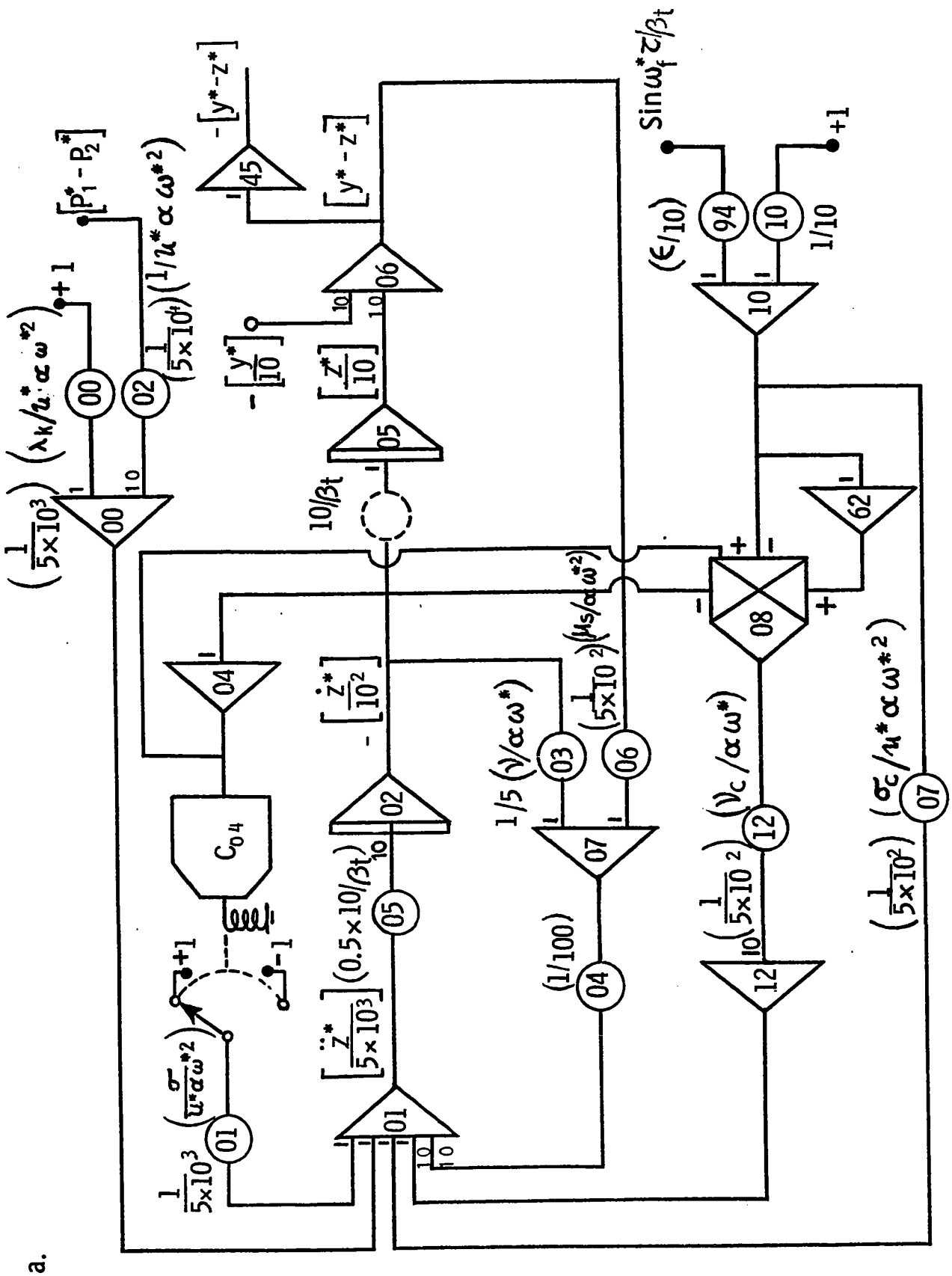
$\left(\frac{1}{5\times10^3}\right)$
$(\lambda_k/u^*\alpha\omega^{*2})$
+1
$[P_1^* - P_2^*]$
$(1/u^*\alpha\omega^{*2})$
$\frac{1}{(5\times10^4)}$
$-[y^*-z^*]$
$[y^*-z^*]$
$-\left[\frac{y^*}{10}\right]$
$\left[\frac{z^*}{10}\right]$
$10/\beta t$
$\sin\omega_f^* \tau/\beta_t$
+1
$(\epsilon/10)$
1/10
$\left[\frac{\ddot{z}^*}{5\times10^3}\right](0.5\times10/\beta_t)$
$-\left[\frac{\dot{z}^*}{10^2}\right]$
$1/5\ (\nu/\alpha\omega^*)$
$\left(\frac{1}{5\times10^2}\right)(\mu_s/\alpha\omega^{*2})$
$(\nu_c/\alpha\omega^*)$
$\left(\frac{1}{5\times10^2}\right)$
$(\sigma_c/u^*\alpha\omega^{*2})$
$\left(\frac{1}{5\times10^3}\right)$
$\left(\frac{\sigma}{u^*\alpha\omega^{*2}}\right)$
C_{04}
+1
-1
(1/100)
00
01
02
03
04
05
06
07
08
10
12
45
62
94
a.

b.

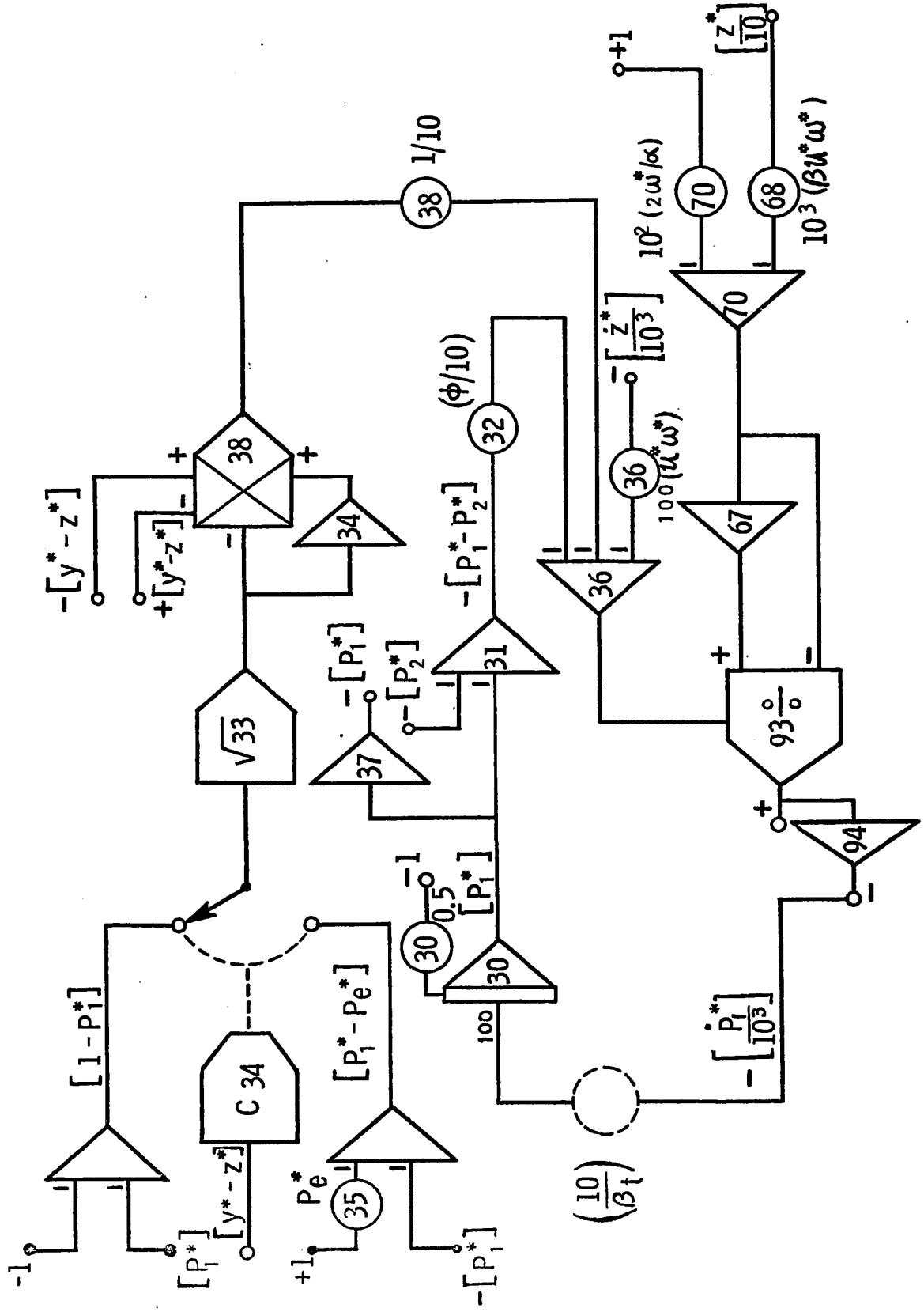
-1
[1-P1*]
[P1*]
[y*-z*]
C 34
+1
Pe*
35
[P1*-Pe*]
-[P1*]
√33
38
1/10
-[y*-z*]
+[y*-z*]
34
(Φ/10)
32
-[P1*-P2*]
-[P1*]
-[P2*]
37
31
-1
0.5
30
[P1*]
30
100
(10/βt)
-[ż*/10³]
36
100(ω*)
36
10²(2ω*/α)
+1
70
70
10³(βu*ω*)
[z*/10]
67
93%
94
-[ṗ1*/10³]

c.

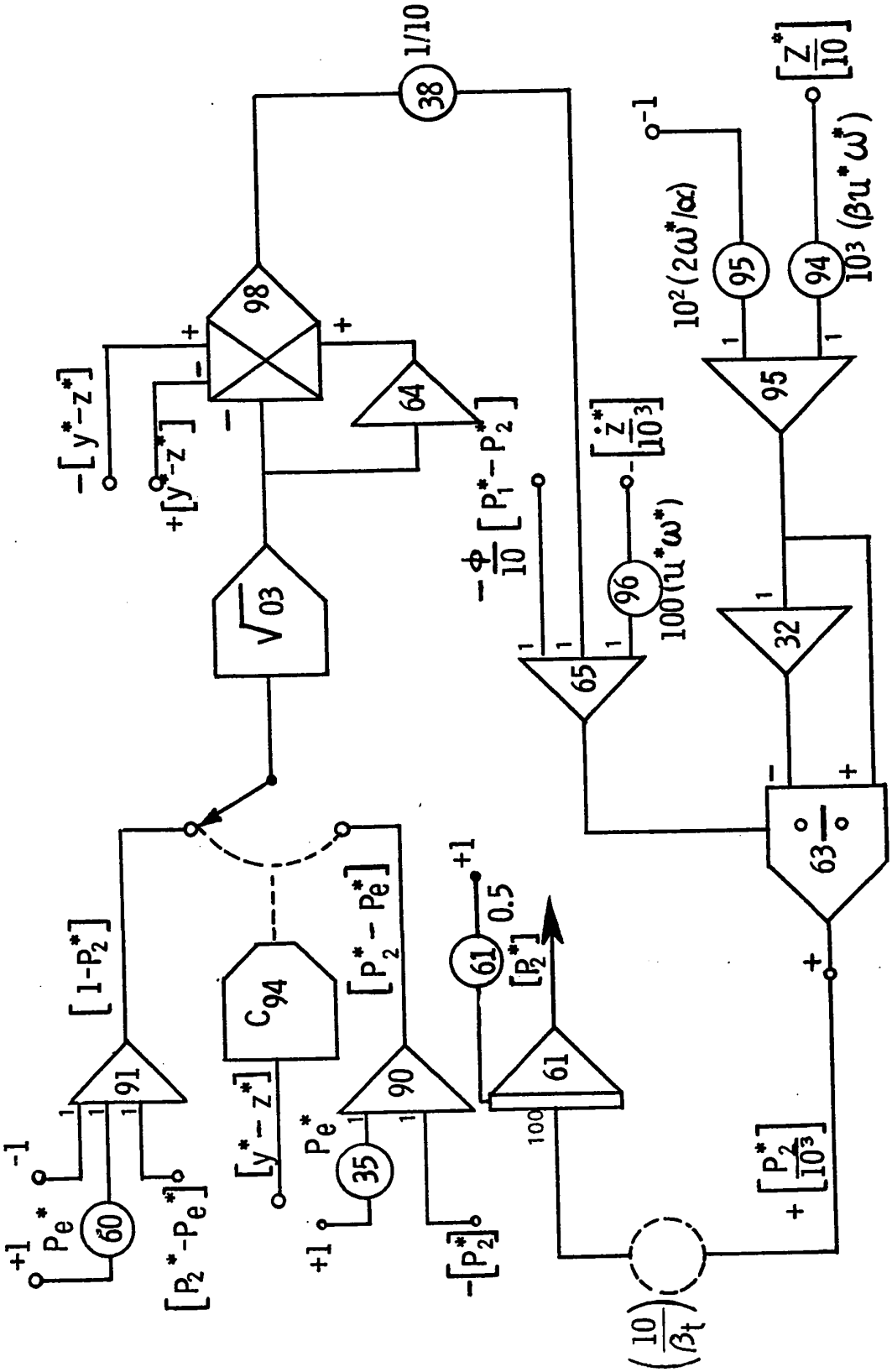
1/10
38
98
64
$\sqrt{03}$
$-[y^*-z^*]$
$+[y^*-z^*]$
$-\frac{\Phi}{10}[P_1^*-P_2^*]$
$\left[\frac{\dot{z}^*}{10^3}\right]$
96
$100(u^*\omega^*)$
65
$10^2(2\omega^*/\alpha)$
95
$10^3(\beta u^*\omega^*)$
94
$\left[\frac{Z^*}{10}\right]$
32
63
$\left[\frac{P_2^*}{10^3}\right]$
$\left(\frac{10}{\beta_t}\right)$
100
61
+1
0.5
$[P_2^*]$
$-[P_2^*]$
$[P_2^*-P_e^*]$
C_{94}
$[y^*-z^*]$
P_e^*
35
90
$[1-P_2^*]$
91
-1
P_e^*
60
$[P_2^*-P_e^*]$

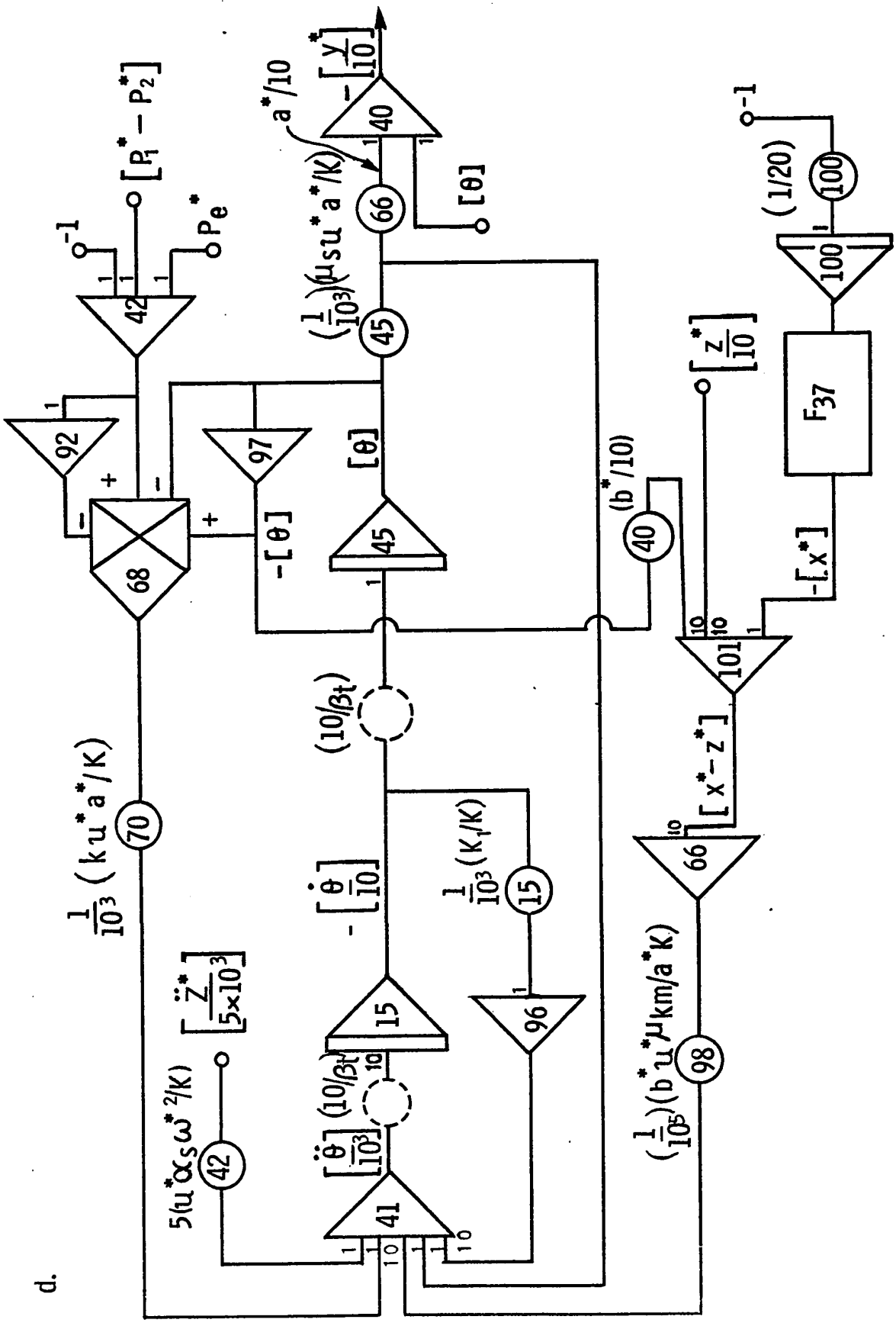
d.
$\frac{1}{10^3}(k_u^* a^*/K)$
70
$5(u^* \alpha_s \omega^{*2}/K)$
42
$[\frac{\ddot{z}^*}{5\times10^3}]$
$[\frac{\dot{\theta}}{10}]$
$[\frac{\dot{\theta}}{10^3}]$
(10/βt)
19
15
41
$\frac{1}{10^3}(K_1/K)$
15
96
$(\frac{1}{10^5})(b^* u^* \mu_{km}/a^* K)$
98
66
$[x^* - z^*]$
101
$-[x^*]$
F_{37}
100
(1/20)
100
-1
$[\frac{z^*}{10}]$
$(b^*/10)$
40
$[\theta]$
45
$(\frac{1}{10^3})(\mu_{su}^* a^*/K)$
45
$a^*/10$
66
$-[\frac{y^*}{10}]$
40
$[\theta]$
$-[\theta]$
97
92
68
42
-1
P_e^*
$[P_1^* - P_2^*]$

A P P E N D I X IV

FORTRAN PROGRAM FOR STYLUS MOTION IN TIME DOMAIN

```
      PROGRAM TEMPCON(INPUT,OUTPUT)
      DIMENSION X(11),Y(11),XT(11),T(11)
C     THIS PROGRAM IS USED TO OBTAIN THE TEMPLATE CONFIGURATION IN TIME
C     DOMAIN.
C     X(I),Y(I) REPRESENT THE COORDINATES OF THE TEMPLATE IN THE
C     RECTANGULAR COORDINATES.
C     XT(I),T(I) REPRESENT THE TIME DOMAIN DISPLACEMENT OF THE STYLUS
C     AND THE REAL TIME
      READ 1, (X(I),I=1,11)
      READ 2, (Y(J),J=1,11)
    1 FORMAT(11F5.3)
    2 FORMAT(11F5.3)
      PRINT 10
   10 FORMAT(1H1,///,20X,4HX(I),10X,4HY(I),//)
      PRINT 30, (X(I),Y(I),I=1,11)
   30 FORMAT(10(19X,F5.3,9X,F5.3,//))
      XT(1)=Y(1)
      T(1)=0.
      PAI=22./7.
      AGAMMA=45.
      V=2.
      GAMMA=AGAMMA*PAI/180.
      SGAMMA=SIN(GAMMA)
      TGAMMA=TAN(GAMMA)
      DO 40 I=1,10
      J=I+1
      DX=(Y(J)-Y(I))/SGAMMA
      XT(J)=XT(I)+DX
      DT=((X(J)-X(I))+(Y(J)-Y(I))/TGAMMA)/V
   40 T(J)=T(I)+DT
      PRINT99, (V,AGAMMA)
   99 FORMAT(1H1,///,30X,1HV,5X,1H=,F5.3,10X,5HGAMMA,5X,1H=,F5.2)
      PRINT 100
  100 FORMAT    (///,20X,28HDISPLACEMENT IN TIME DOMAIN ,10X,5HTIME,//)
      PRINT 120, (XT(I),T(I),I=1,11)
  120 FORMAT(34X,F7.3,19X,F7.3,//)
      STOP
      END
```


X(I)	Y(I)
0,000	0,000
1,367	,233
2,089	,311
2,847	,354
3,239	,361
3,647	,354
4,068	,332
6,273	,127
7,101	,099
7,873	,127
9,746	,255

V =2,000 GAMMA =45,00

DISPLACEMENT IN TIME DOMAIN	TIME,
0,000	0,000
,329	,800
,440	1,200
,500	1,600
,510	1,800
,500	2,000
,469	2,200
,180	3,200
,140	3,600
,180	4,000
,361	5,000

A P P E N D I X V

SYSTEM PARAMETERS

A P P E N D I X V

A	=	$6\ in^2$
a	=	$1\ in$
B	=	$2.5 \times 10^5\ lb/in^2$
b	=	$2\ in$
C_d	=	0.62
C_l	=	$0.01\ in^5/lb.sec$
C_m	=	$600\ lb.in.sec$
F_1	=	$8\ lb$
F_2	=	$140\ lb.sec/in$
F_k	=	$10\ lb$
F_w	=	$100\ lb$
I_m	=	$2\ lb.in.sec^2$
K_m	=	$4 \times 10^5\ lb/in$
K_s	=	$30\ lb/in$
M	=	$0.35\ lb.sec^2/in$
m_s	=	$1.5 \times 10^{-3}\ lb.sec^2/in$
P_s	=	$350\ lb/in^2$
P_e	=	$35\ lb/in^2$
V	=	$60\ in^3$
v	=	$2\ in/sec$
γ	=	$45\ deg.$

A P P E N D I X VI

CALCULATION OF HYDRO-MECHANICAL STIFFNESS C_h AND ITS CONDITION ON STABILITY

A P P E N D I X VI

In analyzing the stability of hydraulic copying systems using linearization method, the stability condition can be written as outlined in Chapter III and is given by:

$$\frac{a_2 a_1}{a_3 a_0} > 1 \qquad \text{(A.14)}$$

Using the values of the coefficients defined in equation (3.20) and assuming that the effect of viscous friction in the cylinder, the leakage past the piston, and the stiffness K_s of the spring are negligible, the above condition can be rewritten as:

$$\frac{C_e}{C_p} < \left(\frac{b}{a}\right) \left(\frac{4AB}{V}\right) \qquad \text{(A.15)}$$

Let

$K_g = \frac{a}{b}$, the kinematic gain

$C_o = \frac{4A^2B}{V}$, the hydraulic stiffness [40].

Then the stability condition in equation (A.15) can be defined in terms of k_g and C_o and is given by:

$$A \left(\frac{C_e}{C_p}\right) < \left(\frac{1}{k_g}\right) C_o \tag{A.16}$$

In order to evaluate the coefficients C_e and C_p, consider the non-linear flow characteristic equations

$$Q_1 = C_d W e \left[\frac{2}{\rho} (P_s - P_1) \right]^{\frac{1}{2}} \tag{A.17}$$

$$Q_2 = C_d W e \left[\frac{2}{\rho} (P_2 - P_e) \right]^{\frac{1}{2}} \tag{A.18}$$

for $e > 0$

and

$$Q_1 = C_d W e \left[\frac{2}{\rho} (P_s - P_2) \right]^{\frac{1}{2}} \tag{A.19}$$

$$Q_2 = C_d W e \left[\frac{2}{\rho} (P_1 - P_e) \right]^{\frac{1}{2}} \tag{A.20}$$

for $e < 0$

Assuming that the valving orifices are matched and

symmetrical, the flow into and out of the cylinder will be the same; that is,

$$Q_1 = Q_2 = Q_l \text{ , say.}$$

Then from equations (A.17) and (A.18),

$$P_s - P_1 = P_2 - P_e$$

i.e., $$P_1 + P_2 = P_s + P_e \qquad \text{(A.21)}$$

Let $$P_1 - P_2 = P_l \qquad \text{(A.22)}$$

Then combining equations (A.21) and (A.22) and rearranging, gives:

$$P_1 = \frac{1}{2}(P_s + P_e + P_l) \qquad \text{(A.23)}$$

$$P_2 = \frac{1}{2}(P_s + P_e - P_l) \qquad \text{(A.24)}$$

Using equations (A.23) and (A.24), the flow rate Q_l can be written as:

$$Q_l = C_d We \left[\frac{1}{\rho} (P_s - P_e - P_l) \right]^{\frac{1}{2}} \qquad (A.25)$$

for $e > 0$

and

$$Q_l = C_d We \left[\frac{1}{\rho} (P_s - P_e + P_l) \right]^{\frac{1}{2}} \qquad (A.26)$$

for $e < 0$

Combining equations (A.25) and (A.26),

$$Q_l = C_d We \left[\frac{1}{\rho} (P_s - P_e - \text{sgn}(e)\ P_l) \right]^{\frac{1}{2}} \qquad (A.27)$$

Then, the coefficients C_e and C_p can be defined as:

$$C_e = \frac{\delta Q_l}{\delta e} = C_d W \left[\frac{1}{\rho} (P_s - P_e - P_l) \right]^{\frac{1}{2}}$$

and

$$C_p = -\frac{\delta Q_l}{\delta P_l} = \frac{C_d We \left[\frac{1}{\rho} (P_s - P_e - P_l) \right]^{\frac{1}{2}}}{2 (P_s - P_e - P_l)}$$

Then

$$\frac{C_e}{C_p} = -\frac{\frac{\delta Q_l}{\delta e}}{\frac{\delta Q_l}{\delta P_l}} = -\frac{\delta P_l}{\delta e} = \frac{2\ (P_s - P_e - P_l)}{e} \qquad (A.28)$$

Therefore,

$$A\ \left(\frac{C_e}{C_p}\right) = -A\ \frac{\delta P_l}{\delta e} = -\frac{\delta}{\delta e}\ [A(P_1-P_2)]$$

Since the total load $\Sigma P = A(P_1-P_2)$

$$A\ \left(\frac{C_e}{C_p}\right) = -\frac{\delta \Sigma P}{\delta e} \qquad (A.29)$$

From the definition of the hydro-mechanical stiffness C_h given in Chapter II, the equation (A.29) can be written as:

$$C_h = A\ \left(\frac{C_e}{C_p}\right) \qquad (A.30)$$

Hence from equation (A.28), the hydro-mechanical stiffness is given by:

$$C_h = \frac{2A\ (P_s - P_e - P_\ell)}{e}$$

Using equation (A.30), the stability condition given in equation (A.16) can be written in terms of C_h as:

$$C_h < \left(\frac{1}{K_g}\right) C_o$$